AEDC-TR-95-10

# AEDC Sensor T&E Methodology

Space Environment Simulation Technology and Analysis Teams
Micro Craft Technology/AEDC Operations

July 1995

Final Report for Period October 1, 1992 — January 31, 1995



Approved for public release; distribution is unlimited.



ARNOLD ENGINEERING DEVELOPMENT CENTER
ARNOLD AIR FORCE BASE, TENNESSEE
AIR FORCE MATERIEL COMMAND
UNITED STATES AIR FORCE

## NOTICES

When U. S. Government drawings, specifications, or other data are used for any purpose other than a definitely related Government procurement operation, the Government thereby incurs no responsibility nor any obligation whatsoever, and the fact that the Government may have formulated, furnished, or in any way supplied the said drawings, specifications, or other data, is not to be regarded by implication or otherwise, or in any manner licensing the holder or any other person or corporation, or conveying any rights or permission to manufacture, use, or sell any patented invention that may in any way be related thereto.

Qualified users may obtain copies of this report from the Defense Technical Information Center.

References to named commercial products in this report are not to be considered in any sense as an endorsement of the product by the United States Air Force or the Government.

This report has been reviewed by the Office of Public Affairs (PA) and is releasable to the National Technical Information Service (NTIS). At NTIS, it will be available to the general public, including foreign nations.

## APPROVAL STATEMENT

This report has been reviewed and approved.

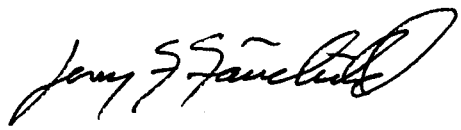

JERRY F. FAIRCHILD
Flight Dynamics Technology
Applied Technology Division
Test Operations Directorate

Approved for publication:

FOR THE COMMANDER

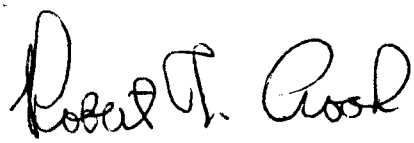

ROBERT T. CROOK
Asst Chief, Applied Technology Division
Test Operations Directorate

# REPORT DOCUMENTATION PAGE

*Form Approved*
*OMB No. 0704-0188*



| 1. AGENCY USE ONLY (Leave blank) | 2. REPORT DATE | 3. REPORT TYPE AND DATES COVERED |
|---|---|---|
| | July 1995 | Final Report -- Oct. 1, 1992 - Jan. 31, 1995 |

**4. TITLE AND SUBTITLE**

AEDC Sensor T&E Methodology

**5. FUNDING NUMBERS**

PE - 65807F
PN - 0104

**6. AUTHOR(S)**

Space Environment Simulation Technology and Analysis Teams
Micro Craft Technology/AEDC Operations

**7. PERFORMING ORGANIZATION NAME(S) AND ADDRESS(ES)**

Arnold Engineering Development Center/DOT
Air Force Materiel Command
Arnold Air Force Base, TN 37389-9011

**8. PERFORMING ORGANIZATION (REPORT NUMBER)**

AEDC-TR-95-10

**9. SPONSORING/MONITORING AGENCY NAMES(S) AND ADDRESS(ES)**

Arnold Engineering Development Center/DOT
Air Force Materiel Command
Arnold Air Force Base, TN 37389-9011

**10. SPONSORING/MONITORING AGENCY REPORT NUMBER**

**11. SUPPLEMENTARY NOTES**

Available in Defense Technical Information Center (DTIC).

**12A. DISTRIBUTION/AVAILABILITY STATEMENT**

Approved for public release; distribution is unlimited.

**12B. DISTRIBUTION CODE**

**13. ABSTRACT (Maximum 200 words)**

For space surveillance systems it is extremely costly, and, in some cases, impractical to provide effective field testing to evaluate operational issues. Even with sufficient systems on orbit, there are significant problems in providing the threat targets. Not only is the launch of a target missile very expensive, but it is also impractical to launch eight or ten missiles simultaneously. System performance is measured at only one set of parameters, and the possibility of acquiring zero data is real. Operational testing of space assets in ground test facilities has been limited as well by the lack of adequate target and threat simulations. AEDC's new direct write scene generation (DWSG) capabilities have overcome this limitation. These capabilities, along with recently upgraded state-of-the-art sensor test facilities and closed-loop DWSG developments, can provide ground-based testing at all levels of system acquisition. This report describes the proposed new approach to surveillance and seeker testing for the next century, which includes the marriage of the traditional DT&E with a new capability to perform early operational assessments and operational T&E prior to deployment. This T&E methodology takes full advantage of existing DoD facility investments, provides testing at lower costs, enables better investigation of the sensor design envelope with actual hardware, allows concurrent DT&E and OT&E, and reduces flight risk for a program.

**14. SUBJECT TERMS**

sensors, test and evaluation (T&E), surveillance, seeker, closed loop, networks, operational testing, development testing, simulations, human-in-control, focal plane array

**15. NUMBER OF PAGES**

122

**16. PRICE CODE**

| 17. SECURITY CLASSIFICATION OF REPORT | 18. SECURITY CLASSIFICATION OF THIS PAGE | 19. SECURITY CLASSIFICATION OF ABSTRACT | 20. LIMITATION OF ABSTRACT |
|---|---|---|---|
| UNCLASSIFIED | UNCLASSIFIED | UNCLASSIFIED | SAME AS REPORT |

## PREFACE

The work reported herein was conducted by the Arnold Engineering Development Center (AEDC), Air Force Materiel Command (AFMC), under Program Element 65807F. The results were obtained by Micro Craft Technology/AEDC Operations, support and technical service contractor of flight dynamics test facilities, AFMC, AEDC, Arnold Air Force Base, TN 37389-4300 under AEDC Job Numbers 0103, 0104, 0106, and 0120. The Air Force Project Manager was Capt. Frank Fairchild, AEDC/DOT. This report describes the work effort initiated on October 1, 1992 and completed January 31, 1995. The manuscript was submitted for publication on May 31, 1995.

## ACKNOWLEDGMENTS

This document was prepared by the Space Environment Simulation Technology and Analysis teams at AEDC. Contributors listed alphabetically are:

| | |
|---|---|
| R. Dawbarn | 615-454-7348 |
| R. Fugerer | 615-454-6889 |
| W. Goethert | 615-454-7665 |
| C. Herron | 615-454-7718 |
| E. Kiech | 615-454-7669 |
| R. Menzel | 615-454-3702 |
| J. Selman | 615-454-3734 |
| S. Steely | 615-454-7730 |
| M. Tripp | 615-454-3754 |

The appendices to this document provide synopses of the technical work which has been accomplished in support of the overall objectives of this project. The technical expert in each of these areas is listed with each synopsis. Additional information in each area can be obtained directly from the investigator listed, or in the referenced documents.

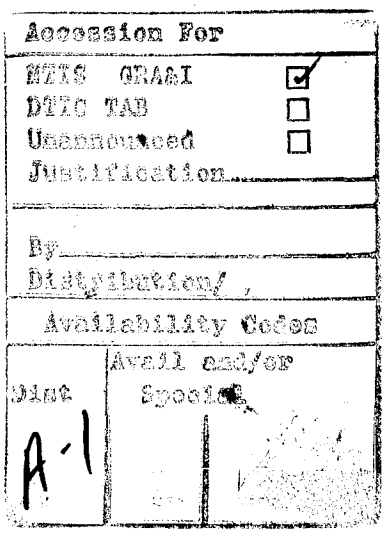

## CONTENTS

## APPENDICES



## ILLUSTRATIONS

# 1.0 FUTURE SENSOR TEST REQUIREMENTS

The development of space test capabilities for the future is based on an evaluation of the types of space systems which will be built and deployed. The types of systems which will be developed will be governed by the missions which they are called to fill and the anticipated state of the technology which can be applied. In the practical world, the requirements and the applied technology will be subject to the political commitment and the available financial resources.

Changes in the world political environment and the end of the Cold War have had a significant effect on the mission of today's sensor programs. The future focus will be on local conflicts rather than on a global war. The current reluctance to commit ground troops in traditional face-to-face combat will grow. There will be more reliance on smart weapons which have their own ability to track and home on preselected targets. The smart weapons will rely on a variety of sensors, with some systems using multiple sensors sharing the same viewing aperture. The selection of targets will require timely, high-resolution reconnaissance information both for the field commanders and for programming weapons systems. The need to provide local surveillance for relatively long periods of time will result in the development of loitering unmanned upper atmospheric fliers with a variety of sensors. The trend in miniaturization will continue, and, in this respect, satellite systems will become smaller. Some satellite systems will be launched from aircraft rather than the traditional launch pads. This will permit the launch of satellites on demand to meet the needs of a specific outbreak of hostilities. The data processing capability will increase, which will permit satellites to become more autonomous. The result will be less reliance on maintaining expensive ground command and control tracking stations around the world. The economic pressures on the development of the new systems will continue. This pressure will result in more emphasis being placed on demonstration of the performance of the proposed systems using modeling, simulations, and emulations with brassboard and prototype hardware rather than expensive flight demonstrations.

The state of the art today is such that surveillance sensor missions, in combination with technology achievements, have led to very complex sensor designs. Platform designs now have multiple sensors with handover capabilities from wide-angle acquisition sensors to high-resolution, narrow-field-of-view tracking sensors. There is a drive to more onboard processing to reduce the amount of data which must be transmitted to the ground stations. Advances in computational hardware allow for faster data rates and higher resolution systems.

## 1.1 IMPACT ON TEST FACILITY REQUIREMENTS

As a result of the anticipated sensor complexities, the test requirements to support the acquisition of these sensors are impacted. The future requirement for better resolution in

surveillance data translates to test facilities with better quality optics and stringent line-of-sight jitter control in ground test facilities. The autonomous handover between various sensors suggests ground test facilities which can handle multiple sensors viewing the same scenes. Multispectral sensors require ground test facilities with high-fidelity spectral targets and backgrounds. Onboard data processing implies the need to provide mission length complex scene simulations. The fact that some advanced systems might require operations evaluation prior to building and deploying flight hardware suggests that ground test facilities must be capable of providing advanced test scenario simulations to brassboard and prototype hardware.

## 1.2 GROUND TEST FACILITIES TECHNOLOGY

Ground test facilities to support sensor testing cannot be designed without first defining the test methodology. The test methodology is developed by examining the advanced sensor concepts and the missions they are designed to fulfill then, and assessing these concepts with the technology available for use in the ground test facilities. Since ground test facilities require a significant lead time for design and construction, those planned for use in the next century must primarily rely on today's technology, yet there must be sufficient flexibility in their design to permit incorporation of potential technology breakthroughs. A further caveat in developing test facilities is that the technology employed should be sufficiently mature so that one is not faced with trying to evaluate an innovative sensor design with an unproven, innovative technology in the ground test chamber.

## 1.3 TEST METHODS

AEDC has developed a long-range plan to support the acquisition of space systems which have optical sensors as part of their surveillance or seeker subsystems. The requirements for future ground test assets are developed from an analysis of the types of systems which must be tested, and a projected test methodology. This report describes the test methodology and the test facilities which are required for its implementation. The proposed new approach to testing for the next century includes the marriage of the traditional development testing with a new capability to perform early operational assessments prior to deployment. This new test methodology provides testing at lower cost, enables better investigation of the sensor design envelope, and reduces flight risk for the program. This approach is in harmony with changes which are being made in the acquisition process.

# 2.0 ACQUISITION PROCESS

In the final analysis all testing should be planned and conducted to support the needs of the decision maker in the acquisition process. The test plan should identify a critical path which directly supports fixed milestone decisions. It is helpful to identify the acquisition cycle and define the types

of tests which should be considered during this cycle. Figure 1 presents the five phases of a traditional acquisition cycle, and identifies the exit milestones. Below this sequence is the contractor acquisition cycle with his deadlines for the various reviews. The acquisition process starts with the user who identifies the need for the space system and the way the system will be used. This process results in the production of several documents. While each of these documents is not primarily produced to define a test program, each can be extremely useful in developing the test plans for the system.

The **Mission Needs Statement (MNS)** and the **Operational Requirements Document (ORD)** are generated by the user and are the foundation for the development of the space system concepts. These documents are supported by a **System Threat Assessment Report (STAR)** which uses the basic authoritative threat assessment, tailored and focused for the specific acquisition program. The threat information is based on Defense Intelligence Agency-validated documents. In conjunction with these documents, the user conducts a **Cost and Operational Effectiveness Analysis (COEA)** to define the costs and benefits of the proposed system with respect to overall military operations. During this process, he establishes a set of **Measures of Effectiveness (MOEs)**. In order to meet the mission requirements a document is produced which identifies the **Measures of Performance (MOPs)** for the system. All these documents are important in developing the test plan. Although they do not identify specific test requirements, they do identify the operational requirements for the final product, and these operational requirements are used to identify critical performance issues. These critical performance issues provide focus points for defining the test plan. The **Test and Evaluation Master Plan (TEMP)** is the basic planning document for all test and evaluation related to the system acquisition. It is used for planning, reviewing, and approving all tests and evaluations throughout the system acquisition. As the acquisition cycle progresses, the TEMP is supplemented with additional documents, each identifying very specific test plans for very specific parts of the space system.

## 2.1 TYPES OF TESTING

There are two types of testing programs associated with the development and eventual deployment of military systems. The first is labeled as development test and evaluation (DT&E). The DT&E program is focused on building demonstration units. Tests are conducted throughout the concept, prototyping, and construction phases of the project. These range from evaluations of materials and components, through 'shake-and-bake'-type tests of subsystems, to integration tests of completed prototypes. The end product of the DT&E program eventually results in operational hardware ready for field tests. At this point in the acquisition process, the emphasis changes to operational test and evaluation (OT&E). For an aircraft, this involves test pilots flying the plane and evaluating its handling, its ability to carry munitions, etc. It also includes evaluating ruggedness, maintenance, and its effectiveness as it is integrated into the larger defense architecture. At present,

space systems follow a similar development test program. However, for space systems it is extremely costly and, in some cases, impractical to provide effective field testing for OT&E. Currently, only two options are available for operational test planners: digital simulations (validated with sparse laboratory data) and on-orbit tests. The former is limited in its ability to test real software and hardware while the latter represents a very expensive alternative with limited threat scenarios and minimal truth data. Recognizing the inherent limitations in the standard procurement practice when considering space systems, DoD has noted that there must be alternative ways of conducting OT&E rather than starting after the completion of the DT&E cycle. The following are examples of such regulations and instructions.

*AFOTECR 55-9*
*"Test support groups (AFOTEC) must coordinate with the implementor (AFMC) to determine which part of OT&E can be accomplished concurrently with DT&E."*
*AFR 80-14*
*"OT&E will begin as early as practical in a system's development ..."*
*".....OA (operational assessment) provides an operationally oriented input in support of decisions prior to milestone III."*
*DoD Instruction 5000.2*
*"Both developmental and operational testers shall be involved early (in the acquisition cycle)."*
*"Testing shall be planned and conducted to take full advantage of existing investment in DoD ranges, facilities, and other (DoD) resources...."*

A standard practice has been to concentrate on the DT&E plan at the beginning of the acquisition process and start the OT&E planning as the system neared the demonstration/validation (dem/val) or flight phase. However, there are severe limitations on what can be accomplished in the area of OT&E in the demonstration/validation and flight programs for space systems. For example, a surveillance satellite on orbit can be tested for such operations as communications, orbit and attitude control, etc., but tests of its primary observation and threat tracking functions are extremely limited. Dedicated launches of missiles are extremely expensive, and it is impossible to launch sufficient numbers to represent a credible threat. Even with limited dedicated launches, there is a hesitancy to launch a threat with the satellite at a minimal viewing angle since it is not cost effective to spend millions of dollars on the dedicated launch of a threat missile and get a zero data point. Targets of opportunity are few and far between, especially if the dem/val satellite is in low orbit and therefore has limited viewing windows. The emphasis for including some method of operational assessment in the development tests is because of these limitations of flight tests for space systems. There are also other important reasons for conducting operational tests early in the acquisition cycle. Testing provides an opportunity to detect deficiencies in the concept or design early in the program when it is still economically possible to make changes. In the case of competing contracts, testing provides the opportunity to make down-selects earlier in the program, thus reducing overall

costs. In the case of advanced technology demonstration programs, testing provides a means of assuring that the concept and the technology as applied are mature enough to develop into a deployable system without expensive flight tests. Figure 2 couples the stages of system development and acquisition with the two types of testing. The new approach as presented in this report provides for early operational assessment of the system at the brassboard and prototype unit stages. As is noted in Fig. 2, instead of development testing handing over to operational testing, these phases are merged together so that there is a gradual shift in emphasis from DT&E to OT&E throughout the acquisition cycle. The desire to conduct operational assessment tests early in the acquisition cycle is an important factor in developing a test methodology and defining the required ground test facilities.

## 2.2 MODELING AND SIMULATION

A comprehensive Modeling and Simulation (M&S) program should underlie the entire acquisition program. This program begins with models to support the concept, develops into models which support the development and construction cycles, and eventually leads into simulations to evaluate the operational effectiveness of the system. In the ideal case, this process of modeling and simulation is seamless from concept support through complex simulators for wargaming. Modeling should be used extensively to help define test requirements, to predict test outcomes, and to evaluate the test results. In the test process suggested in this report, M&S plays an important role in adapting DT&E test facilities for early operational assessment of space systems.

# 3.0 EVOLUTION OF AEDC's SENSOR TEST METHODOLOGY

AEDC has been in the sensor test business for many years and has tested more than 30 sensors. In addition to sensor testing, AEDC has tested nearly 90 focal planes. Historically, these tests have been conducted in an open-loop configuration to support DT&E. However, there has been a continuous effort at AEDC to examine the future of sensor systems, their test requirements, and the types of facilities required. Through this experience and the planning process, a recommended sensor testing methodology has evolved which will test both open- and closed-loop configurations in support of DT&E, Early Operational Assessment, and OT&E.

## 3.1 SDIO-SPONSORED STUDIES

In 1986, a study was sponsored by SDIO and directed by AEDC to develop conceptual designs for a flexible developmental testing capability for advanced space sensors with apertures up to 3 meters in diameter. The study was conducted by the Ralph M. Parsons Company. A key result was the recommendation for three separate capabilities: (1) a test chamber with a cryogenic liner and an all-transmissive optical collimator to test full sensor assemblies; (2) an associated Free-

standing High Fluence Radiation Test Facility to test for nuclear hardening; and (3) a separate Focal Plane Array Facility which could test the sensors at a brassboard level of development. The total cost was estimated at $850 million.

AEDC next contracted with two companies to further define the focal plane facility. Both Boeing and Hughes developed concepts and estimated costs for such a facility at approximately $40 million. The critical component of such a facility is the scene projection system, however, and neither company had an operational concept for the scene projector.

AEDC then started an in-house technology program to develop such a scene projector based on laser scanning techniques. OSD(CTEIP)/Boost Surveillance and Tracking System (BSTS) funded the cost for a demonstration of this new technology. This resulted in a prototype test capability called the Transportable Direct Write Scene Generator (TDWSG). The program was extended to provide a test capability based on this prototype which is called the Focal Plane Array Test Chamber (FPATC). The FPATC was completed in late FY94.

In a concurrent effort, BMDO (then SDIO), through the AF Phillips Laboratory, funded the development of a test chamber at AEDC to characterize the focal plane chips used in sensor systems. The chamber is called the Focal Plane Characterization Chamber (FPCC).

Changes in the BMDO (SDIO) program saw sensor apertures shrink to 1 meter or less and therefore negated the Parsons concept for a large sensor test chamber. The Rockwell Company was contracted to develop a new concept for a future sensor test chamber. This chamber was based on an all-reflective 1-m collimator housed in a cryogenic vacuum chamber with a large seismic mass optical bench to provide microradian line-of-sight stability. The estimate for this chamber was around $100 million, which was more than BMDO could afford within the existing budget. The $100 million request was placed in the MCP program for future funding, and AEDC was asked to provide estimates to modify the existing 7V and 10V facilities for an interim capability. BMDO has invested $25 million in an upgrade of the 7V (completed in FY94), and is in the process of funding a $15 million upgrade for 10V.

Separation of the radiation effects testing from the other sensor test facilities is being accomplished through Defense Nuclear Agency (DNA) siting of its DECADE facility at AEDC. This facility will provide X-ray simulation of nuclear weapons effects on ensembles and subsystems over a 1-$m^2$ test area in a vacuum environment. This $100 million facility will reach Initial Operational Capability (IOC) in late FY96.

The recognition that sensor test requirements cannot be met in a single facility due to both cost and technical barriers was the basis for AEDC's development of a new test methodology. A suite of required test facilities was identified: the FPCC which tests at the focal plane level; the FPATC, which tests the focal plane and its signal processor; and the 7V and 10V, which test the sensor, its signal processor, and its telescope optics. Following the Parsons recommendations, the DECADE facility provides a separate nuclear effects test facility. The sensor test facilities at AEDC have all been upgraded since 1986 to reflect this new sensor test methodology. Each test facility is described in Section 4.0.

As a part of the overall development of the test methodology, it was determined that future testing would involve interfacing government and industry test capabilities over an information network. In FY93, AEDC, in conjunction with AFOTEC, contracted with SAIC to perform a surveillance Sensor Test Bed Study (Ref. 1). This work produced a high-level network plan for interfacing sensor test and modeling facilities.

## 3.2 DEFINITION OF LEVELS OF TESTING

The strategy for ground testing of a modern sensor system must be decomposed into a hierarchy of manageable levels that parallel the requirements for each phase of the program. As the level increases, the complexity of the ground test increases, but the program risk decreases. The test objectives for validation of a space surveillance system can be considered at four levels as the system progresses from initial concepts to final operational assessment. As previously noted, all the test levels are supported by a continuous M&S program. Definitions for each level are as follows:

Level 0: Modeling and simulation
Level 1: Calibrations and characterizations
Level 2: Open-loop mission functional performance
Level 3: Sensor and platform closed-loop performance
Level 4: Sensor and platform networked into an integrated system test

### 3.2.1 Level 0 Definition

Modeling and simulations and test and evaluation play a significant role in the acquisition cycle. The role of Modeling and Simulation (M&S) starts at the concept stage and continues to be utilized throughout the program life. The models should grow "seamlessly" from the early stages into the later models used to develop and support the test programs. Eventually, they should support system performance evaluations and, finally, the integration of the simulated system in the larger defense architecture for wargaming and military exercises. It is important that there should be a total M&S plan which reflects this overarching set of requirements.

Modeling plays an important role in the test process in that it can be used to perform sensitivity analyses to define the critical areas where testing should be focused. Modeling is also used in the test process to anticipate test results and then to analyze and compare experimental data. Figure 3 illustrates the supportive role of modeling in the test cycle.

### 3.2.2 Level 1 Definition

The first level of testing is required to verify that as-built components and prototypes meet design specifications. The first level of testing can be described as calibrations and characterizations. Required test facilities must be able to simulate the space environment, provide high-fidelity infrared sources, and provide extremely stable line-of-sight alignment capabilities, with all measurements traceable to National Institute of Standards and Technology (NIST). At this early stage of development, the OT&E testers can start their program, but must rely primarily on computer modeling. With appropriate monitoring of the DT&E tests, however, data can be acquired to upgrade the fidelity of the computer models, and theoretically derived characteristics can be replaced with empirical results.

### 3.2.3 Level 2 Definition

The second level of testing verifies that the system can perform mission tasks in an end-to-end simulation. For a sensor system this means a test scenario presented to the sensor and object track data exiting the data processing computer. These tests require a test facility which can accommodate the sensor and data processors and can provide a high-fidelity simulation of specific mission functions. For example, this might be a faint high-fidelity plume target moving against a complex background for initial acquisition. A second mission task might be the discrimination of objects to identify targets and decoys. The test requirement is then for multiple targets with accurate signatures in close proximity for closely spaced object (CSO) discrimination. This second level of testing primarily supports DT&E. However, it is becoming of greater relevance to OT&E analysts as it can also provide real hardware data inputs to the modeling activities.

### 3.2.4 Level 3 Definition

The third level of testing exercises the system over a full mission profile and includes simulations of the complete surveillance platform or the seeker vehicle. The complexity of these mission profile tests has significant value for DT&E testers, but is now entering the domain of OT&E. As already noted for space systems, it is extremely expensive to field space system hardware and then provide the required targets for observation by the system. In the case of significant military missions, it is impractical to launch enough targets to provide the desired threat density. A significant cost savings can be realized if the space system hardware can be tested in ground

simulation facilities against very complex realistic scenes. However, such testing has not been possible in the past because of the limitations of providing adequate mission simulations in ground test facilities. AEDC has developed an infrared (IR) laser writing scene projection test facility which plays a key role in providing the additional ground test capability required for mission simulation. The test technique will be described in some detail beginning in Section 4.7.

### 3.2.5 Level 4 Definition

The final level of testing has its primary emphasis on OT&E issues. This level requires extending the full mission ground tests to provide operational assessment testing for multiple surveillance platforms or seeker interceptors. In these tests AEDC would be networked to an operations center or battle management control center where personnel can communicate and receive data from the ground-based test facility. The test facility would have operational hardware (prototype or flight qualified) simulating surveillance platforms on orbit. This level of capability then permits integrating a program such as a surveillance system with other elements of the Theater Missile Defense (TMD) architecture such as ground-based interceptors and battle management elements to better evaluate the operational effectiveness of the surveillance element in larger distributed interactive simulations (DIS). One of the long-range goals of military strategy is to couple the information from surveillance assets such as orbiting surveillance platforms directly to the pilot in the plane. Evaluations of the effectiveness of such an approach can be made with ground simulations of the surveillance asset coupled to pilots in ground simulation aircraft.

## 4.0 EXISTING AEDC SENSOR TEST FACILITIES

The simulations and environments required for testing space systems are very complex. As noted in the introduction, there is no single test facility which can meet all the test needs. The test methodology requires several test assets. The test assets which have been developed and are being constructed at AEDC are listed in Fig. 4. They consist of the DECADE facility, the Focal Plane Characterization Chamber (FPCC), the 7V sensor characterization test chamber, the 10V sensor mission issue test chamber, the Focal Plane Array Test Chamber (FPATC), and the Advanced Sensor Test Capability (ASTC), the latter being an extension and integration of all the test assets. Each test asset is focused for a particular level of testing. Since AEDC's prime charter has been to assist in the DT&E of space systems, the current chambers focus support on Level 1 and Level 2 testing. The objective of the long-range test asset development program is to extend the DT&E test capability to support Level 3 and Level 4 testing. As is noted by the diamonds in Fig. 4, there is some degree of overlap in the capabilities of each test chamber. In the case of the 10V and the FPATC test chamber, they can already provide a limited amount of Level 3 testing. Each of these facilities will be described further in the following paragraphs. These descriptions will be followed by our proposed plan to extend these test assets to support full Level 3 and Level 4 testing. There

are several other items of note in Fig. 4. First is the fact that information is designed to flow from each test level to the next test level, building on well-understood results. Tests which rely on relative data without reference to standards should be avoided, since these data are useless outside of the specific test environment. As noted previously, in the overall test program the emphasis should slowly shift from DT&E to OT&E in an integrated manner (Ref. 2). Modeling and simulation can and should play an important role in planning the tests and evaluating test results. As noted in this figure, there should be a symbiotic relationship where the models help direct the tests and the test results in turn enhance the model's fidelity.

The final note of importance is that the test facilities to support the Level 3 and Level 4 test capability do not yet fully exist. As will be noted later in this document, the AEDC technology program is focused on extending the FPATC technology, thus providing the closed-loop Level 3 testing. An extension of these AEDC test facilities networked to other testbeds can then provide the human-in-the-loop type of test capabilities required for Level 4 testing.

## 4.1 DECADE X-RAY SIMULATION FACILITY

The DECADE X-ray Simulation Facility, shown in Fig. 5, is being built by the Defense Nuclear Agency (DNA) and sited at AEDC to verify that critical DoD systems can perform their missions in harsh radiation environements. The name DECADE arose from the goal of an order of magnitude increase in the dose exposure area product that is attainable at existing DoD facilities. At present, the large area bremsstrahlung mode planned for IOC will have an exposure area of 1 $m^2$ and a dose of greater than 10 kRad (Si). Planned Product Performance Improvements will include reduced endpoint voltage, reduced pulsewidth, multiple pulses, a small area bremsstrahlung mode, and a plasma radiation source capability that will include Al and Ar radiation lines. DECADE will be the only DoD above-ground X-ray simulator capable of testing entire large-area operating electronic ensembles such as satellite surveillance, communication, and missile navigation subsystems. The primary purpose of this premier test facility is to provide a user-friendly systems developer test capability; however, the simulator may also be used to develop and advance technologies for X-ray simulators. The simulator will produce 30–40 TW of power for a period of 40–50 nsec. The energy required to produce the X-rays is stored in the Marx capacitor banks at the rear of the simulator. The Marx banks are discharged through closing switches, pulse forming lines, magnetically insulated transmission lines (MITL), and a plasma opening switch. When the plasma opening switch is activated, the resulting energy pulse is derived from the energy being released to the diode source plate through the downstream MITL. The diode converts the electrical energy to X-rays through the bremsstrahlung process. These X-rays expose the test article, which is located in a vacuum chamber or ambient conditions. Test articles up to 1.5 m in diameter by 2 m in length can be accommodated in the vacuum chamber; larger test articles may be tested at ambient conditions. The facility is designed with a number of user-oriented features such as 1,000 $ft^2$ of user

data acquisition needs, dedicated test setup area, user shop, and classified testing capability, along with data analysis and storage capabilities.

## 4.2 MARK I OAR TEST CAPABILITY

One chamber which is not listed in Fig. 4 is the Mark I chamber. It is used for a variety of tests of large spacecraft assemblies. These have ranged from fairing separation tests, through firing of separation rocket motors, to thermal balance tests of a complete satellite. Mark I offers a unique capability in the context of sensor testing where it is suited for conducting tests to measure the off-axis rejection (OAR) characteristics of the telescope and sunshields of sensor systems as indicated in Fig. 6. The Mark I chamber is 42 ft in diameter and 82 ft high. In the OAR configuration the Mark I OAR system has a 50-cm-diam collimating mirror and provides a maximum off-axis beam irradiance over the sensor entrance aperture of approximately 0.001 W/cm$^2$. A gimballed sensor mount allows pitch, yaw, and roll movement so the OAR can be measured from a near on-axis to an off-axis angle approximately 35 deg from the line of sight of the sensor.

## 4.3 FOCAL PLANE CHARACTERIZATION CHAMBER (FPCC)

The Focal Plane Characterization Chamber (FPCC) shown in Fig. 7 is a state-of-the-art radiometric calibration and characterization facility for infrared detector and hybrid focal plane arrays (Ref. 4). Certain features inherent in the chamber design and various operational aspects of the facility make the FPCC well suited to test focal plane arrays (FPAs) fabricated for both tactical and strategic applications. The chamber specifications include a pressure of $< 10^{-7}$ torr, a GHe liner temperature of < 25 K, and a minimum background of $10^9$ ph/sec-cm$^2$. Target source temperatures of 200–800 K are provided with background source temperature of 77 to 500 K. The theoretical spot size is 71 μm at 10.6 μm. Test capabilities in the FPCC include flood source calibration, parametric evaluations, in-band spectral measurements, crosstalk, radiometric flash recovery, and target blooming.

There are many unique features of the FPCC. The NIST-traceable target source and FPA are in the same test volume and there is no optical element between the source and FPA in the flood mode. It provides the desired target temperature and uniform FPA illumination with reduced radiometric uncertainty. There is independent background and target radiation control which improves the simulation and test condition capability. There are also multiple test capabilities in a single test installation along with an FPA injection system. This provides a thorough performance evaluation in the FPCC with good economy of operation.

In proximity to the test chamber there is a full complement of electronics to provide bias voltages, clock frequencies, etc. to drive the chips. These electronics can be configured to meet many drive requirements. A 20-channel simultaneous data acquisition system is provided to reduce test time and increase processing flexibility. The data acquisition system is supported by an extensive data analysis capability.

## 4.4 7V CHAMBER

The 7V Chamber, shown in Fig. 8, has been the primary sensor calibration facility at AEDC since 1969. Since its inception, it has supported the functional checkout and calibration of approximately 30 sensors. A recent performance upgrade has made the 7V a state-of-the-art cryo/vacuum facility providing calibration and mission simulation against space backgrounds (Ref. 5). Key features of the facility include high-fidelity scene simulation with precision track accuracy and *in-situ* target monitoring, diffraction limited optical system, NIST-traceable broadband calibration, normalized spectral throughput, and outstanding jitter control. The upgrade has also added a new 50-cm-diam cryogenic collimator, contamination-free vacuum pumping, enlarged 20 K refrigerators, a Class 100 clean room, and a new control room and data acquisition system. A schematic of the 7V Chamber is shown in Fig. 9. The sensor under test is located in the left end of the chamber, the center section houses the optical collimator, and the infrared sources are located in the right-hand end of the chamber. While the focus of the 7V is for calibration and characterization, it can also track single and CSO targets against a space background. One of the single target sources can be operated as a moving target which can grow in size to simulate the conditions of a seeker closing on a threat. The chamber is designed to simulate space background conditions; however, the system can operate at warmer temperatures if this is required for testing Earth-looking sensors. The sensor antechamber is fitted with an isolation valve so that it can be sealed from the main test chamber and brought back to atmospheric conditions, thus providing quick access to the test article, should that be required during a test period.

## 4.5 10V CHAMBER

The 10V Chamber, shown in Fig. 10, is undergoing major refitting to configure it as an infrared test facility to provide a Level 2 test capability. Chamber 10V is located in the same building as the 7V and shares the control room and some of the support infrastructure; however, both chambers can operate simultaneously and independent of each other. The chamber is 10 ft in diameter by 30 ft long. One of the most important components of the 10V is the large isolated seismic mass under the chamber. This is the optical table to which all the internal chamber elements, including the test sensors, are attached via soft vacuum feedthroughs. The vacuum chamber and all the pumping systems are thus isolated from the optical systems. The seismic mass provides the rigidity and the vibration isolation required to maintain a 2-μrad line-of-sight stability while still

permitting scan mirrors and the sluing gimbals of the test sensors to be operational. The chamber is designed for full space background simulation, although the scene projection equipment can provide simulations of plume targets against Earth backgrounds. The 60-cm-diam collimator in the 10V is designed for testing sensors operating at wavelengths ranging from the far IR to sensors with visible focal planes.

## 4.6 TEST CONSTRAINTS OF TRADITIONAL COLLIMATOR TEST CHAMBERS

One of the fundamental requirements for a ground test chamber used to test sensor systems is to simulate the large distance between the sensor and the target. This is accomplished using a collimator in the test chamber. The sensor, therefore, must "look" into this collimator to see the simulated scene. Since the test chambers must be able to provide a wide range of spectral radiances ranging from the visible to the far infrared, the collimators must be all reflective. The state of the art for the field of view of large, reflective collimators which can operate in the cold environment of the test chamber is only a few degrees. Therefore, there is a constraint on the amount of scene which can be simulated at any one time. The typical field of view of a collimator in a test chamber is shown in Fig. 11. As can be seen, if the sensor was simply installed in the chamber and allowed to operate with its normal scan pattern, it would only "see" a target and scene when its field of view passed through the small collimator field of view. Although the collimator field of view is large enough to conduct tests to assure that the sensor can accomplish specific mission tasks within the timeline such as acquisition of dim targets against the background or resolution of closely spaced objects or hand-over, it is limited in providing a sufficiently large scene to have the system conduct a complete mission. This limitation is even more obvious if, in order to test an SWIR-to-MWIR handover task, two sensors must be installed in the test chamber and simultaneously look into the collimator to see the same scene. The full sensor test constraints affect the ability to perform some aspects of Level 2 testing in the 7V and 10V Chambers, where the high-fidelity targets and scenes are presented to the sensor through the telescope. However, with the development of the scanning IR laser capability, this physical test constraint is relieved, since the scene is projected directly onto the focal plane.

## 4.7 FOCAL PLANE ARRAY TEST CHAMBER (FPATC)

In 1991, the technology development to provide an infrared scene projection capability based on scanning IR lasers was initiated at AEDC. The proof-of-principle system was designated the Transportable Direct Write Scene Generator (TDWSG) and was successfully demonstrated in 1992 (Ref. 6). The follow-on scene generation test capability, called the Focal Plane Array Test Chamber (FPATC), was completed at the end of FY94 (Ref. 7).

In the Focal Plane Array Test Chamber (FPATC), the optical properties of the sensor telescope and the motions of the gimbal systems are incorporated in the laser writing system (Fig. 12), and the scenes are written directly on the focal plane of the sensor. Relieved of the physical constraints of the collimator/telescope interface (Fig. 13), a full mission profile for any type of scanning or staring sensor can be simulated. In this facility the complex backgrounds, the target sizes, radiances, and motions as influenced by the optical properties of the telescope, the optical transfer function (OTF), is reproduced within the content of the mission scenes. The OTF can be obtained in two ways. The first is to develop a theoretical OTF from the telescope design using an optical design tool such as Code V®. However, in the real-world there are aberrations caused by manufacturing and alignment errors which influence the final OTF. One of the technology tasks has been to develop a realistic OTF prediction method for a sensor telescope from the optical design. A more detailed report on the effort is contained in Appendix A. The second method of obtaining the OTF is to measure it from the as-built telescope. A second part of the technology program has focused on defining the approach to measuring the OTF of telescopes. Further information on this effort is contained in Appendix B.

The FPATC system consists of a cryogenic test cell which houses the focal plane array from a sensor. Several sizes of cryogenic test cells can be used. The one shown in Fig. 14 can accommodate scanning focal plane arrays which are up to 24 in. long. Small test dewars are used to support testing focal planes up to 2 in. square.

The test cell is fitted with an optical window and a cryogenic laser line filter so that the laser equipment can be operated under ambient conditions, but the focal plane can still be maintained at cryogenic conditions with low background radiation. The laser beams (0.514, 1.06, 5.4, and 10.6 μm) are modulated and scanned by acousto-optic cells which are driven in turn by high-speed radio frequency (RF) drivers modulated to carry the scene content. The modulated and the step-scanned laser beams are focused on the focal plane so they can paint the radiation on each pixel of the array. The laser writer is synchronized to the clocking frequency of the array such that each frame of the scene is painted during each focal plane integration period. As presently built, the FPATC can paint radiances onto the FPA for a mission scenario composed of a precalculated and stored set of scene frames. These scene frames are precalculated and stored in a 3-Gb disk farm. The mission scenario times which can be supported by the present equipment are a function of the size and number of focal planes in the test article. For a 256 × 256 focal plane, the present disk storage system can provide up to 10 min of mission scenario. These scenes can include hundreds of objects consisting of targets and decoys all moving against a complex background. This type of test scenario permits the evaluation of the capabilities of the time-dependent processor (TDP) and object-dependent processor (ODP) to extract information from the complex background structure and establish track files. More details on the construction and operation of the FPATC can be found in Refs. 6 and 7. The laser writing system in its present configuration is designed for open-loop operation, and does not provide for any real-time scene manipulation.

# 5.0 TRANSITION FROM LEVEL 2 TO LEVEL 3 TEST CAPABILITY

As noted in Fig. 4, the FPATC can be enhanced to provide Level 3 test capability. The following sections describe the current mode of operation and identify the areas which would be enhanced.

## 5.1 CURRENT MODE OF OPERATION FOR FPATC

The FPATC was designed to provide a Level 2 test capability. In this operating mode, the test scenario is determined prior to the test, and the images are precalculated and stored on a large disk farm. Since the scenario is prescripted, the OTF can be convolved into these scene data. The individual frames are played back in sync with the framing rate of the focal plane. As shown in Fig. 15, the radiance data undergo blackbody calibration processing and direct write scene generator processing before being projected via laser beams onto the focal plane array. On a surveillance satellite, the platform manager or the tracking data processor requires two pieces of information to fulfill its mission of detecting targets and providing target location and track handover information. One is the data from the focal plane for each frame, and the other is the line-of-sight pointing vector for each frame. These two pieces of data are used by the processors to establish target track files. The platform manager is supplied with a line-of-sight (LOS) pointing vector from the disk farm, along with each frame of the scene which is written onto the FPA. This method of testing uses a scripted scenario and provides a sequential set of scene frames with complex background and targets to test the performance of the time-dependent and object-dependent processors. The sensor's ability to extract the targets from the backgrounds and to form accurate track files can then be compared to the well-known background and target inputs.

## 5.2 ENHANCED MODE OF OPERATION OF FPATC

The Level 3 test capability is an extension of the existing Level 2 and thus builds upon the in-place test resources at AEDC. Figure 16 shows how the basic FPATC architecture is supplemented for use in a closed-loop test mode. This first change from the current mode of operation (Fig. 15) is in the way the scenes are generated and stored. The closed-loop test approach is also based on a prescripted database but, unlike the present operation of precalculated frames of data, this data set consists of the global irradiance map of the complete scenario. The irradiance map is separated into two components, the background irradiance and the target irradiances. For example, the background irradiance map for a surveillance system can be generated using the Strategic Scene Generation Model (SSGM) and is specific for a particular set of weather conditions (clouds, atmospheric water content, temperature, etc.) and for a particular satellite orbit and sun orientation. The target irradiance maps which are generated for the scenario are stored as differences between the background irradiance and the target irradiance as seen against the background and through the atmosphere. Thus, if a specific dim target obscures a bright background at some part of its trajectory, the irradiance value for that target could possibly be a negative value. When added to the background value, the net irradiance would be correct, i.e., target only and no background. One of

the technology efforts is focused on developing these scenario databases for a range of sensor missions using both SSGM and synthetic scene generation techniques. More details on this work are contained in Appendix C. As noted, the targets and their tracks which are chosen for a particular test scenario are generated separately. Since the target track databases are much smaller than the backgrounds, they can be changed quickly and thus provide the capability of performing sets of tests for a wide variety of mission scenarios (i.e., different target signatures, different numbers of targets, different target launch and impact points, etc.). The most obvious addition to the enhanced FPATC architecture as shown in Fig. 16 is the inclusion of a series of emulators. The hardware under test (the FPA, the data processors, and the platform manager) is coupled to the emulators which provide the simulation conditions that cannot be duplicated in a ground test facility. These include such things as the platform motions in the reduced-gravity environment or the live firings of the attitude control motors. These emulators provide the feedback information needed to simulate the operation of a complete satellite system. An example of the emulators' operation perhaps best illustrates their use. If the platform manager commands the sensor gimbals to slew to the line of sight, the entire platform's attitude will be disturbed when the sensor moves under the reduced-gravity conditions. The Inertial Measurement Unit (IMU) senses this platform tilt and relays the information to the platform manager. In turn, the platform manager might command the attitude control inertial wheels to speed up to offset this disturbance. The net result would be a pointing vector that would be a composite of all these movements and, as with any coupled system, would have oscillations and damping factors associated with the motion. One of the technology tasks initiated in FY94 starts to define the requirements for these emulators. A summary of the results of this effort is included in Appendix D.

As noted in Fig. 16, the net pointing vectors determine the particular set of data which must be taken from the database and projected onto the focal plane. Since the satellite orientation might also be affected by an induced roll, one of the requirements is that the FPATC now provide a real-time capability to translate and rotate the content of the scene to be included in each frame.

A second implication of this unpredictable line-of-sight selection is that the effects of the optical telescope cannot be precalculated and included in the stored database. These effects must be added to each particular frame of data as it is extracted from the database. Therefore, an additional real-time operation on the scene data frame must be to add the OTF. Significant progress has been made in developing the concepts and the algorithms required to perform these two operations. A more detailed summary of the work accomplished to date is included in Appendix E. Details on the methodology and status of enhancing the existing FPATC signal processing hardware and software are described further in Appendix F.

Guiding the work in developing scene generation techniques, manipulating lines of sight, generating OTFs, and constructing emulators is a fundamental study of the characteristics of present and future sensor systems and the anticipated mission requirements. This study results in

the definition of the driving parameters in both the development of the ground test equipment and the operational algorithms. Line-of-sight pointing accuracy, target resolution, spectral characteristics of targets and backgrounds, dynamic ranges of radiance within scenes, etc., must all be considered. One of the FY94 technology tasks concentrated on accumulating these data to support the ongoing developmental effort. More details of these requirements for surveillance systems are contained in Appendix G.

## 6.0 IMPLEMENTATION OF LEVEL 3 TESTING

Figure 17 introduces the fundamental ideas for the Level 3 OT&E approach. When engineers plan for a ground test of a sensor system, the onboard program manager and the data processors become part of the ground test hardware while the remaining subsystems on the platform are represented by emulators operating in real time. Early in the acquisition process, the testing can be conducted with prototype hardware and breadboarded processors. Later in the program, the hardware can be upgraded to flight-qualifiable test items. As illustrated in Fig. 17, several different spectral wavebands can be tested per sensor suite. Using the FPATC, multiple focal planes are stimulated with multiple laser writers. Each laser writer is driven by the appropriate scene calculated using the bandpass of the particular focal plane. These scenes can be representative of multiple sensors or of single sensors with multiple focal planes. While not shown, it is quite possible to include visible systems along with the infrared sensors.

With this interactive architecture, both commanded and autonomous operation of the platform/sensor combination can be tested for pointing, acquiring, and tracking of multiple target sets against a variety of background clutter conditions. At this level of testing, real-world operational assessment issues can be explored for the evaluation of system performance. Foremost is the autonomous operation of the platform under a well-controlled test environment, i.e., a scripted scenario database. Unlike on-orbit testing, operational hardware and software can be tested with controlled backgrounds and target complexity. Boundaries of the operational envelope can be explored beyond that specified in the original design. Level 3 testing assures that the hardware and software performance is adequately tested as an integrated surveillance system.

## 7.0 DEVELOPMENT OF A LEVEL 3 TEST CAPABILITY

Two Proof-of-Principle (PoP) demonstrations are planned to be conducted in the process of establishing a Level 3 capability. The implementation roadmap for Level 3 is shown in Fig. 18. Figure 19 identifies the estimated costs of the PoP demonstrations for the FPATC operating with a closed-loop, Level 3 capability. The modified hardware and software developed under the PoP programs will be capable of providing a level of closed-loop testing which can support some early operational assessments for programs in the FY97/98 timeframe. The PoP programs will

use existing FPATC hardware with minimal modifications in order to reduce costs. The FY94 and FY95 investment for PoP 1 is provided from AEDC technology tasks. Since there are other space test requirements, this level of effort will be reduced in the outyears. The estimated AEDC investments and the anticipated shortfalls are noted for FYs 96 and 97. As is noted, the PoP demonstrations are followed by an investment of $3 million to underwrite the design and construction of the parallel processor boards in the FPATC. These boards will permit operation at frame rates appropriate for advanced sensor systems. This funding will also produce a prototype laser drive system. A following investment of $5 million will extend the prototype system to handle multiple focal planes of a satellite platform and include the development of prototype emulators to provide an early operational capability. Another $5 million investment in FY00 will provide the expansion of the hardware required to provide a full operational capability to support Level 3-type testing for advanced surveillance and seeker systems. The present plans are to develop this capability within the existing buildings at AEDC. The following sections describe the objectives of the PoP demonstrations.

## 7.1 PROOF-OF-PRINCIPLE TO DEMONSTRATE REAL-TIME SCENE MANIPULATION

One of the bottlenecks in handling the amount of data for the interactive scenes is the transmission between computational nodes. Therefore, the approach being considered for the implementation of this enhanced capability is to transition to parallel processing, locating these processors within the FPATC electronic drive system. This approach involves developing fast algorithms which are matched to the FPATC processors. The new architecture will provide onboard scene translations and rotations, as well as the optical convolutions and the laser and RF calibrations. PoP 1 combines the algorithms developed to manipulate the scenes with the parallel processing hardware, and transmits the resulting scene to the laser writer. Details of the technology task to build the PoP demonstration hardware are contained in Appendix F. The real-time LOS input for this demonstration will be a manual joystick which can be operated to change the pointing vector and the rotation for each focal plane frame.

## 7.2 PROOF-OF-PRINCIPLE TO DEMONSTRATE INTERACTIVE EMULATORS

The second PoP (PoP 2) couples emulators to the FPATC to provide the feedback loop to the laser writer. In this demonstration, these emulators will perform the I-O functions, but will not be high-fidelity emulators of a specific system. For example, the platform will be a rigid body 6-DOF emulator. It will not have the bending modes and resonant vibrations of a contractor design. However, it will permit parametric studies in that bending modes and vibrations can be incorporated as a jitter imposed on the scene being written by the laser. The later implementation of Level 4 closed-loop testing will incorporate the more detailed emulators.

## 8.0 IMPLEMENTATION OF LEVEL 4 TESTING

Level 4 brings the surveillance platform (already tested and with defined performance) into the larger battle management, command, control and communication ($BMC^3$) architecture. Studies have indicated that given the predicted message traffic and data rates between the platform and the element operational command center, the AEDC could be connected with a T1 link to the $BMC^3$ remotely located (Ref. 8).

The principal benefit of the Level 4 test methodology is that "interaction" between the surveillance platform and the command center can be established. The primary emphasis of Level 4 testing is placed on operational issues which include the functions of a ground-based operational center communicating with the surveillance satellites on orbit, controlling their operation and interpreting the returned data. Figure 20 is an illustration of satellites in orbit communicating with a ground control station. An operational ground test facility which could provide multiple Level 3 test chambers would simulate these satellites using virtual satellites operating in ground test chambers.

The proposed configuration for a Level 4 test links an operational center to the test bed at AEDC. Multiple platforms which were tested at Level 3 are now configured in a surveillance sensor suite and are connected to the command and control element by a high-speed data link. With a Level 4 test configuration, the higher-level integration issues are addressed: interoperability of the element subsystems, tasking response, human-in-control (HIC), effects of data latency, etc. One of the principal benefits of the Level 4 test methodology is that "interaction" between the surveillance platform and the command center can be established. Advanced test issues can be addressed such as interfacing a surveillance element to the larger overall battle simulations as envisioned in the Distributed Interactive Simulation (DIS).

## 9.0 NETWORK INTERFACES

Linking test beds has been underway for testing tactical systems. An excellent review of the digital communications technology used to integrate intra- and inter-range information transmission is given in Ref. 8. The article discusses how conventional links can be used to connect such test ranges as the Air Force Flight Test Center and the Naval Air Warfare Center-Weapons Division. The authors project that in the future, Synchronous Optical Network (SONET) standards with 100 Mb/sec (Mbps) bandwidth will be available for T&E. Reference 9 discusses the future issues (protocols, bandwidth, management, and cultures) associated with tying LANs together.

A block diagram showing a feasible "breakout" of a surveillance element into a geographically distributed test bed is shown in Fig. 21. This example links the proposed Level 3 AEDC test bed to the Integrated System Test Capability (ISTC) test bed located at an Army test site in Huntsville. The ISTC test bed is designed to evaluate the operation of prototype computer

hardware and software in an interactive mission scenario. It includes ground-based $BMC^3$ elements, ground-based radars, and defense interceptors. All element or system level testing conducted on the ISTC can be conducted as before, but would now include surveillance elements simulated at AEDC.

## 9.1 LINKING AEDC TO ISTC WITH THE DSI TECHNOLOGY

A recent white paper (Ref. 10) addresses the use of the DIS technology for connecting geographically distributed ISTC simulation nodes or hardware test facilities. ISTC already conforms to DIS protocol. The DIS employs standard interfaces at each node called protocol data units (PDU). The PDUs are the "language" of the DIS and represent the key to the interoperability of simulations and test beds not originally designed to be interfaced. PDUs provide information on entity states, entity interactions, test control, and environment conditions. The white paper study concludes that the DIS could be a feasible solution if an additional PDU needed to effect the real-time simulation/emulation of system communications is added to the network architecture.

### 9.1.1 Local and Wide Area Networks

One means of implementing the Level 4 test capability network is to employ commercial networks for the wide area network coupled with local area networks already in place at most defense facilities. A review of the network technology will show that this option is a feasible approach.

In creating Local Area Networks (LANs), Wide Area Networks (WANs), LAN-to-LAN connections, and LAN-to-WAN-to-LAN connections, there are several options available in today's technology. The choice of distributed systems architecture options is a function of distance, bandwidth required, security required, error tolerance, and a number of other related factors. A few typical ways in which these distributed systems may be created and interconnected are discussed in this section. This is a high-level outline of network technology. Exact requirements will require detailed analyses.

### 9.1.2 Bandwidth

The first area for discussion is the bandwidth of the various Wide Area Network connections or WANs. Table 1 lists a range of connectivity options as a function of bandwidth and location. ATM-type systems are in the 200-Mbps range, while simple modems are on the very low end of the frequency spectrum at 14.4 Kbps. If security is a concern, a simple STU III device is suitable for low data rates up to 9,600 baud and a KG 94A is available for T1 or fractional T1 connections up to 1.544 Mbps. Special encryption and decryption devices must be inserted into the network architecture.

### 9.1.3 Network Links

Figure 22 illustrates the two types of connections discussed in Section 9.1.2, plus a third possibility -- a data connection called packet switching. As indicated in the figure, the use of packet switching requires additional hardware. Not indicated in the figure are the redundant lines which are normally part of the packet-switched network to increase reliability.

## 9.2 LEVEL OF ELEMENT INTEGRATION

The network interfacing discussed in this section represents a *minimum* configuration needed to support element-level and system-level DT&E, Operational Assessments, and OT&E. This baseline network concept can be expanded to include additional hardware such as a suite of sensor hardware, the platform manager, communication hardware, and even operators of prototype terminals associated with the Element Operation Control Test site. It is possible to consider OT&E of the entire surveillance element in a Level 4 test environment using the AEDC ASTC.

# 10.0 DEVELOPMENT OF A LEVEL 4 TEST CAPABILITY

The concept for Level 3 and Level 4 testing requires an enhancement of the FPATC test capability to include a real-time interactive test capability and an interfacing of the complex of test facilities at AEDC with other test centers. At present, the ASTC consists of the test chambers described in this document plus the following elements:

1. Multiple closed-loop laser writers and their associated emulators as developed for Level 3 testing.

2. The computers which will permit interfacing the test chambers to an external network.

3. The transmission links, either via dedicated hard lines or via satellite to a battle management center such as the ISTC or the National Test Facility.

The possibility of including prompt and total dose radiation simulation with the direct write test capability has been considered and appears feasible. The facility for this type of application includes an X-ray simulator along with a radioactive source to provide the gamma ray simulation. Inclusion of the radiation components would require that the test chambers developed for the Level 3 testing be housed in a radiation-shielded environment. Therefore, a request for a building, along with the radiation equipment, has been planned as a long-range military construction project.

## 11.0 CONCLUSION

It is extremely costly, and, in some cases, impractical to provide effective field testing to evaluate operational issues for sensor systems. Even with sufficient systems on-orbit, there are significant problems in providing the threat targets. Not only is the launch of a target missile very expensive, but it is not practical to launch eight or ten missiles simultaneously. Because of the cost of live firings, there is also the reluctance to evaluate the operation of the surveillance system in marginal viewing configurations with the attendant possibility of zero data points.

One of the barriers to providing these levels of operational testing in ground test chambers has also been the limited capability to provide adequate target and threat simulation. The laser writing technology has overcome this barrier. AEDC has been developing test technologies and a test methodology, and is in the process of upgrading test facilities needed to provide a level of simulation which, using system hardware, will permit the evaluation of surveillance and seeker systems in realistic engagements in ground tests. These test beds can be used to perform operational assessments prior to construction and deployment of space-qualified assets.

## REFERENCES

1. Pipes, J. and Dawbarn, R. "Network Plan to Use DT&E Test Facilities at AEDC as a Node to Simulate Surveillance Systems." ITEA 3rd Annual Joint Combat and Weapons Integration T&E Workshop, Sandestin, FL, February 1995.

2. Dawbarn, R., Mattasits, G., and Pipes, J. "Development of Ground Test Facilities at AEDC to Conduct DT&E and OT&E for Space Surveillance Sensors." 15th Aerospace Testing Seminar, Manhattan Beach, CA, October 11–13, 1994.

3. Christensen, L. S. and Whitehead, G. L. "Decade X-ray Effects Test Facility." 15th Aerospace Testing Seminar, Manhattan Beach, CA, October 11–13, 1994.

4. Nicholson, R. A. and Steele, C. A. "AEDC Focal Plane Array Test Capability." AEDC-TR-90–31, January 1991.

5. Simpson, W. R. "The AEDC Aerospace Chamber 7V: An Advanced Test Capability for Infrared Surveillance and Seeker Sensors." 18th Space Simulation Conference, Baltimore, MD, October 31–November 3, 1994.

6. Lowry, H. S., Elrod, P. D., and Layne, T. C. "AEDC's Transportable Direct Write Scene Generator Test Capability." SPIE *Proceedings*, Vol. 1687, 1992.

7. Lowry, H. S., Tripp, D. M., and Elrod, P. D. "Current Status of Direct Write Scene Generation at AEDC." SPIE *Proceedings*, Vol. 2333, 1994, pp. 26 ff.

8. Switzer, E. and Straigley, E. "Digital Communications — Integrating T&E in the 21st Century." *ITEA Journal*, March 1993.

9. Smith, B. and Udell, J. "Linking LANS." *Byte* Magazine, December 1993.

10. McBride, E. "DIS PDU's and ISTC, Distributed System Simulation and TMD UOES System Exerciser." SEIC/MM White Paper, March 1993.

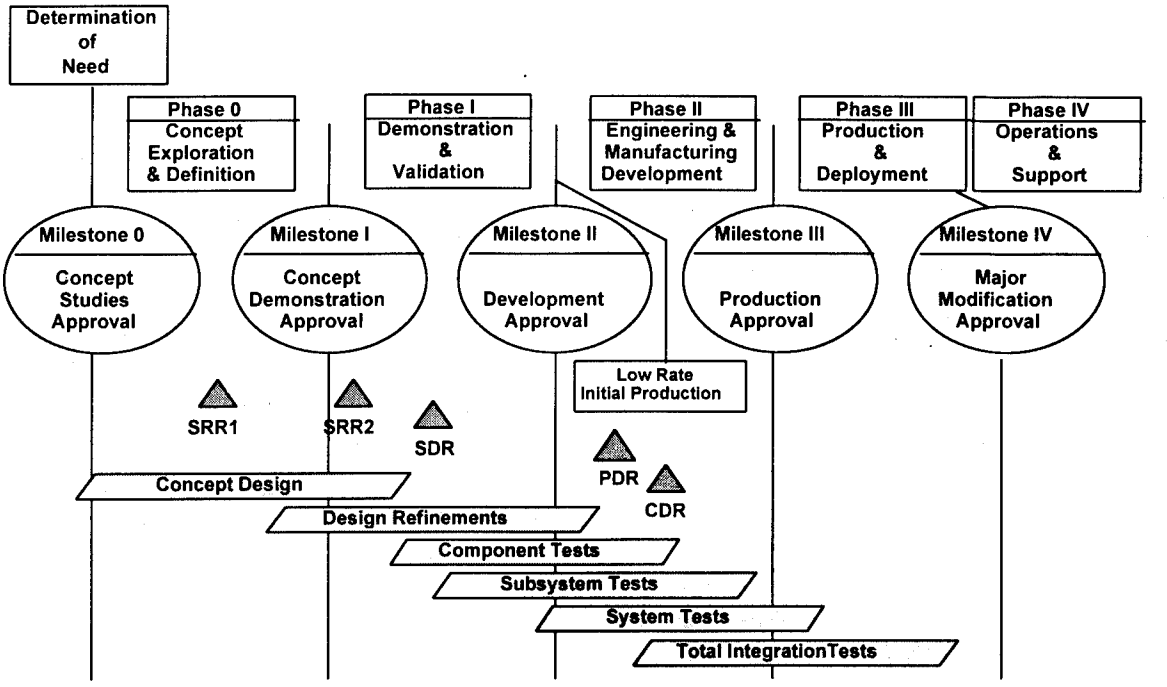


Figure 1. Acquisition and test phases.

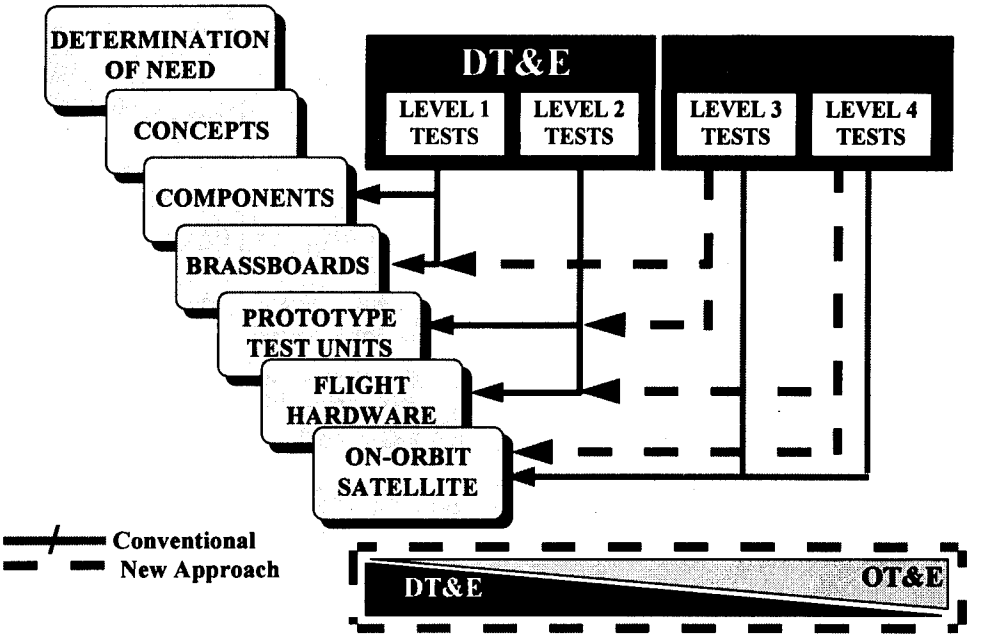


Figure 2. Types of testing.

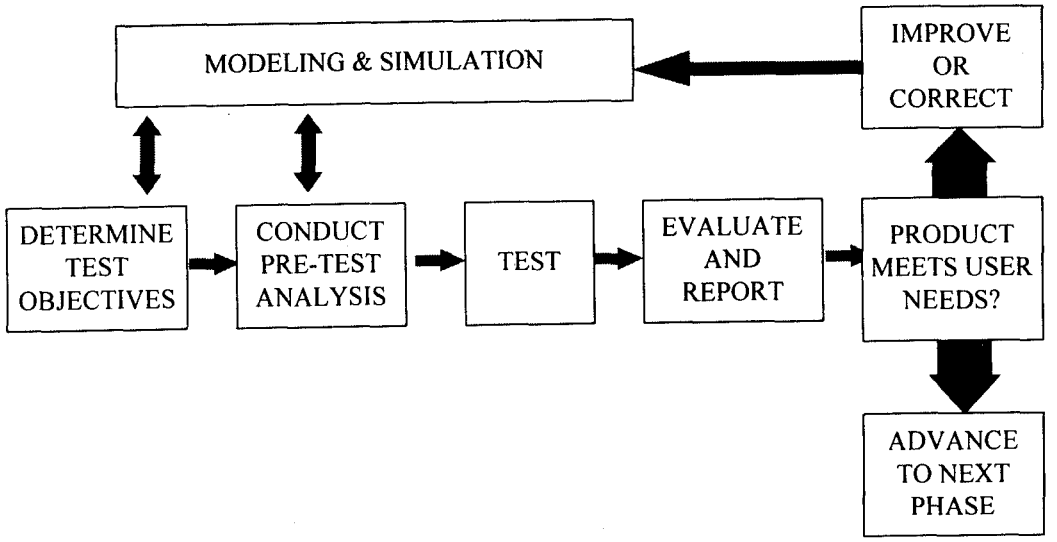


**Figure 3. Test process.**

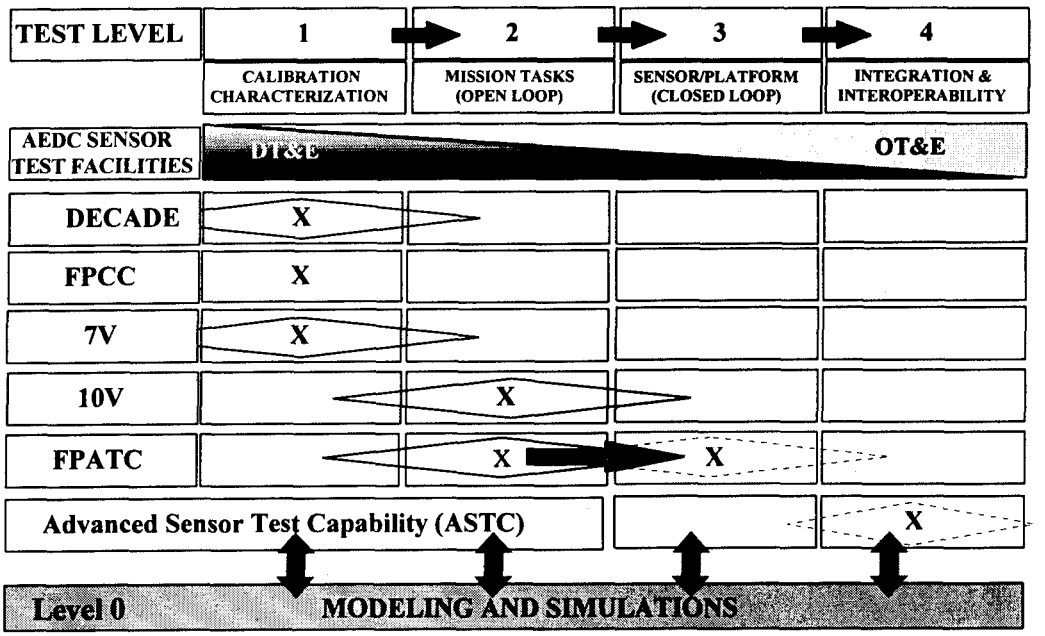


**Figure 4. Test levels.**

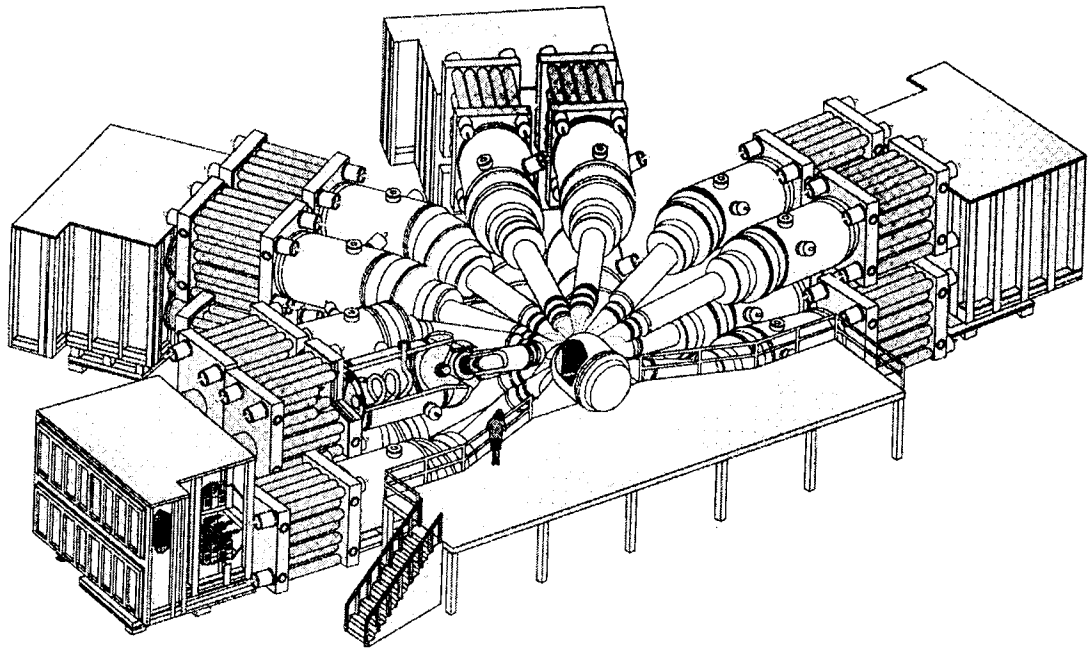

**Figure 5. DECADE X-ray Simulation Facility.**

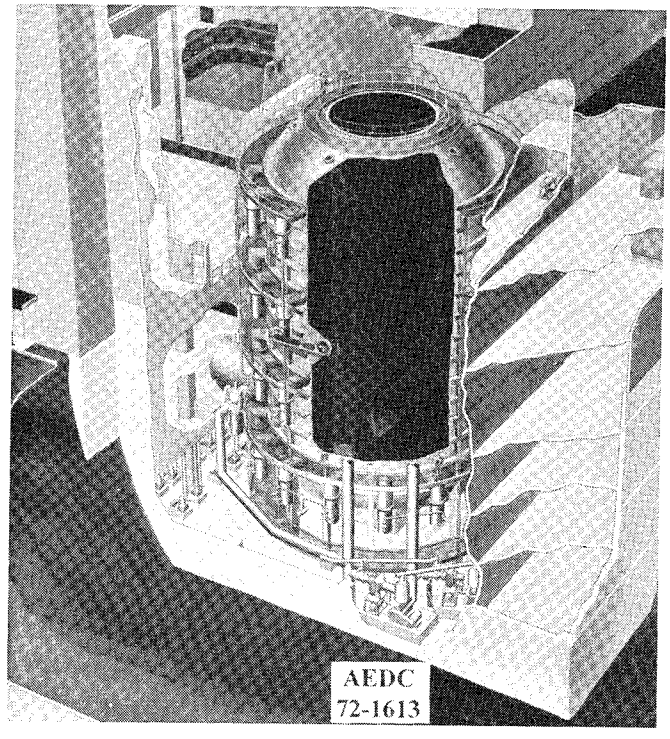


**Figure 6. Mark I Chamber with OAR test installation.**

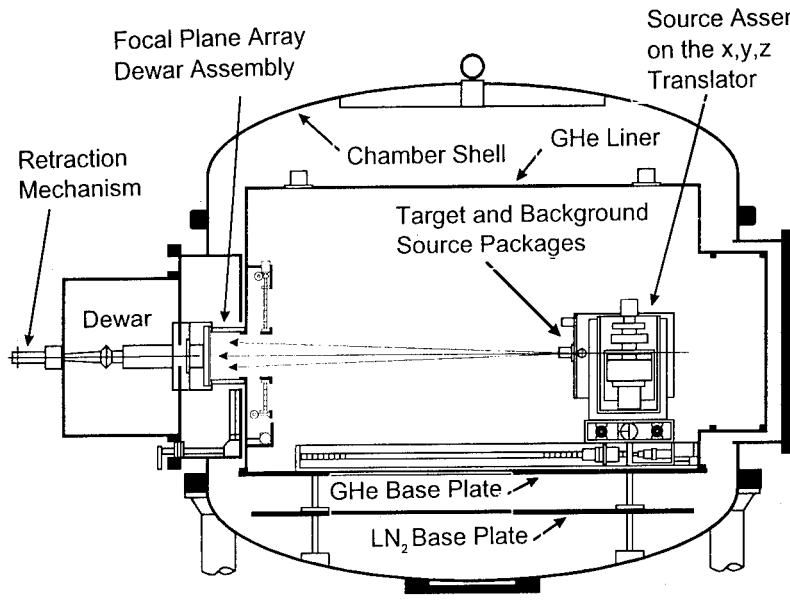


**Figure 7. Focal Plane Characterization Chamber (FPCC).**

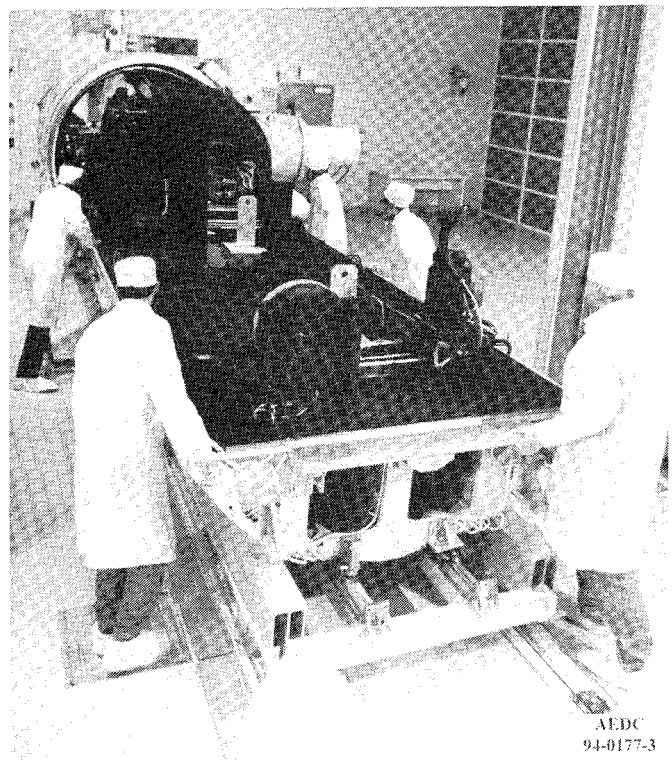


**Figure 8. 7V Chamber optical bench.**

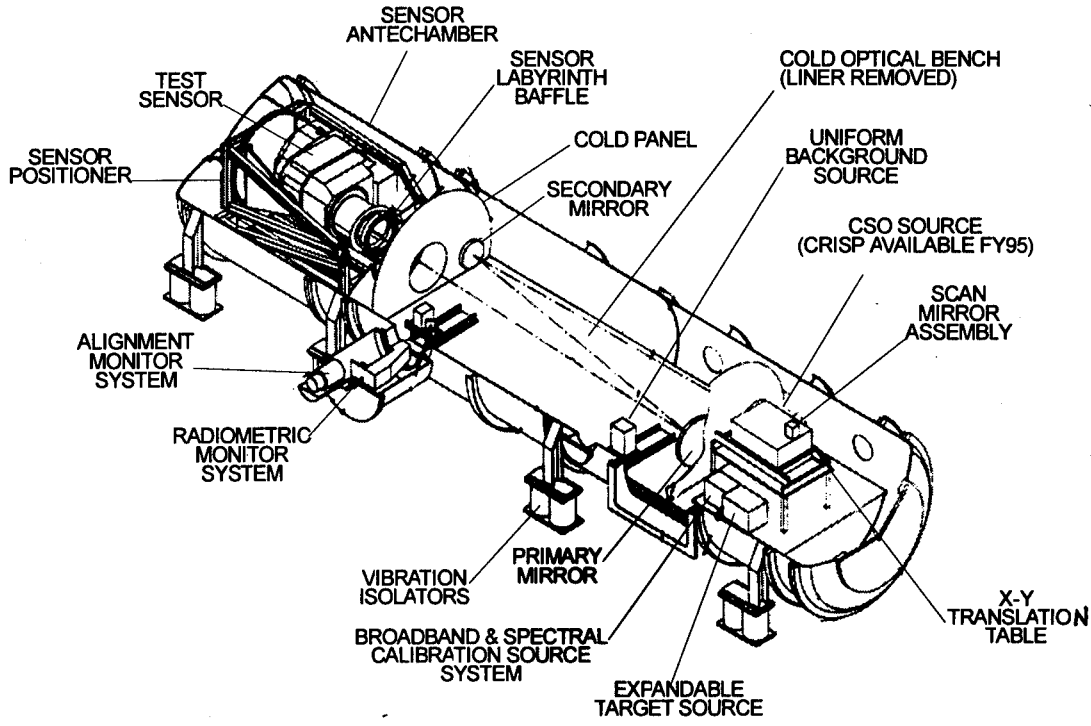


**Figure 9. 7V Chamber schematic.**

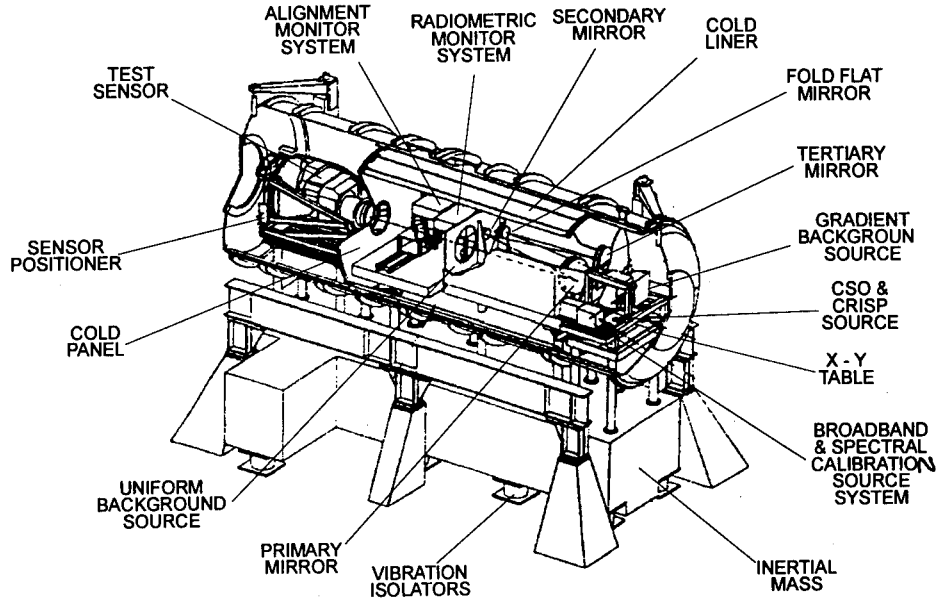


**Figure 10. 10V Chamber schematic.**

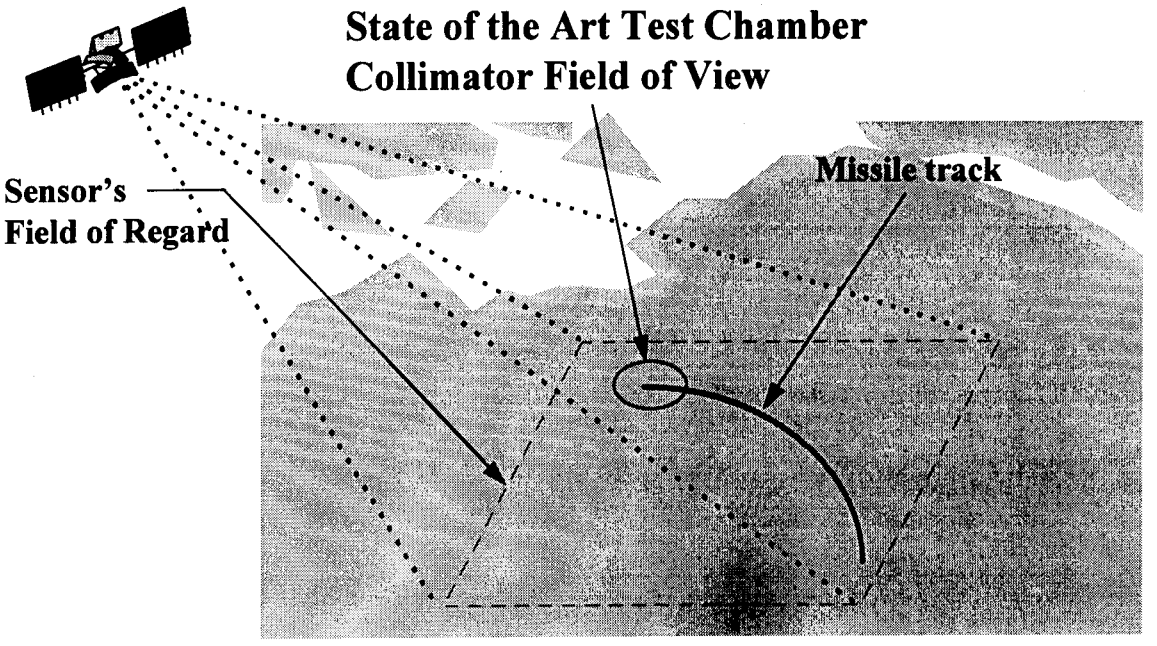


Figure 11. Full sensor test constraints.

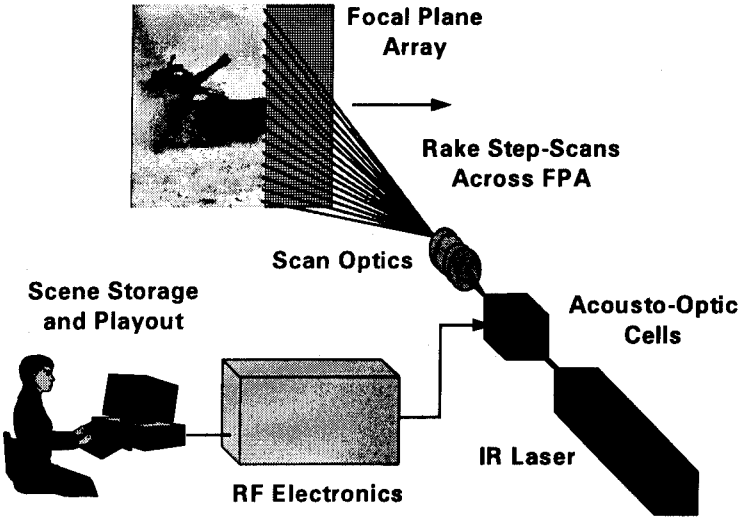


Figure 12. DWSG technique.

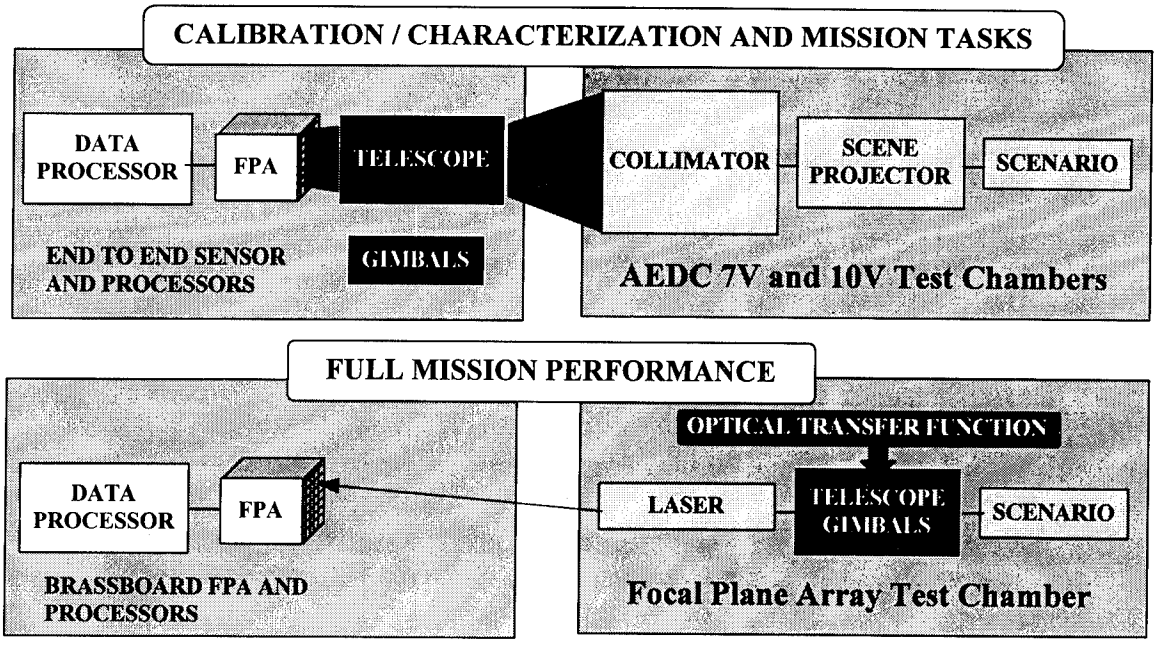


**Figure 13. Full mission performance testing using the FPATC versus testing in the 7V and 10V Chambers.**

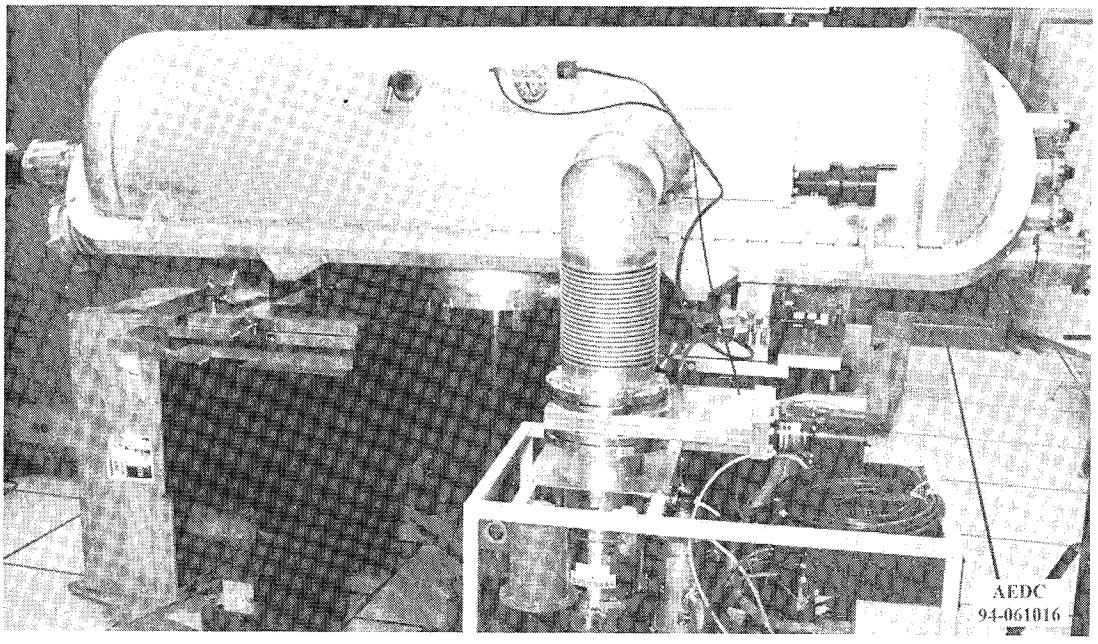


**Figure 14. Focal Plane Array Test Chamber.**

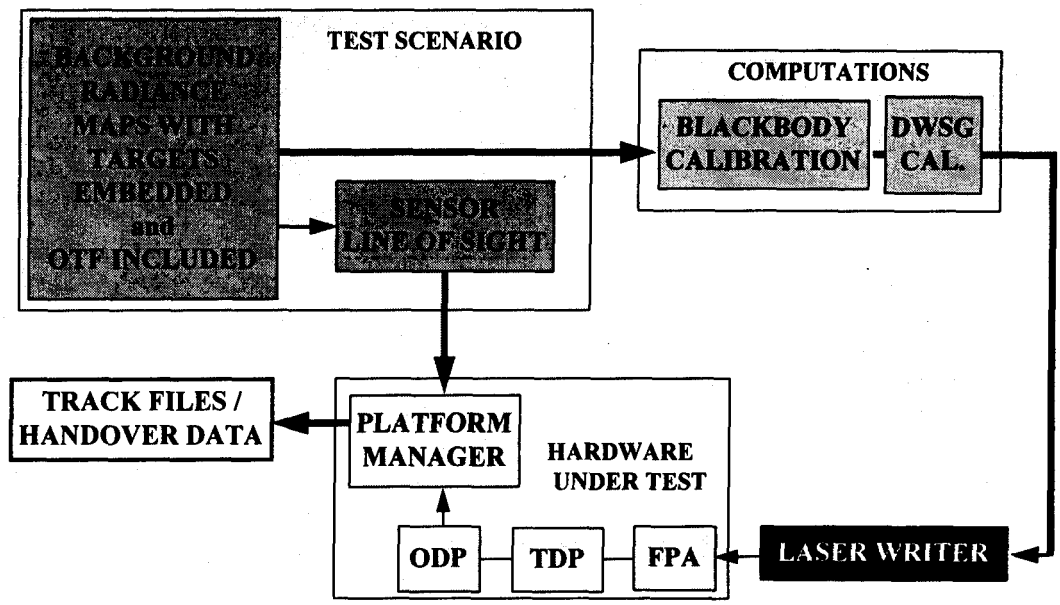


**Figure 15. Open-loop surveillance sensor testing in the FPATC.**

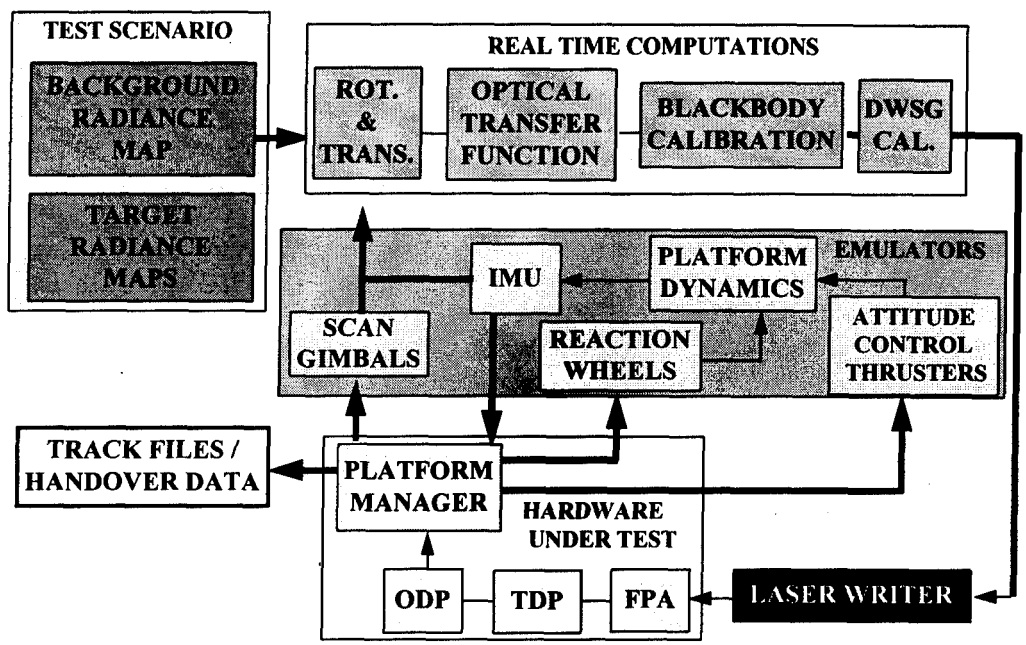


**Figure 16. Closed-loop T&E implemented using FPATC.**

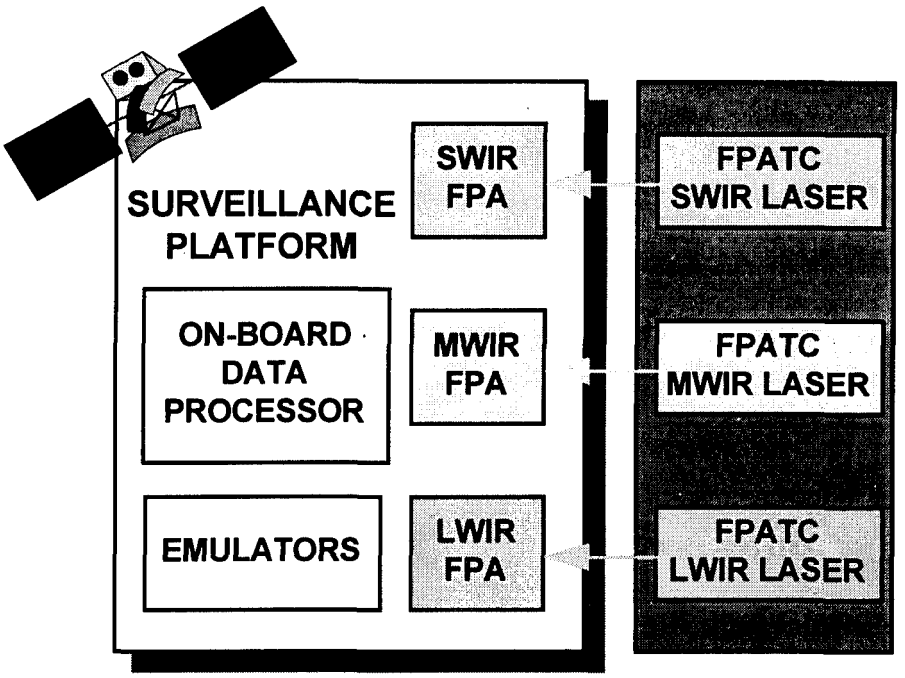


Figure 17. Elements of Level 3 testing.

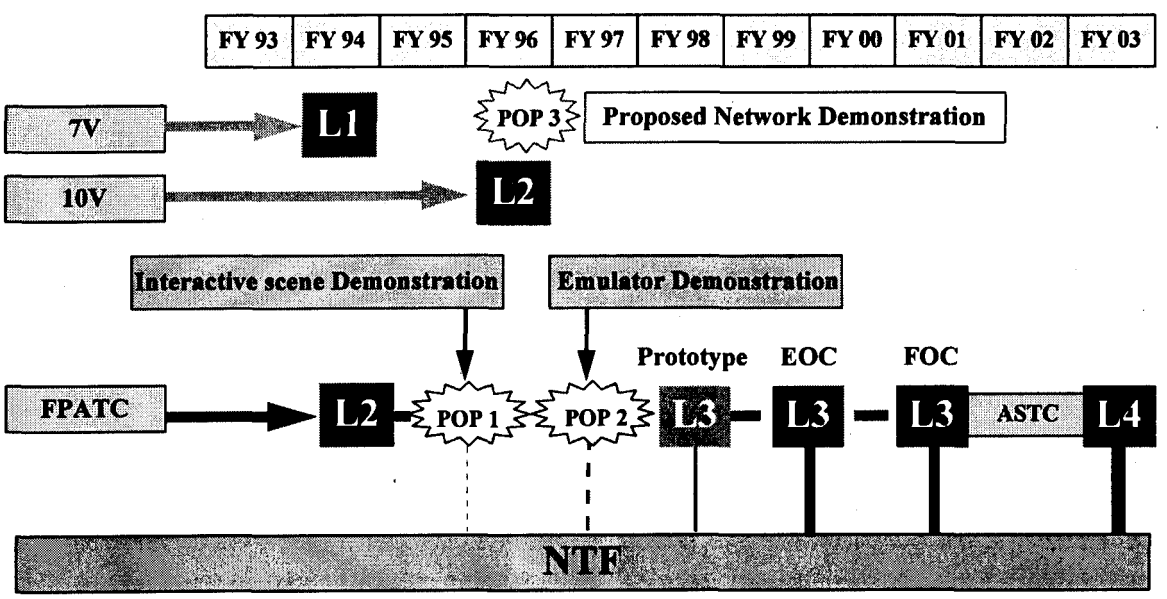


Figure 18. Level 3 development roadmap.

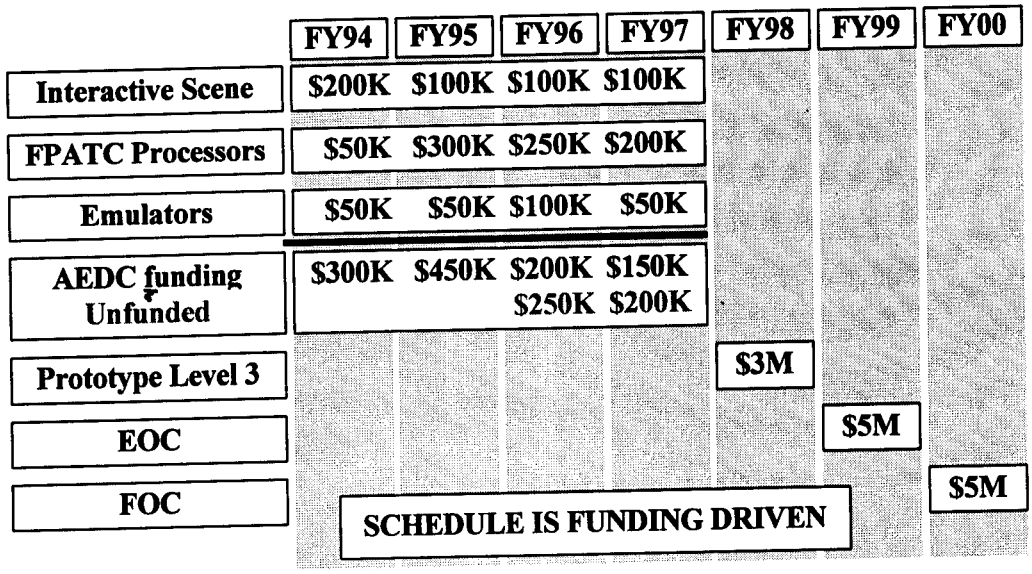


**Figure 19. Funding profile to achieve Level 3 test capability.**

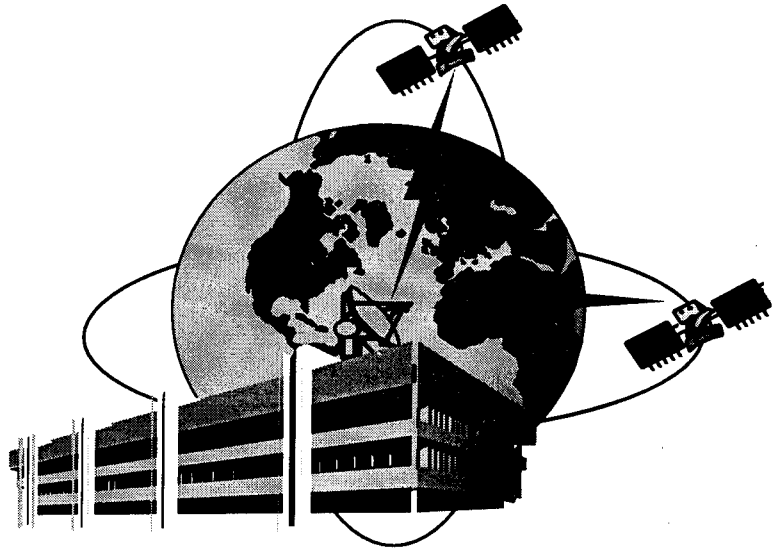

**Figure 20. Level 4 testing.**

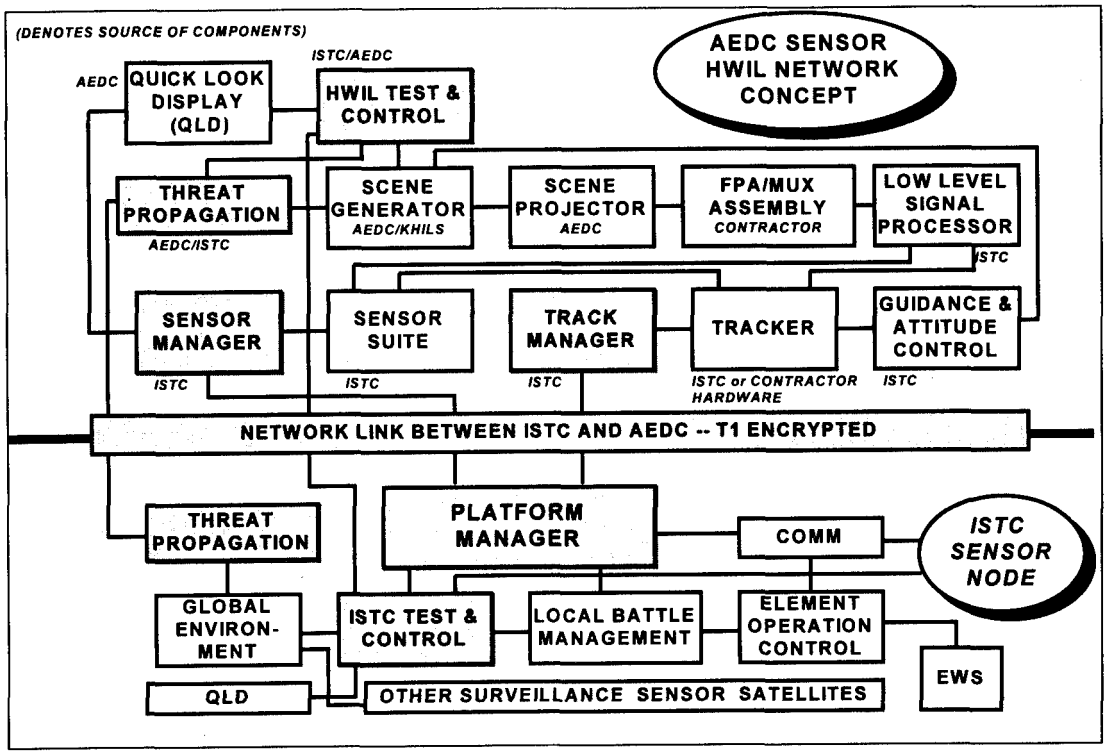


**Figure 21. Network plan for integrating AEDC into ISTC.**

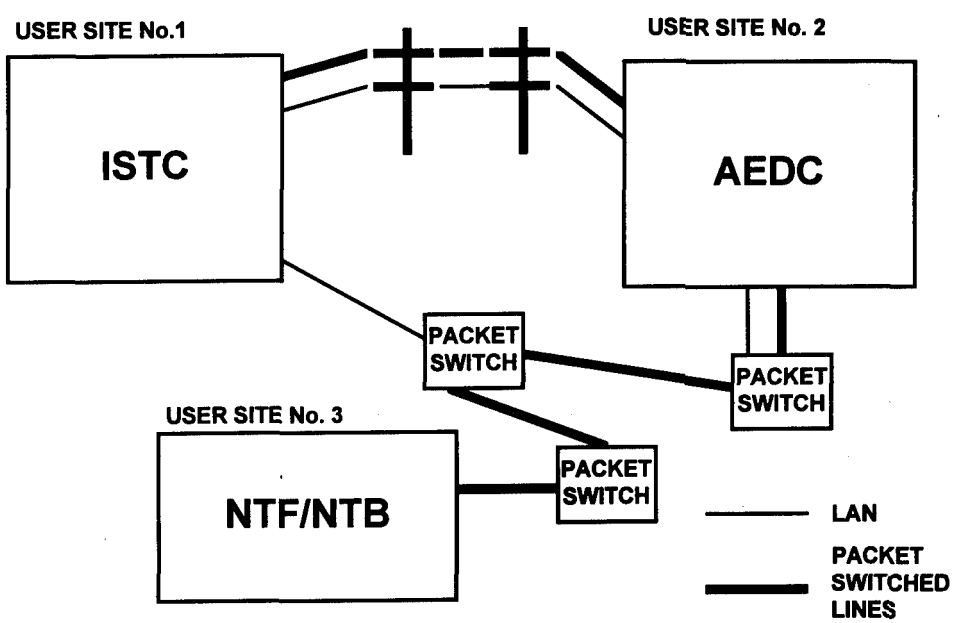


**Figure 22. Architecture for linking test beds**

**Table 1. Typical Network Devices and Baseline Specifications.**

| Line Speed | Sending Network | Long Distance Connectivity | Receiving Network |
|---|---|---|---|
| 200 Mbps | ATM | | |
| 100 Mbps | FDDI | | |
| | | T3 | |
| 20 Mbps | 16-Mbps Token Ring | | 16-Mbps Token Ring |
| | Ethernet | | Ethernet |
| 10 Mbps | | | |
| | | T1 | |
| 1 Mbps | | | |
| 64 Kbps | Basic Rate ISDN: Two 64 Kbps and one 16 Kbps channels. | | |
| | | Switched 56 | |
| 15 Kbps | Voice modem to 14.4-Kbps connection. | | |

## APPENDICES

# APPENDIX A
# OTF FROM THE SYSTEM DESIGN INFORMATION

J. Selman

When optical system performance is numerically simulated and quality is evaluated, no other metric is more widely used than the optical transfer function (OTF) and its absolute magnitude, the modulation transfer function (MTF). Accurate rendition of the system OTF enables the modeler to computationally reproduce the observed structure and energy distribution in the image. The MTF, when presented as spatial frequency curves or surfaces, presents a quantitative display of system quality. OTF calculations have been the subject of many papers and technical books. The reader is referred to standard references such as Goodman (Ref. A-1) and Williams (Ref. A-2) for tutorials on the mathematical techniques involved in OTF calculations. Practical methods of computing the OTF from first principles are presented in a series of technical reports issued in the 1970's by The Aerospace Corporation as development for the original POLYPAGOS optical design software (see Ref. A-3). Two viable methods will be presented for obtaining a realistic OTF from optical design information.

## A1.0 INTRODUCTION TO THE OTF

Exactly what the OTF is may be better understood by what it represents. In optical system terminology, a point source is a light radiator having the ideal characteristic of no physical dimensions. A star viewed by a telescope on Earth would be a close approximation to a point source at infinity. Optical systems simply cannot focus a point source into a point image. Even if a perfect, aberrationless optical system images a point source, the image is not itself a point.

Two inherent properties of the optical system cause degradation of the image. First, a practical optical system does not have an infinite pupil size and thus cannot collect all the radiation from the point source. Any finite pupil diameter and shape will cause Fresnel diffraction of the entering wavefront. This phenomenon gives rise to diffractive optical effects. Second, differences in optical path (that is, the difference in path traveled by any given ray as compared to a reference ray through the center of the optical elements) induced by the optical system will alter the entering wavefront. These alterations are called geometrical aberrations and will also cause the image to degrade.

The point-source image intensity distribution will spread and warp because of these diffraction and geometric effects. This distortion is called the point spread function, or PSF. This effect, caused by the optical system on radiation from a perfect point source, can be used to provide a transfer function. This transfer function, called the OTF, describes a range of spatial frequencies which are passed or attenuated by the optical system, and which are available for creation of the image.

## A1.1 CALCULATING THE OTF FOR A GIVEN SYSTEM

Determining the OTF for a given design starts with a mathematical description of the system and uses raytrace information to define a wavefront aberration function (WAF). The WAF is essentially a map of optical path differences (OPD) calculated from raytraces (Ref. A-3). The WAF is typically formatted as an array of values normalized by the wavelength of interest. Locations in the array are keyed to spatial positions in the exit pupil of the system. The WAF is combined with the normalized pupil amplitude to form the exit pupil phase and amplitude (EPPA) function. The complex optical impulse response function is then calculated by Fourier transforming the EPPA. The square of the magnitude of this impulse response function is called the PSF. A Fourier transform of the PSF provides the complex OTF. Simply stated, the PSF is an array of intensity values in the image plane, and the OTF is a complex array of spatial frequency values representing the spatial frequency content (and phase) of the system. These values are heavily dependent on the wavelength chosen for system evaluation. The reader is referred to Refs. A-1, A-2, or (especially) A-3 for the explicit equational formats.

In practice, the OTF is calculated from a series of convolution integrals. Hand calculation of these convolution integrals becomes exceedingly difficult for any but the most basic optical systems. With the advent of Fast Fourier Transform (FFT) algorithms, convolution calculations can be performed quickly on array representations of the various quantities. The two main concerns in calculation of the OTF for an optical system then become obtaining the array representations of either its WAF or PSF, and acting on the array with the appropriate sequence of FFT operations.

Two software tools are available to determine the OTF of an optical system. One tool calculates the performance data of the optical system; the second tool operates on the performance data to find the nominal OTF.

The first tool, CodeV®, is used to express the system mathematically. In the model, the surfaces are specified in terms of location and shape. Optical quantities such as wavelength, pupil diameter, indices of refraction, etc., are included in this system model. Geometrical aberrations are calculated by way of fast raytracing through the system. Diffractive effects are also included. Output from CodeV includes all standard optical data such as aberration coefficients, spot diagrams, spot sizes, etc. CodeV does not provide the critical OTF array directly. The user may obtain an array of either the WAF or the PSF as output from one of two options in CodeV. Because the PSF is the immediate step prior to the OTF calculation, the PSF array output becomes the quantity of interest. Formatting of the CodeV PSF array output file is covered in detail in Ref. A-4.

The second software tool is the Interactive Data Language® or IDL®. IDL brings two main functions to the OTF calculation. First, IDL provides high-quality display of data. Second, IDL

provides a library of mathematical operations that may be performed on various formats of data. Using the IDL macro language, the CodeV PSF array may be displayed directly, and the Fourier operations on the PSF performed sequentially. As an example of this capability, Fig. A-1 shows the IDL surface plot of the PSF for a perfect lens system. The perfect lens in CodeV has no geometrical aberration, but does include diffraction effects caused by pupil size and shape. Note in Fig. A-2 that a source (an ideal point source) is shown imaged into a Bessel function (see Refs. A-1 and A-3 for an explanation of the mathematics involved). Figure A-2 shows the OTF for this perfect lens as calculated by Fourier transform in IDL. The cone shape is typical of a diffraction-limited system where the only degradation comes from diffraction caused by a circular pupil with finite diameter.

## A1.2 METHODS OF OBTAINING A REAL-WORLD SYSTEM OTF

Two methods have been evaluated which may be used to calculate a realistic OTF for a given system. One method depends on measured interferometric data. This method folds actual measurements of system performance into the design information. This requires optical access to both the entrance aperture and the focal plane of the telescope. The second method calculates the OTF from the optical design parameters and can be applied before any hardware is constructed, or to systems which cannot be accessed for direct measurement. It adds reasonable stochastic changes to the design which would be expected due to manufacturing errors, misalignments, and operating conditions. The first method, which will be termed the measurement method, is by far the more desirable of the two. The 7V Chamber optical system has been studied in detail using the measurement method. The second method, which will be termed the predictive method, relies more on random perturbation of the optical parameters in the model. Comparisons between the 7V measurements and predictions from the 7V optical design have been made.

### A1.2.1 Measurement Method

Three types of data are required to develop the numerical models. First, as the system components are constructed, interferograms are made of the surfaces. This process is routinely accomplished by the optical house during the manufacturing phase. Second, with the system in place, ray intercepts on system surfaces are measured by projecting a pencil beam (laser) through the system. These intercepts must, of course, be referenced to some global coordinate system that allows correlation of the ray-surface intercepts. Finally, the assembled system is measured interferometrically. Typically, this measurement is made by autocollimating the interferometer through the system with a retroreflecting surface. Each source of system data controls increasingly fine adjustments to the system model.

Coarsest alignment of the model is obtained by reconciling the beam trace through the optical system. By tilting and tipping surfaces in the model, a reasonable mathematical reproduction of the

set of actual ray-surface intercepts can be realized. This reconciliation of optical system to model creates a firm basis for applying the interferometric data. CodeV is used to reconcile the optical measurements with the design parameters with an optimization routine. This routine uses system variables (i.e., 6-DOF movement of surfaces), creative system constraints, and user definition of the error (or merit) function using a high-level macro language.

When an assembled optical system can be measured interferometrically, the interferogram is recorded at the exit pupil of the system. Standard interferometer software such as ZAPPC® enables interferogram capture, digitization, analysis, and output formatting. CodeV has the useful capability of "attaching" these formatted interferograms to the exit pupil of the modeled system. Although raw, measured OPD data can be attached to the exit pupil, stability in the optimization of the numerical model is enhanced by using a polynomial expansion to represent the OPD. The generally accepted polynomial expansion for optical calculations is the set of Zernike polynomials. These orthonormal polynomials are discussed in Ref. A-5. The Zernike expansion is not available in CodeV as a standard mathematical surface description; therefore, user-defined surface descriptions using the Zernike expansion have been created. As a starting point in the optimization, component interferograms can be placed on the model surfaces by way of a Zernike expansion. Difficulties can arise if the component interferograms are not well-fiducialized. Small variations in the spatial location of the attached component interferograms can cause major departures in the wavefront calculation. Again using the CodeV optimization routine, the active surfaces in the numerical model can be modified by Zernike expansion to reproduce the exit pupil wavefront. Generally it is necessary to rotate and shift the interferogram on the surface, as well as modify the expansion coefficients to achieve reasonable correlation of the exit pupil wavefront.

Employment of this method successfully reproduced the wavefront of the 7V Chamber Optical System (COS) as measured in the performance test. After a detailed geometric reconciliation of raytrace information, the 7VCOS model matched observed alignment ray locations. When the surface decenters of the optimized CodeV model were placed in the CAD/CAM model, good correlation between component mount footprint locations at ambient conditions was observed from bench to CAD/CAM. Modifying the mirror surfaces by Zernike expansion also produced model OPD maps that closely resembled the measured OPD maps, especially at the inner field points. Figure A-3 is an OPD plot for the on-axis field point of the 7VCOS. Similarly, Fig. A-4a is an OPD plot from the modified model for the same measured field point. Comparison of Figs. A-3 and A-4a shows that a close reproduction is possible.

Reproduction of the measured exit pupil wavefront essentially re-creates the actual set of exit pupil OPD in the model. Obtaining the realistic OPD pupil map is the crucial step, since CodeV can then routinely calculate the PSF from the OPD modified system model. PSF data can subsequently be transferred to IDL for further reduction into the OTF.

### A1.2.2 Predictive Method

When the optical system is inaccessible to interferometric measurement, as may occur when a sensor telescope and FPA cannot be separated, then the OTF can be generated from the design by a predictive method. The chief disadvantage in the method is that there are no measured OPD data for comparison. The chief advantage is that only the optical design information is required.

Departure of the physical characteristics of an optical system from the optical design comes from small errors induced by manufacturing of the optical elements and the support structures, alignment of the system as it is assembled, and the extreme cold or high accelerations of the operating environment. Manufacturing imprecision derives from errors in constructing the individual components of the system. For example, the radius of curvature of a powered element may vary from the design specification by a small, but unknown amount. Alignment imprecision is error induced by placing the components in the optical train. Finally, the operating conditions affect the final configuration of the system. For example, cooling the 7V optical system down to operating conditions causes a 7-cm shift in the effective focal length of the system. The entire system shrinks towards the fixed center of the optical bench as the temperature changes from ambient to cryogenic.

To simulate the performance of an unmeasured system adequately, imprecisions from all three sources must be realistically estimated. Unfortunately, except for some known behaviors, estimation of this imprecision must be based on the past experience of optical engineers familiar with the characteristics of previously examined systems. Known behaviors that can be folded into an optical system may include quantities such as the coefficient of thermal expansion of materials, variations of the index of refraction of materials based on temperature and wavelength, or gravity sag of heavy optical elements. Again as an example, thermal contraction of the aluminum used for the 7V optics and bench could be applied in a known manner to the model to give a good starting point for the cryogenic solution. Also, modeling of the large BK7 window under the pressure loading between the atmosphere and the vacuum provided assurance that the window would contribute little to the overall wavefront error in the 7V performance test.

Random perturbations of the remaining optical parameters -- the degrees of freedom of the individual surfaces and the surface characteristics (radius of curvature, conic constant, etc.) — in a controlled manner are used to simulate the imprecisions caused by manufacturing and alignment. Sensitivity studies can be conducted to indicate which parameters are most critical for the optical performance of the system. Limits on the set of perturbations are used in the macros as parameters in the sequence call. These limits may be more intuitive than quantitative and thus rely on the operator's experience. Values chosen for limits typically will be derived from tolerances stated by the manufacturer or specified by the user. Figure A-4 shows an OPD map derived from the design 7VCOS compared to a perturbed 7VCOS model. Because the applied perturba-

tion is random and not measured, actual wavefront artifacts in the system generally will not appear in the model. Once the OPD map is obtained in CodeV, the PSF follows directly by exercising the correct option in the software.

## A2.0 SUMMARY

In the AEDC FPATC, where the sensor optics are removed and the scenes are written directly on the focal plane, the optical properties of the telescope must be included in the scenes. The OTF is an important parameter in evaluating the performance of an optical system and is essential for the correct performance of the DWSG. It can be obtained by measurements of the optical system (see Appendix B for details on specific methods of making these measurements) or from the optical prescription of the system. Computational tools such as CodeV and IDL have been supplemented with custom software to provide a capability to define the OTF. These tools, coupled with the experience gained from detailed measurements and analysis of optical systems installed in AEDC test chambers, have produced a capability to determine the most likely optical performance of ambient and cryogenic systems from their optical design information.

## REFERENCES

A-1. Goodman, Joseph W. *Introduction to Fourier Optics.* McGraw-Hill, San Francisco, 1968.

A-2. Williams, Charles S. and Becklund, Orville A. *Introduction to the Optical Transfer Function.* John Wiley and Sons, New York, 1989.

A-3. Parsons, John R. "*Sampling Functions and their Effect in Optical Systems Evaluation.*" Aerospace Report Number TR-0059(6311)-3, (Air Force Report SAMSO-TR-71-78), December 1970.

A-4. *CodeV Reference Manual, Volume II.* Optical Research Associates, Pasadena, California, 1993.

A-5. Wang, J. V. and Silva, D. E. "Wave-Front Interpretation with Zernike Polynomials." *Applied Optics*, Vol. 19, May 1980, pp. 1510–1518.

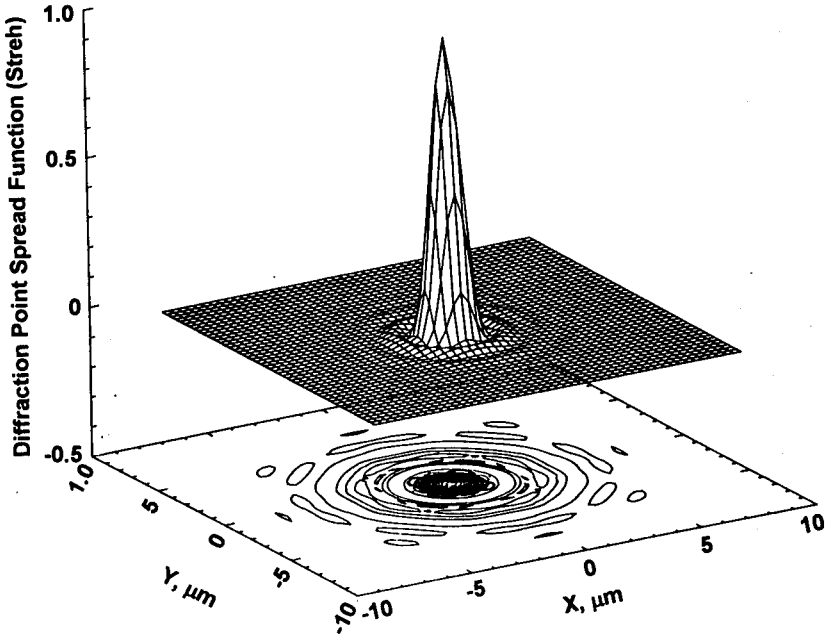


**Figure A-1. Diffraction PSF for a perfect optical system with a circular pupil.**

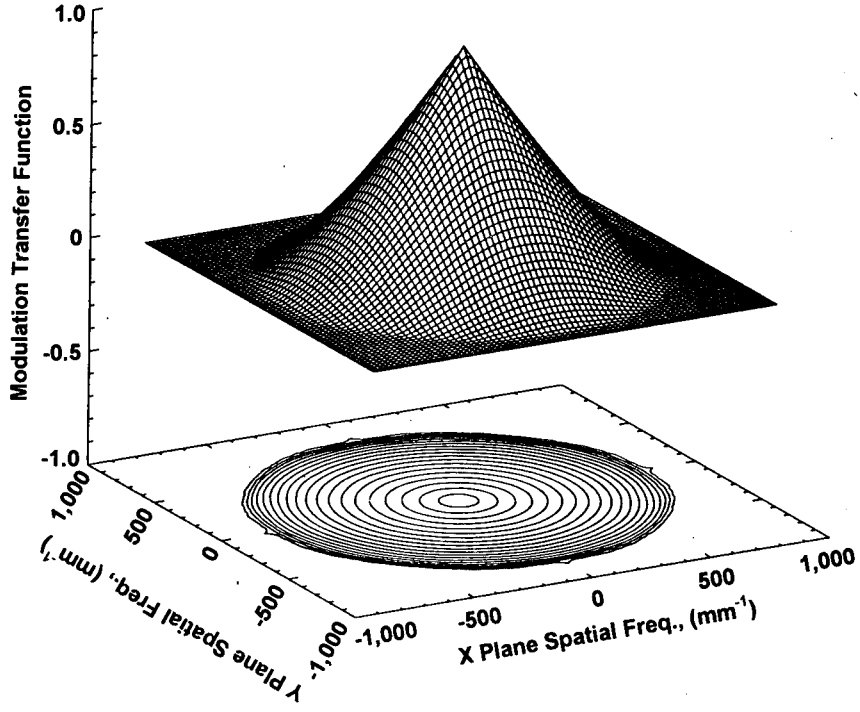


**Figure A-2. Diffraction MTF for the perfect optical system (generated from the PSF in IDL).**

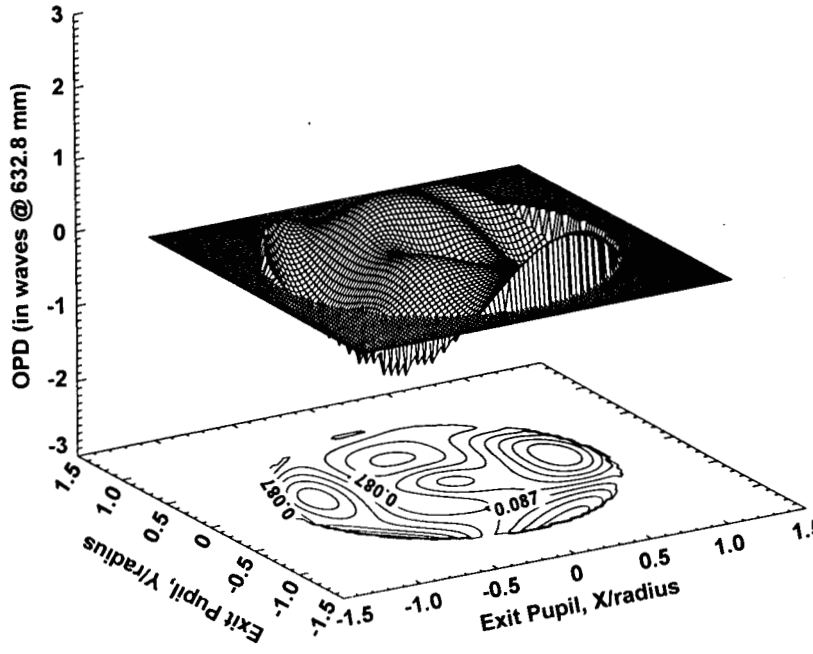


**Figure A-3. Interferometrically measured OPD for 7VCOS (on-axis field point).**

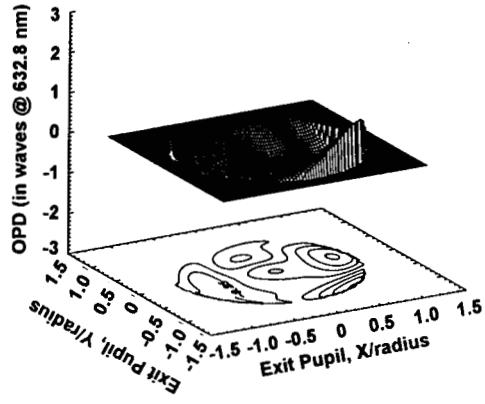


**a. OPD generated from data fitted to measured 7VCOS (on-axis field point).**

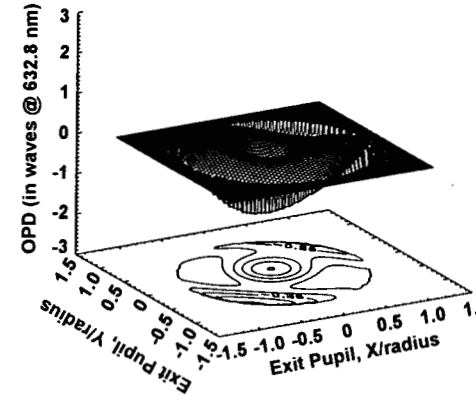


**b. OPD map generated from random perturbation of the 7VCOS design (on-axis field point).**

**Figure A-4. Optical path differences from a modified model.**

# APPENDIX B
# OTF DETERMINATION OF SENSOR SYSTEMS IN CRYOVACUUM CHAMBERS

W. H. Goethert

## B1.0 MEASUREMENT TECHNIQUE

There are several factors which must be considered prior to defining the measurement technique to be applied to determine the OTF of a sensor. The first is whether the telescope can be detached from the focal plane so that there is optical access. The second is whether the optics are to be operated at ambient or cryogenic temperatures.

Some knowledge of the OTF for the sensor optics is generally known prior to a test. This information is derived from the design optical codes and, in some cases, verified with interferometric evaluation (Appendix A). What is generally not known is the OTF change due to cyro/vacuum stresses. These physical changes originate from telescope optical distortions and slight focal changes upon cooling. Very small focal changes can have a profound effect on the OTF.

Testing with and without the FPA will be considered first, followed by considerations for cryogenic measurements.

## B1.1 INFLUENCE OF TEST SYSTEM COMPONENTS

Test system components contribute to the measured OTF over and above the OTF of the unit under test (UUT). If these additional OTF contributors are understood and can be analytically predicted or independently measured, their contribution can be divided out of the end-to-end measurement. A discussion of these additional factors contributing to the OTF measurement follows.

Performance evaluation of a sensor system in a test chamber such as the AEDC 7V space chamber facilities will be computed by cascading the optical properties of each system component in the testing system. The mathematical form of the OTF consists of a real and an imaginary component. The absolute magnitude is defined as the square root of the sum of the squares of both components. This is called the modulation transfer function (MTF).

The general makeup of a complete MTF response of the testing facility (which includes the UUT) is written in general form as

$$MTF_{total} = MTF_{testchmbr} \times MTF_{UUT} \times MTF_{display}$$

The overall MTF consists of three primary contributors: the test chamber, the Unit Under Test, and the display. A breakdown of each of these primary MTF contributors is as follows.

$$MTF_{testchmbr} = MTF_{source} \times MTF_{LOS} \times MTF_{optics}$$

where $MTF_{source}$ = due to the source contributions such as target not being adequately resolved
$MTF_{LOS}$ = due to chamber line-of-sight jitter
$MTF_{optics}$ = due to the test chamber optics

The UUT-related MTF consists of three primary factors, specifically the optics, focal plane array effects, and the electronics that follow the FPA.

$$MTF_{UUT} = MTF_{OPT} \times MTF_{ARR} \times MTF_{ELEC}$$

where $MTF_{OPT}$ = *sensor optical system contribution*

$MTF_{ARR}$ = *detector array contributions*
= $MTF_{sample} \times MTF_{det} \times MTF_{tef}$

where $MTF_{sample}$ = due to sampling effects
$MTF_{det}$ = due to detector spatial effects
$MTF_{tef}$ = due to CCD transfer efficiency

$MTF_{ELEC}$ = *UUT output electronics*
= $MTF_{amp} \times MTF_{pre\text{-}f} \times MTF_{dig\text{-}f} \times MTF_{post\text{-}f}$

where $MTF_{amp}$ = *due to amplifiers*
$MTF_{pre\text{-}f}$ = *filter prior to A/D*
$MTF_{dig\text{-}f}$ = *digital filter*
$MTF_{post\text{-}f}$ = *post A/D filter*

If a display is used for the sensors' output, losses in resolution due to the display are given here by a composite display MTF as

$MTF_{display}$ = *the display contributions*

Each specific MTF entity given above will have a theoretical bound. The derivation and specific equations for each MTF component are provided in Refs. B-1–B-6.

## B1.2 SENSOR OPTICS TESTING

An OTF evaluation of a sensor, excluding the focal plane array, is accomplished either by interferometric or geometrical scanning. Interferometric techniques use a single optical frequency approach, usually with a phase measuring interferometer. The geometric scanning approach scans an image of a bar target, a subresolution source, or the image of a step function (knife edge).

### B1.2.1 Interferometric Approach

An interferometrically measured pupil function of an optical system can be used to determine an OTF for an optical system. The interferometers' software calculates the OTF either by an auto-correlation technique or a Fourier approach. Although the autocorrelation approach is a one-step process, the actual calculation is slow and calculation-intensive (Ref. B-1). Consequently, the Fourier approach is generally used to generate the OTF.

An interferometrically generated OTF, although simple to implement, has some disadvantages. First, the measurement is made at a single wavelength, usually in the visible spectrum. Care must be taken in extrapolating the results to the infrared domain. Second, the wave-front error cannot exceed some maximum error value dictated by the characteristics of the interferometer. Usually this is less than 2 wavelengths of the operating wavelength of the instrument. The interferometer is not able to detect more than 1 fringe/pixel. For optical systems designed and built to be diffraction limited, the interferometer is a good choice, since its strength lies in the ability to detect less than a tenth wave variation. Large system aberrations, such as 30 waves, however, would dictate a geometric approach to OTF determination.

### B1.2.2 Geometric Approach

The theoretical basis for OTF evaluation using a geometric approach lies in determining the spatial frequency response of the optical system when it images a point source (similar to the impulse response concept in electronics).

A user-supplied sensor system is designed to image objects located, for all practical purposes, at infinity. Since the OTF test is based on the system response to a point source at infinity, an additional optical system must be provided to establish this "collimated" input to the UUT. A high-quality collimator such as the 7V and 10V Chamber Optical System (COS) provides this function. It must be understood that the OTF of the COS will be part of the cascaded terms contributing to the measured end result. An interferometric measurement has already been conducted on the 7V COS. Therefore, the chamber optic contributions are known.

A point source is located at the focal point of the test chamber collimator and is thus focused at the focal plane of the optics under evaluation. This image is subsequently scanned at the focal plane of the sensor telescope by a detector with a small instantaneous field of view (IFOV). The small IFOV will ensure a negligible MTF contribution from the "scan" detector. Specifically, the detector will have limiting frequency response given by the inverse of the IFOV. Hence, a small "scan" detector will necessarily have a high spatial frequency cutoff.

Scanning across a point source image, however, has two drawbacks: (1) the scan must be through the center of the image, which is not easy to locate; and (2) the energy from a point source is usually too low for adequate detection. Therefore, point sources are generally not used because of energy throughput considerations.

### B1.2.2.1 Use of Bar Targets

A direct MTF measurement can be obtained by imaging a bar target of specific spatial frequencies. The resulting image will be convolved with the transfer function of the optical system. This viable but less-used technique makes a measurement of image contrast which is directly related to the MTF of the system.

In an optical system that is both linear and continuous, the contrast is given as

$$MTF = \frac{B_{max} - B_{min}}{B_{max} + B_{min}}$$

where "B" are adjacent maxima and minima responses in the imaging system. A bar target such as the USAF resolution targets or a rotating circular grating permits direct measurement of image contrast by observing the maximum intensity and the adjacent minimum intensity. Since the normalized maximum and minimum contrast is a mapping of the MTF for a specific frequency, direct determination of MTF at each bar target frequency will be required. The availability of various bar target frequencies is finite, and the requirement to move the detector and the source tends to be a difficult calibration problem. This technique is cumbersome for system MTF determination.

The bar target approach is often employed for system focusing determination. Focusing is usually effected by choosing a spatial frequency, usually near one-half of the spatial frequency cut-off for precise focusing of an optical system. The task is then to maximize the MTF (maximum/ minimum measurement) by varying the detector focus position.

A variation on the bar target technique is the use of a sinusoidal amplitude target. Fabrication of these types of targets is difficult, and they are seldom used.

#### B1.2.2.2 Use of Line Sources

There are two types of line sources:

1. Thin heated wire
2. Narrow slit (inverse of the heated wire)

The heated wire and the narrow slit generate the LSF directly, thereby eliminating the differentiation process. Not requiring a blackbody source illuminating the back side of the knife edge is a distinct advantage with the wire technique, but accommodating the wire and its electrical connections has its own difficulties. A slit source overcomes the difficulties of heated wire technique but requires a radiation source. Fabrication of the slit is a definite issue to be addressed if this approach is to be used.

#### B1.2.2.3 Use of Knife Edge Targets

Use of a knife edge (step function) instead of the point source generates a one-dimensional slice through the center of the two-dimensional OTF. The spatially continuous knife edge image is scanned perpendicular to the edge. This scanned image is termed the edge spread function (ESF) or sometimes the edge trace function, ETF. Differentiation of the ESF yields the line spread function (LSF). A Fourier transform of the LSF yields the desired OTF along one axis. Reorienting the knife edge at 90 deg provides the orthogonal OTF information.

The spatial frequency range of the knife edge is not limited by the target collimator focal length as a slit would do (Ref. B-2). All things considered, the knife edge approach seems to be the best method for the OTF determination. The discussions that follow will concentrate on the knife edge test methodology.

#### B1.2.2.4 Test Approach Using the Knife Edge Method (Method 1)

Figure B-1 shows a testing scheme for the OTF measurement in a 7V Chamber configuration. A sub-resolution slit is placed in front of a suitable source and located at the focal point of the test chamber collimator. This assembly is mounted on a translation stage.

The test article is placed near the centerline of the collimated output of the chamber optical system. The knife edge is placed at the focal plane of the sensor. A precise positioning mechanism is required to perform the knife edge scan, position the knife edge at the focal plane, and rotate the knife edge as needed. The knife edge scan device will require a precision traversing device that has movement resolution of better than 1 μm. Translation devices are available with resolution better than 0.1 μm. Calibration of the traversing device at cryogenic temperature will require care. Fine position resolution is required to ensure sufficient data samples for the data reduction. Following the knife edge is a condenser lens for concentrating the light into an appropriate detector.

### B1.2.2.5 Test Approach Using the Knife Edge Method (Method 2)

An alternate method consists of interchanging the knife edge with the slit. The scan resolution on the knife edge is relaxed by the ratio of the magnification of the test chamber collimator to the UUT collimator. Placement of the sub-resolution slit in the sensor focal plane, however, will be a more difficult task.

Choice of the appropriate method will depend on the hardware configuration of the sensor.

## B2.0 TEST METHODOLOGY

The edge trace data can be obtained either by scanning the edge and recording the transmitted intensity or by fixing the knife edge in the focal plane of the sensor and scanning the "source" end (see Fig. B-1). Generally, the scanning is performed by a "step-read" procedure; however, continuous scanning has also been implemented (Ref. B-3). Knowledge (calibration) of position versus time appears to be the limiting factor. The resolution and timing requirements on the scan traversing unit for a continuous scan method are high.

Ultimately, the edge trace function (ESF) must be sampled to implement the differentiation process. Differentiation of the ESF yields the line spread function (LSF) of the optical system. Traditionally, the knife edge technique allows for oversampling the continuous image. Oversampling assures that aliasing does not distort the transfer function.

An optical system will not transmit spatial frequency higher than

$$f_{max} = \frac{2N.A.}{\lambda} = \frac{1}{\lambda f\#}$$

where $f\#$ is the f-number of the optical system. The sampled value will need to be at least twice $f_{max}$ to comply with the Wittaker-Shannon sampling theorem.

J. P. Chauveau, et al. (Ref. B-4) experimentally determined an optimum sampling on the ESF to be two times greater than the required Nyquist sampling, which is defined as twice the maximum frequency passing through the system. This necessarily implies that the LSF should be sampled at least 4 times greater than the maximum spatial frequency in the system.

Oversampling is limited by the (1) overall hardware system stability, (2) accuracy of the scanning device, and (3) the time needed to process each data point, i.e., differentiation and Fourier transforming.

## B2.1 DIFFERENTIATION OF THE ESF

There are two methods for differentiation of the ESF. The first consists of taking the difference of adjacent values of the sampled edge spread function. The second approach curve fits the raw data and differentiates the results. The primary difficulty with obtaining the line spread function from the edge trace is noise. One noise reduction technique averages the oversampled ESF and resamples from this data set.

A differentiation technique reported in the literature employs a "successive difference" method. Differencing adjacent samples results in an approximation of the LSF, which is proportional to the first derivative of the ESF. Figure B-2 represents the process. Closely spaced samples can easily have difference value ranging from negative to positive values. This averaging/ resampling is shown in Fig. B-2. Oversampling the ESF ensures that sufficient values are available for averaging

The spline interpolation method is another well-known differentiation technique which provides some averaging by locally fitting a polynomial of narrow intervals and forcing the slopes to be equal at the end points. The major benefit derived by this technique is that the points that are used for the resampling do not necessarily need to fall on a sampled point of the ESF.

An alternate differentiation approach that effectively eliminates the noise problem is curve fitting the ESF to a differentiable function. Such a function was reported by Tzannes (Ref. B-5). The form of the equation is

$$f(x) = \frac{a}{e^{(x-b)/c} + 1}$$

This has nearly the same shape as the edge trace and, more importantly, it is differentiable. According to Tzannes (Ref. B-5), the actual measured function does not necessarily fit well about the midpoint of the rising or falling edge; however, a combination of three of these functions was

found to give good results. The curve fitting will consist of minimizing 10 variables in the summed equation

$$F(x) = D + \sum_{i=0}^{2} \frac{a_I}{e^{(x-b_i)} + 1}$$

where $D$, $a_i$, $b_i$, $c_i$ for $0 \leq i \leq 2$ are constants to be minimized. Since the function of the edge trace is known, the LSF is given by the derivative of equation F(x) as

$$LSF = \left|\frac{dF(x)}{dx}\right| = \left|\sum_{i=0}^{2} \frac{a_i e^{(x-b_i)/c_i}}{\left(c_i e^{(x-b_i)/c_i} + 1\right)^2}\right|.$$

The resulting function can be sampled at a high enough sample rate to completely avoid aliasing in the Fourier transform.

## B2.2 FOURIER TRANSFORM OF THE LSF

Taking the Fourier transform of a line spread function results in the OTF of the system. The MTF is obtained by taking the square root of the sum of the squares of the real and imaginary parts of the OTF. The Fourier transform requires that the total sampled values of the LSF must be a power of 2, i.e., the total number of points must equal $2^P$ where p is an integer. A second requirement of the Fourier transform process is that the sampling interval, $\Delta x$, must be constant.

Choosing the number of points to sample along with its sample interval is not straightforward. The total sample length of the line spread function will affect the frequency resolution of the MTF. Let $L$ be the sample length. Consider the number of samples, N, to be at least twice that required to resolve the maximum frequency, then

$$L = 2\ \Delta x N$$

The maximum frequency that can be resolved would be

$$f_{max} = \frac{N}{L} = \frac{1}{2\Delta x}$$

To assist in choosing the sample width, one can determine the maximum frequency that will be transmitted by the sensor optics. This maximum frequency is given by

$$1/\lambda f\#$$

where $\lambda$ is the mean wavelength transmitted by the optics, and $f\#$ is the system f-number.

where $\lambda$ is the mean wavelength transmitted by the optics, and $f\#$ is the system f-number.

Equating these two maximum frequencies results in

$$2\Delta x \geq \lambda f\#.$$

This equation requires the sampling interval to be equal or greater than half the mean wavelength times the f-number of the optics. Data resolution in frequency space will be given by $1/L$.

## B3.0 THE FPA INCLUDED IN OTF TESTING

Including the focal plane detector array to the unit under test adds a new dimension to the problem of making an OTF measurement. One of the difficulties is access to the output of the detector array. A second difficulty arises from having to sample the image by the detectors in the sensor. As a rule, the detector array inherently undersamples the image, causing problems. These problems will distort the OTF results.

The two types of imaging systems are the scanners and the staring arrays. Scanners sample the scene in the cross scan direction using the discrete location of the detectors in the array. Data from the scan direction are generated from an A/D converter tied to the "mechanical" scanning of these devices. The staring arrays utilize the discrete location of detectors to sample the scene in both vertical and horizontal directions. When one samples an image with a detector array, he must consider the aliasing and phasing effects in the output of the detected image.

Aliasing is a digital effect caused by the undersampling of the image as a result of the finite size of the detector pixels and their spatial separation. Specifically, spatial frequency components above the Nyquist cutoff frequency fold into the frequency domain below the Nyquist frequency.

Aliasing and phasing effects induced by focal plane array sampling will greatly affect the OTF testing procedure for a sensor with an installed focal plane. The previously described procedures used for testing an optical element will need to be altered when the focal plane array is present. Needless to say, access to the user-supplied sensor output will be imperative. Several techniques have been explored. These are:

1. Scan slit or knife edge across one detector (Refs. B-6 – B-7)
2. Sample LSF using pixel array (Ref. B-6)
3. Sample ESF using pixel array (Refs. B-6 – B-7)

## B3.1 SCAN SLIT OR KNIFE EDGE ACROSS ONE DETECTOR

When it is not possible to remove the focal plane array, a pixel near the center of the array is designated as the sensor for the OTF measurement. The output of this pixel is recorded as the image of a slit, or a knife edge is scanned over the designated pixel. OTF analysis will be similar to the analysis discussed previously. Any nonuniformity in the response of the chosen pixel to the irradiance range can be independently measured. The aliasing problem is avoided since the sampling is accomplished with small subpixel steps with the scanning process.

The point spread function of the single pixel can be determined by stepping a fine laser beam spot across the pixel. Translating this PSF to the LSF can be achieved by mathematical means. This will allow a calculation of the single-axis MTF using this pixel. The finite width of the detector element will become part of the cascaded MTF in the overall measurement.

Scan line averaging will also be advisable. Each separate scan line, using the same pixel detector, will need to be registered spatially to obtain a true result. A misregistration will broaden the ESF which, in turn, will decrease the MTF roll-off calculated.

## B3.2 SAMPLE THE LSF USING THE DETECTOR ARRAY

A line spread function can be produced directly with a thin heated wire in the focal plane of the test chamber collimator. When the discrete detectors are used to sample the line spread function, a position (spatial phase) independence can be achieved only if the LSF is not apodized by the detector sampling pitch (Ref. B-6). This is generally not the case, so this approach to OTF evaluation is seldom used.

## B3.3 SAMPLE THE ESF USING THE DETECTOR ARRAY

In an alternate technique, the edge spread function is produced by a knife edge in the focal plane of the collimator system. Sampling of the ESF is accomplished by sampling along a scan. As implied above, the detector array will add its own contribution to the measured OTF. MTF degradation from the array is due to the limited number of detectors, the detector pitch, and detector size

However, this line-scan approach can be modified to alleviate or at least minimize the aliasing and phase problem. The technique uses a slightly tilted knife edge relative to the detector array. Edge tilt should not exceed one pixel width over the range of the line scans to be analyzed. Many scan lines are sampled, each being slightly displaced relative to the knife edge (see Fig. B-3). The scan lines are registered using estimates of the knife edge location and subsequently averaged. Shifting each scan line to align the edge points of the knife edge requires some technique to

determine their sub-pixel location. Using this "averaging' technique, the step edge sampling frequency is greatly increased, thereby eliminating the undersampling, along with aliasing and phase effects.

Averaging many scan lines from the tilted knife edge will also reduce the noise. This averaging/resampling is shown in Fig. B-4. Oversampling the edge trace ensures that sufficient values are available for averaging and, more importantly, avoids aliasing.

When line spread functions are obtained from a scan line, care must be taken that "dead pixels" are not seen by the trace. Nonuniformity of the pixel response must be also be taken into account. Background measurements of the maximum and minimum intensity to the array can be used for data correction.

### B3.2.1 Methods for Sub-pixel Edge Location

Determining the edge step function accurately can be difficult. Several empirical techniques have been used that rely on the assumption that the line spread function is symmetrical. The exact position of the edge is therefore located at the maximum slope in the LSF. Usually, few data points are available from the successive difference calculation. This has inspired the development of empirical techniques such as the "Center of Mass" calculation of three adjacent values. Alternate methods assume a parabolic shape or a Gaussian shape, and fit the sparse data to that assumed shape. Unfortunately, the LSF shape will change with different focusing conditions. Other methods have been developed that produce superior results in the edge location. Two of these techniques will be discussed below.

#### B3.2.1.1 Least-Square Fitting

Attempts to locate the knife edge step to sub-pixel accuracy by curve fitting and differentiating to find the maximum slope are frustrated by insufficient samples. Usually, there are four or less noisy samples. This method estimates edge location based on a least-square curve fit as presented by Reichenbach (Ref. B-8) and is listed as follows.

1. Estimate the edge location in each scan line. A reasonable starting estimate is at the one-half intensity points between maximum and minimum light levels.
2. Use a linear regression to fit a line through the individual edge estimates.
3. Use the regression line to improve the estimate of the edge location of each line scan.

Reichenbach (Ref. B-8) indicates that when a large number of scans are used with this estimating technique, sample/scene phase bias, residual noise, and misregistration errors become negligible.

#### B3.2.1.1 Generating a Linear and Symmetric Filter

A second procedure having excellent sub-pixel edge step locating capability is suggested by Seitz (Ref. B-9). The argument is made that the imaging of an edge is made by linear and symmetrical filters near the edge and along one scan line. Blurring due to focusing error, diffraction of the pupil, motion blur, and other so-called low-pass filtering, is indeed linear and symmetric in the mathematical sense. Seitz (Ref. B-9) writes, "It is easy to prove that an ideal edge signal filter with a linear and symmetrical filter, has a (local) maximum in its first derivative at the location of the edge, independent of the exact shape of the filter."

Since any shape can be assigned to the filter, a Gaussian curve is used since it can be constrained to avoid aliasing

$$g(x) = \frac{a}{\sqrt{\pi}} \exp(-a^2 x^2)$$

since its Fourier transform is also a Gaussian

$$G(\omega) = \exp\left(\frac{-\omega^2}{4a^2}\right)$$

The constant "$a$" is chosen to bound G ($\bar{\omega}$) to $-\pi, +\pi$. This constraint will ensure aliasing will not occur, i.e., the transformed function value at $\pm\pi$ is, for all practical purposes, zero. This forces the constant "$a$" to be equal to $\pm 4$.

An important aspect of this method for edge location is that the LSF need not be derived from a focused system. The edge can be located precisely as long as the "filtering" is linear and symmetric.

## 4.0 SUMMARY

Use of a point source to generate a point spread function presents difficulties from low signal levels and alignment problems; hence, it is seldom used.

There are several options for testing sensor telescopes without the FPA. The LSF can be sampled directly, thereby eliminating the differentiation requirement. As noted, noise is accented at the higher frequencies in the differentiation process. The line spread function can be generated

with either a heated wire or a narrow slit; however, both are difficult to fabricate and maintain. Most laboratories engaged in OTF testing use the knife edge due to its simplicity and ease of fabrication.

A user-supplied sensor telescope without an FPA is best evaluated with the knife edge at the focal point of the sensor telescope. The resulting image is probably best scanned at the source end of the collimators in the 7V or 10V test chambers, since the scanning (sampling) in the chamber collimator focal plane will be considerably less stringent.

If the FPA is included in the sensor system, the skewed knife edge technique is recommended for the OTF determination. Oversampling can be achieved if scan lines are shifted and aligned along the step edge using a sub-pixel edge determination procedure. Averaging of the scan lines greatly reduces noise in the measurement. Resampling of the edge trace also reduces noise and provides the input to the Fourier transform procedure. Curve fitting to the resembled data can also be performed to give a noise-free OTF.

## REFERENCES

B-1. Stahl, H. P. "*Infrared MTF Measurement of Optical Systems.*" *Lasers & Optronics*, April 1991, p. 71.

B-2. Pinsky, Howard J. "*Determination of FLIR LOS stabilization errors.*" *SPIE*, Vol. 1488, 1991, p. 334.

B-3. Brot, J. M. "Evaluation of thermal imaging optical systems." *SPIE*, Vol. 590, 1985, p. 152.

B-4. Chauveau, J. P., et al. "Microcomputer Controlled MTF Measuring Equipment for Infra-red and Visible Wavelengths." *SPIE*, Vol. 590, 1985, p. 144.

B-5. Tzannes, A. P. and Mooney, J. M. "Toward the characterization of infrared cameras." *SPIE*, Vol. 2020, 1993, p. 472.

B-6. Bradley, D. J., et al. "*The Modulation Transfer Function of focal plane array systems.*" *SPIE*, Vol. 807, 1987.

B-7. Chazalett, F, et al. "*Theoretical bases and measurement of the MTF of integrated image sensors.*" *SPIE*, Vol. 549, 1985, p 131.

B8. Reichenbach, S. E, et al. "Characterizing digital image acquisition devices." *Optical Engineering*, Vol. 30, No. 2, Feb. 1991, pp. 170–177.

B-9. Seitz, Peter. "Optical super-resolution using solid-state cameras and digital signal processing." *Optical Engineering*, Vol. 27, No. 7, July 1988, p. 535.

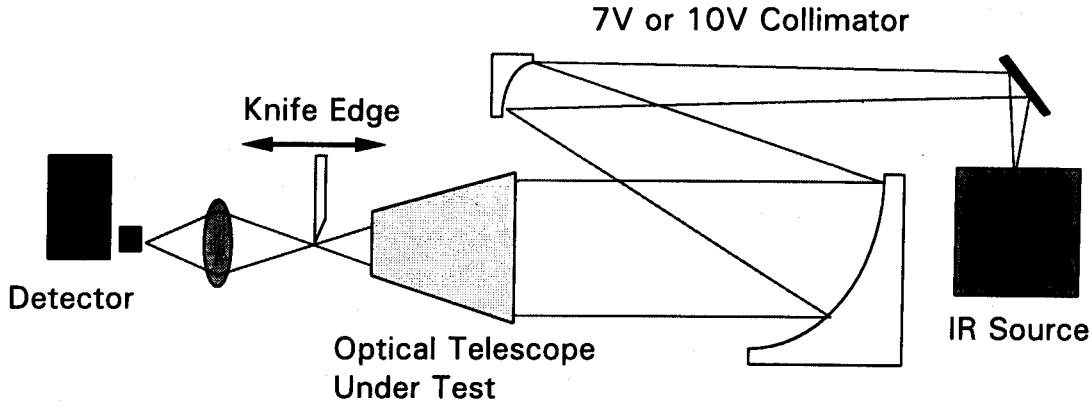


**Figure B-1. Schematic of test setup #1.**

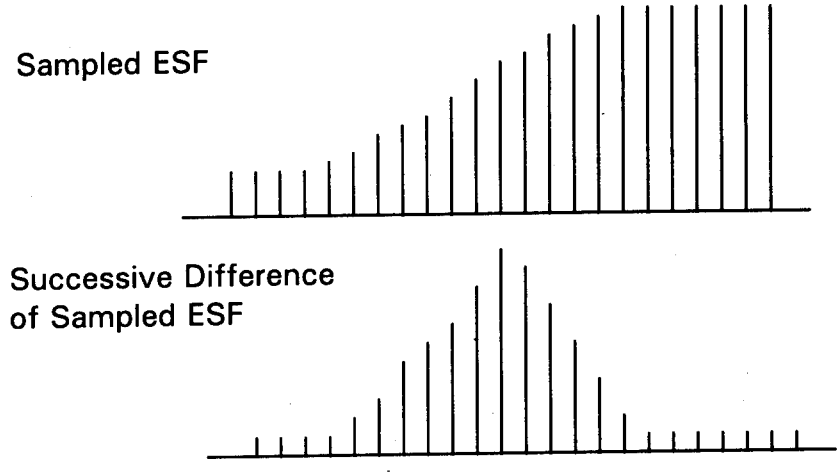


**Figure B-2. Sampled low-pass filtered ESF; differentiation by successive differences technique.**

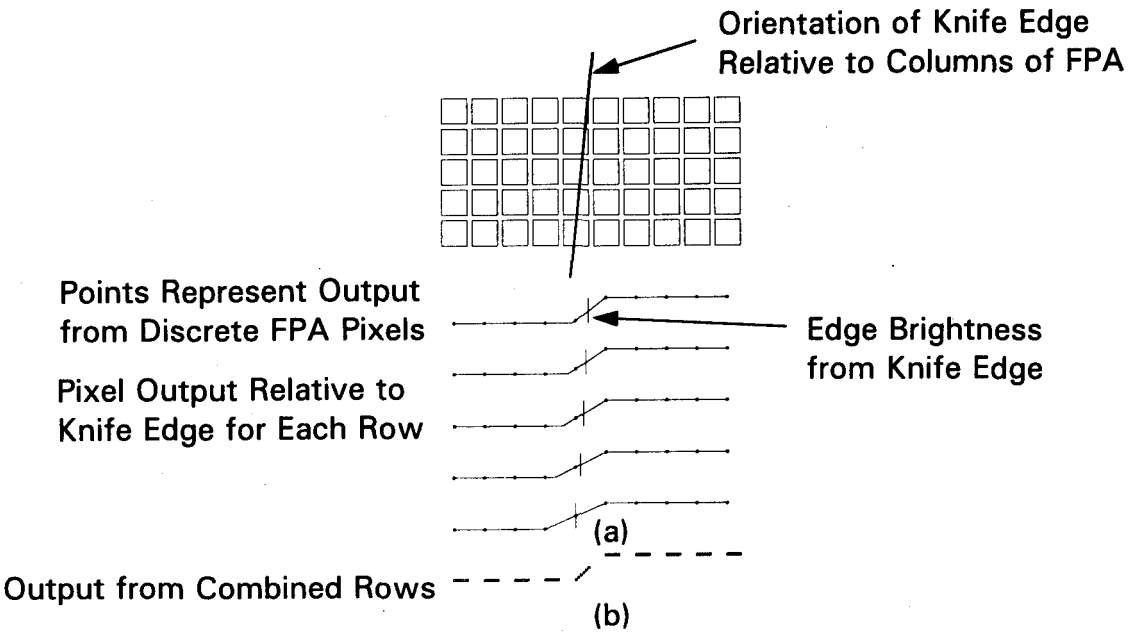


**Figure B-3. Scan line sampling of an FPA.**

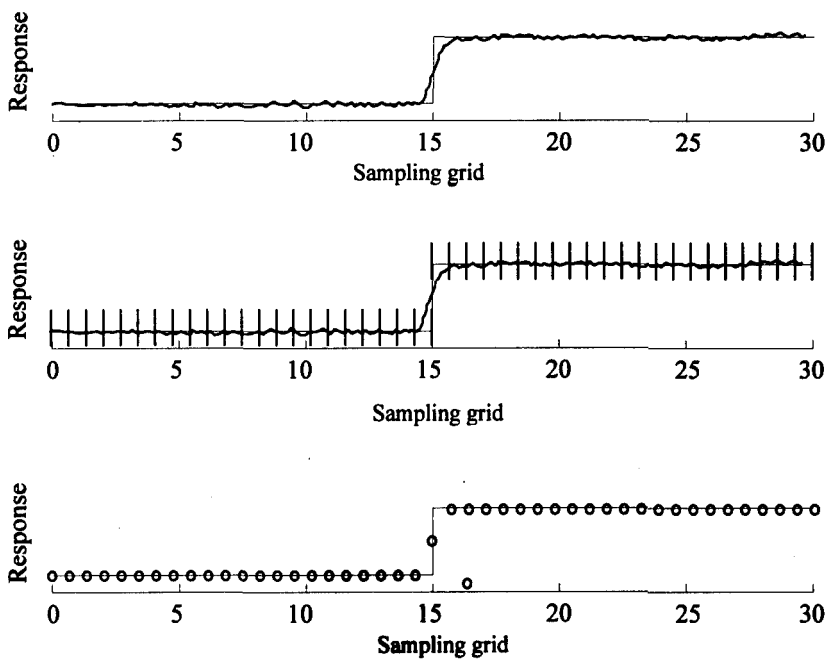


**Figure B-4. Averaging and resampling of ESF.**

# APPENDIX C
# SSGM AND SYNTHETIC SCENE GENERATION

E. Kiech

## C1.0 INTRODUCTION

The scenes for the closed-loop demonstration will be composed of an Earth background with several plume targets. The Earth backgrounds will include contributions from terrain and clouds. The targets will be typical of a Scud-type missile which has a 600-km range. Effects of atmospheric absorption and cloud obscuration will be included in the scenario.

## C2.0 STRATEGIC SCENE GENERATION MODEL (SSGM)

The primary source for the scenes will be the Strategic Scene Generation Model (SSGM) (Ref. C-1) computer program. A limited set of realistic terrain and target data is included in the SSGM. This program consists of software and input databases which provide the capability to generate two-dimensional time-sequenced scenes and data intended for use in the design, development, and test of strategic surveillance and weapons systems, and for strategic engagement simulations.

The SSGM builds a scene radiance map by combining several user-specified elements. An observer position (i.e., the satellite location in its orbit), field of view, date, and time are required to define the geometry and sun angle. The various other inputs such as terrain background, clouds, and targets are chosen from the library of databases. The geometry of a typical SSGM scenario is depicted in Fig. C-1, which shows the various line-of-sight, observer-cloud, sun-cloud, and scattering angles. A typical scene is calculated by taking the apparent radiance of a terrain background as modified by atmospheric (including possible cloud) optical properties and including the effects of target absorption and radiance again as modified by intervening atmospheric optical properties where applicable. Although a field of view is specified, there is no provision for modeling OTF (i.e., perfect optics are assumed). Appendices A, B, and E describe the work in progress to include OTF effects in the calculated scenes.

The current SSGM database includes nine different terrain types with various sizes, pixel resolutions, and representative materials. Table C-1 lists the pertinent parameters for each terrain type. Each terrain is intended to be representative of a typical Earth background and can be positioned at any latitude/longitude. When the terrain is viewed at an oblique angle, the apparent size of the terrain background will necessarily be smaller due to projection effects. The basic materials include various forms of water, ice, snow, soil, rock, flora, and urban commercial and residential areas. Each of the

nine terrains is based on a satellite image of a very small area of the Earth where each pixel has been characterized as one of these basic materials. An emissivity and temperature is assigned to each of the pixels in the scene, and the resulting radiation is calculated for a prescribed infrared bandpass. Using the viewing geometry and the atmospheric conditions that have been defined, the program calculates the atmospheric absorption and produces a pixel irradiance matrix for the sensor. A short-wavelength infrared bandpass (2.6- to 2.8-micron) irradiance map based on the 'land and sea' terrain is shown in Fig. C-2 to illustrate a typical SSGM background. This particular background covers an area of approximately 400-km square and was created from a satellite image of the southern California area. The darker areas represent water (Pacific Ocean) while the lightest areas represent desert sand.

In addition to the nine terrain elements, the SSGM contains an extensive atmospheric absorption model and 17 representative cloud types including altostratus, cumulus, and cirrus. The cloud scenes have been modeled similarly to the terrain elements in that 17 satellite images of various cloud types were decomposed into materials with known optical properties. These cloud materials are 'water,' 'ice,' 'water/ice,' 'water/ice mix,' and 'ice cloud.' In addition, an altitude distribution was assumed for each of the materials comprising a particular cloud scene. In this way, targets flying under clouds, breaking through clouds, and flying above clouds can be properly handled.

Four types of target scenarios with generic missile characteristics and associated trajectories are included in the SSGM database. The launch point latitude, longitude, and azimuth can be specified by the user. Target type #1 is a generic one-stage missile scenario lasting 105 sec and reaching an altitude of 85 km. Target type #2 is a generic two-stage missile with the first stage reaching an altitude of 66 km at 110 sec, and the second stage reaching an altitude of 316 km at 265 sec. Target type #3 is another two-stage generic missile with the first stage reaching an altitude of 77 km at 125 sec, and the second stage reaching an altitude of 322 km at 290 sec. Target type #4 is a generic three-stage missile with the first stage reaching an altitude of 27 km at 65 sec, the second stage reaching an altitude of 91 km at 130 sec, and the third stage reaching an altitude of 250 km at 220 sec. Multiples of each type and combinations of types can be included in the same scenario.

Given the optical properties of the terrain, clouds, and intervening atmosphere and the optical properties and trajectory of a target, the program can calculate irradiance maps for specified targets in specified wavelength bands at appropriate view angles and times. These irradiance maps are only approximations of what would actually be seen by a sensor because of the various simplifying assumptions outlined above. For example, the terrain databases do not include contributions from city lights or any transient sources such as forest fires or local weather effects.

## C3.0 CLOSED-LOOP DEMONSTRATION METHODOLOGY

The SSGM scene for the closed-loop demonstration will consist of a single background data set which includes terrain and cirrus clouds. This database will consist of a matrix of 512 × 512 pixels. It will not be oversampled and, thus, each terrain pixel will correspond to a sensor pixel. The sensor's instantaneous field of view in the demonstration will be 64 × 64 pixels. Each frame of 64 × 64 pixels will be selected and extracted from this 512 × 512 database. The location of the 64 × 64 array selected will be defined in real time by the line-of-sight pointing vector of the sensor.

The target trajectories will be calculated prior to the demonstration. In the closed-loop demonstration, the satellite orbit and the satellite position in this orbit at any time is defined *a priori*. Since the satellite position is known as a function of the scenario time-line and the sensor is viewing the scene at a known framing rate, it is possible to precalculate the target irradiance within the background for each frame time of the sensor. The unknown is the actual line-of-sight pointing of the sensor on board the satellite; in the actual test, the sensor may or may not view the target. However, if the sensor does point in the correct direction, the target will be at the correct location against the background for each frame. In practice, the target database will consist of a series of data sets. The information in each data set will consist of two pieces of information for each target: the current target position and irradiance with all atmospheric effects at that position included, and a negative value for the irradiance at the previous frame location. During the conduct of the scenario, these target frames are added to the background database at the sensor's clocking frequency. Each frame adds the new target irradiance and subtracts the old target irradiance, thus providing a continuously updated database.

One concern which had been voiced with this concept is that the irradiance from the background may not be constant due to the changing viewing angle of the sensor. Therefore, a test case was calculated using the SSGM model where constant background parameters were defined and the sensor was placed in a 30-deg, 1,600-km inclined orbit. The irradiance values at the sensor were calculated for an initial and final view angle for 5 min. The results showed that the model provided identical background irradiance maps. This outcome can be expected, based on the fact that the radiance from the background is diffuse, the change in sun angle and the viewing geometry is small in the test time period chosen, and the parallax changes between clouds and Earth are similarly negligible.

## C4.0 DEVELOPMENT OF SYNTHETIC SCENES

Although realistic scenes play an important role in sensor system evaluation, there is also a need for artificial scenes in sensor testing. The random variables in real-world scenes produce problems in evaluating the operational characteristics of a sensor and its data processors. This is

especially true if the system is not performing as expected and the test data must be used to diagnose the problem. Therefore, there is a need for a complex but better-defined scene. The features of synthetic scenes such as spatial frequencies are more easily controlled and can be used to elicit behavior which might be obscured in more complex real-world scenes. For example, Fig. C-3 is a spatial frequency map of the SSGM terrain data shown in Fig. C-2, and shows the relative complexity of 'realistic' scenes. Synthetic scenes can be constructed with various degrees of complexity and thus provide a parametric capability for evaluations. To accomplish this, several techniques are being investigated to create synthetic scenes with the desired properties. A preliminary investigation of fractal techniques indicates that they could serve a useful purpose in creating randomly varying scenes whose overall properties still satisfy some predetermined characteristics. One of the areas of investigation is to provide a method of comparing the characteristics of typical real-world scenes such as types of clouds and typical types of terrain with synthetically generated equivalent scenes.

An additional benefit offered by synthetic scenes is that they can be manipulated, compressed, and stored much more efficiently. This will have a significant benefit for eventual use in a real-time test capability, where large background databases will be required for long test scenarios. In these there will be real-time changes in the background needed because of significant changes in sun angle and viewing geometry.

Fractal techniques can also be used to artificially extend the resolution in a real-word scene which does not have sufficient resolution. This technique eliminates the appearance of individual pixel artifacts. Figure C-4 shows a small portion of a low-resolution scene from an SSGM database with obvious pixel structure. Figure C-5 shows the results of synthetically interpolating the data from Fig. C-4 to increase the fine structure. There will be a continuing effort to further investigate the creation of synthetic scenes and the particular properties they need to have to serve as useful test scenes.

## C5.0 SUMMARY

This initial database which will be used for the infrared scenes will be the SSGM. For proof-of-principle tests, the database is adequate. However, the eventual test needs for oversampling and enlarged scenarios will require some supplemental data. The present focus of this task is to evaluate the characteristics of the scene content from typical SSGM scenes, the objective being to eventually provide synthetic scenes which have the required extent and resolution and, at the same time, have the infrared characteristics of the real-world modeled scenes.

## REFERENCES

C-1. Photon Research Associates, Inc. "Strategic Scene Generation Model, Release 5.0, Users Manual." February 1993.

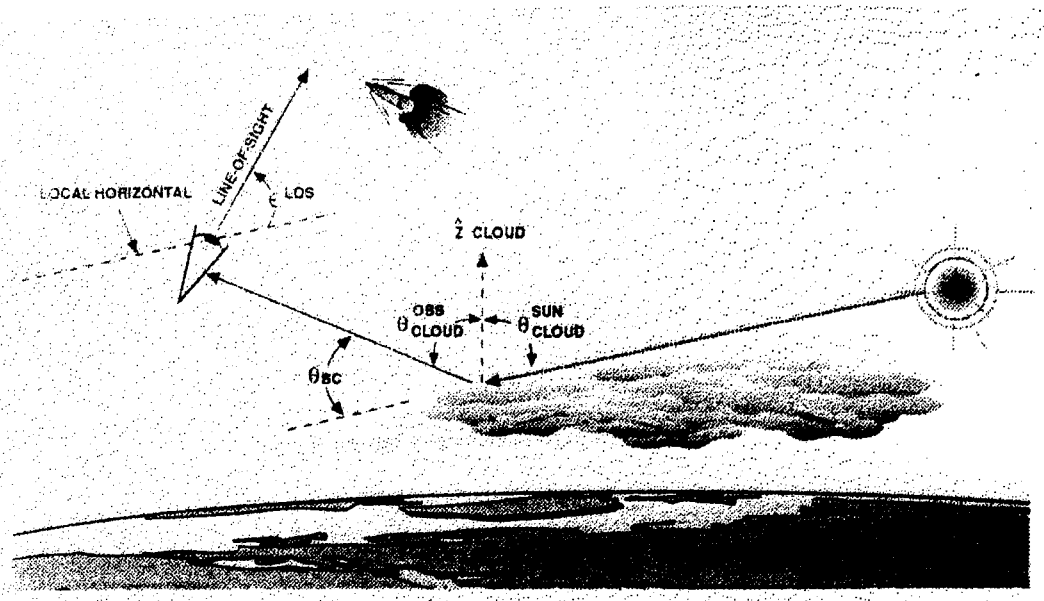


Note:

$$\cos\theta_{sc} = \cos\theta^{OBS}_{CLOUD}\cos\theta^{SUN}_{CLOUD} - \sin\theta^{OBS}_{CLOUD}\sin\theta^{SUN}_{CLOUD}\cdot\cos\Delta\theta$$

$\epsilon_{LOS}$ = LOS Elevation from Observer
$\theta^{OBS}_{CLOUD}$ = Observer Zenith (referenced to Cloud Patch)
$\theta^{SUN}_{CLOUD}$ = Solar Zenith (referenced to Cloud Patch)
$\theta_{SC}$ = Scattering Angle (Sun-Cloud-Observer)

**Figure C-1. SSGM geometry.**

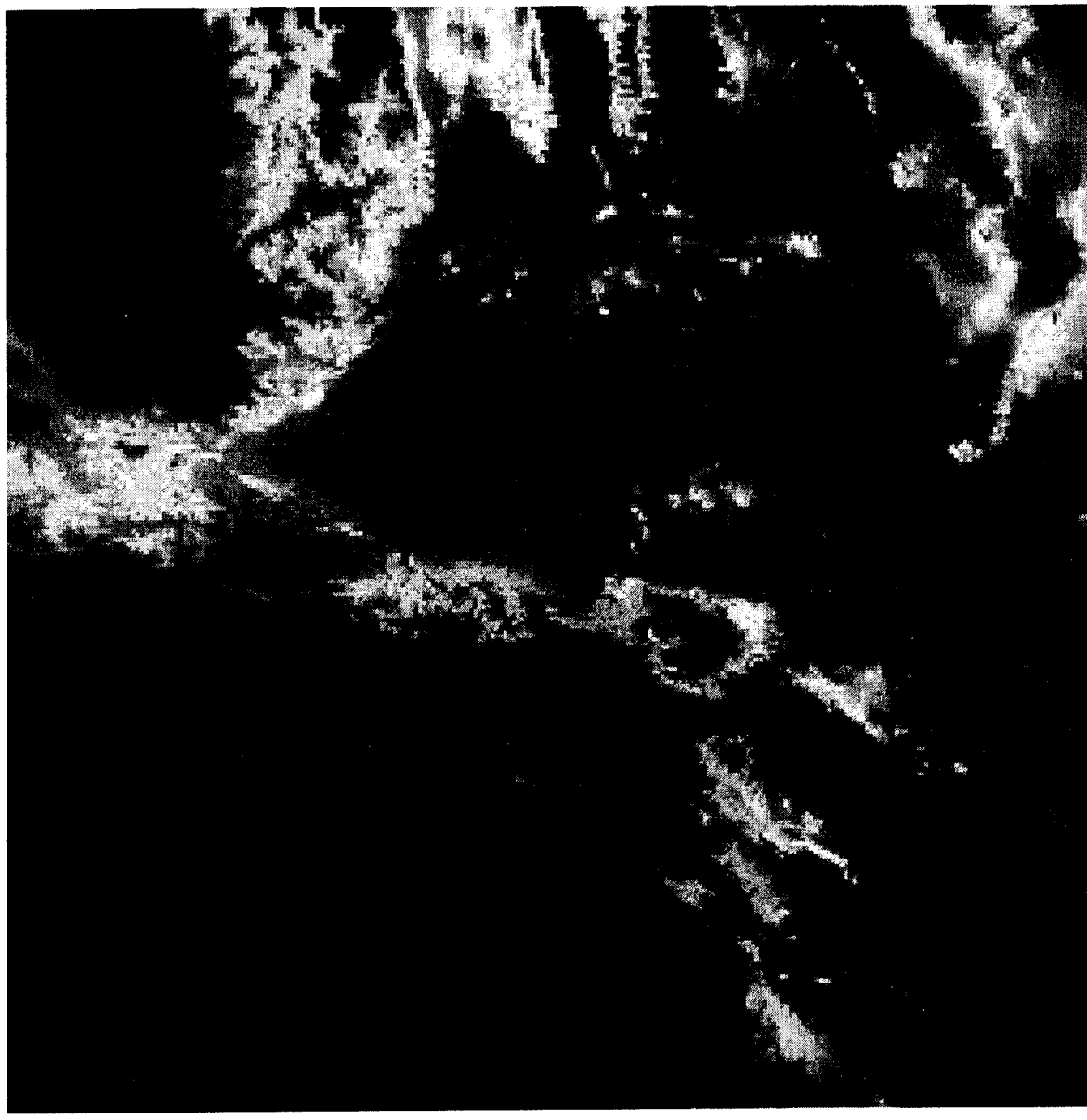

**Figure C-2. SSGM 'land and sea' terrain background.**

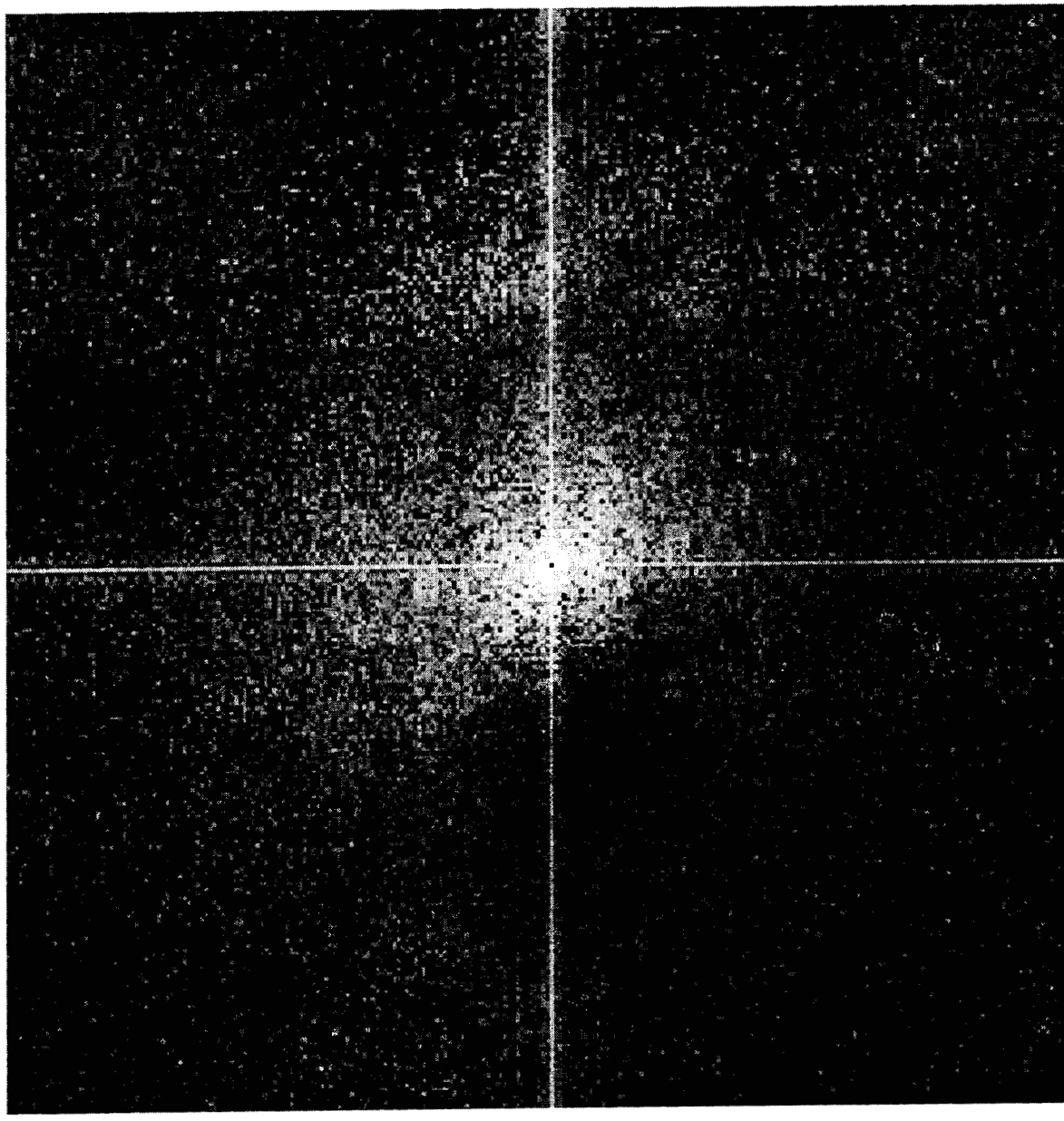

**Figure C-3. Spatial frequencies in 'land and sea' terrain data.**

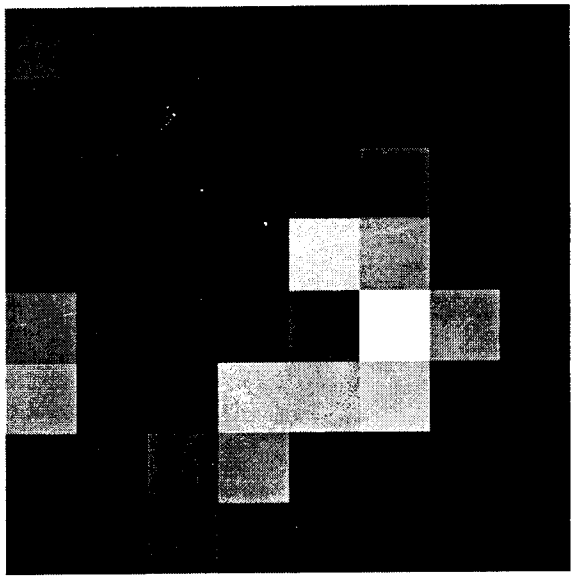

Figure C-4. Sparse data set.

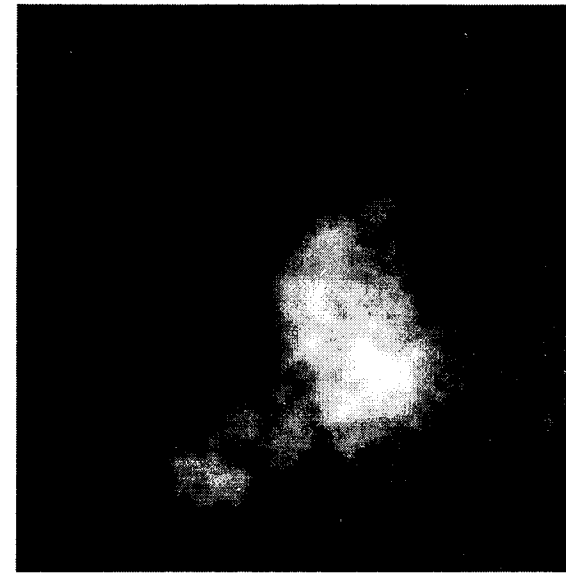

Figure C-5. Interpolated data.

**Table C-1. Current SSGM Database**

| Name | Size Cols/Rows | Resolution, m | Materials Represented |
|---|---|---|---|
| Land and Sea | 1,024/1,024 | 400 | Water, Compacted Soil, Tilled Soil, Sand, Rock, Agricultural Crops, Meadow Grass, Scrub, Pine Forest, Urban Residential |
| Tundra | 1,024/5,000 | 30 | Water, Compacted Soil, Rock, Meadow Grass, Pine Forest |
| Sea Ice | 1,024/5,000 | 30 | Water, Ice, Old Snow |
| Ocean | 1,024/5,000 | 30 | Water |
| Iraq/Syria | 1,024/1,210 | 120 | Water, Varnished Sandstone, Limestone/Silt, Varnished Sand, Dry Silt Playa, Wet Playa, Pure Salt/Silt, Agricultural Crops, Urban Residential, Urban Commercial |
| Iran | 1,024/1,244 | 120 | Wate, Dry Silt/Salt Flats, Wet Silt/Salt Playa, Silt/Sand, Agricultural Crops, Meadow Grass, Scrub, Broadleaf Forest, Pine Forest, Old Snow |
| N. Korea | 1,024/1,024 | 120 | Water, Fresh Snow, Ice, Compacted Soil, Tilled Soil, Sand, Rock, Scrub, Concrete, Urban Residential, Urban Commercial |
| Pakistan | 1,075/1,240 | 120 | Water, Compacted Soil, Sand, Rock, Agricultural Crops, Scrub, Meadow Grass, Pine Forest, Old Snow |
| Kern/River | 128/128 | 400 | Water, Compacted Soil, Tilled Soil, Rock, Agricultural Crops, Scrub, Broadleaf Forest |

# APPENDIX D
# EMULATOR REQUIREMENTS FOR THE DWSG CLOSED-LOOP TEST CONCEPT

M. Tripp

## D1.0 INTRODUCTION

The objective of this document is to provide a general understanding of spacecraft dynamics, a review of existing software and hardware which emulate spacecraft attitude dynamics, and a basic concept for conducting real-time space platform emulation to support a proof-of-principle (POP) demonstration of the closed-loop test concept.

## D2.0 BACKGROUND

Astrodynamics is the field of study which determines the orientation and movement of objects in space; it is broken into two major areas, celestial mechanics (or orbit dynamics) and attitude dynamics. Both of these areas have been studied extensively, and this document will not attempt to recreate the theoretical formulations which are already documented in a number of sources. This document will attempt to establish an understanding of the basic principles governing the dynamics of spacecraft in order to promote the conceptual spacecraft platform emulation described later.

A rigid body in orbit has six degrees of freedom, three of which are associated with the translation of the body's center of mass through space and three which deal with the rotation of the body about its center of mass. A spacecraft which has gimbaled sensors, attitude control wheels, steerable antennas, etc., has additional internal degrees of freedom. The orientation of all these additional items is referenced to the spacecraft primary structure. All motions can be represented using vectorial notation. If a triad of right-handed orthonormal vectors of unit length are used as the frame of reference, the orientation of any single vector (**v**) can be uniquely specified by a set of direction cosines (or Euler angles) between **v** and the chosen reference frame (see Fig. D-1). Although there is not a "standard" frame of reference to which all space systems must adhere, a convenient set of coordinate systems consists of an orthogonal set centered in the Earth and an orthogonal set centered at the center of mass of the satellite. This second set is oriented such that one axis always points to the origin of the Earth-centered coordinates as shown in Fig. D-2. The measurement of the spacecraft platform attitude is provided by sensors on the spacecraft. Optical sensors are used to measure the position of selected stars. Sensors such as inertial or laser gyros continuously measure changes in attitude. However, since over time they exhibit a slow drift, they require a periodic calibration from the reference sensors. The number and accuracy of these sensors

are determined based on the spacecraft mission requirements and the stabilization technique used in the craft's design.

The mission success of the surveillance spacecraft depends on its ability to accurately determine the line-of-sight pointing of the sensors. This in turn requires absolute knowledge of the position and attitude of the spacecraft relative to the reference frame at any point in time. The complex interactions caused by several dynamic systems all mounted on a semirigid platform are not well-formulated. A March 1995 flight of the space shuttle *Endeavour* carried an instrumented small satellite platform called the Mid-deck Active Control Experiment (MACE). This package consisted of a semirigid space platform with a steerable sensor on one end and a scanning sensor on the other. This platform was heavily instrumented. During the space flight the experimental package was released in the shuttle bay area, and data were acquired to determine the interactive modes of motion as the scanning system and the steerable sensors were operated. These data will be used to develop and validate dynamic interactive models. In addition to the interaction of operating sensor systems, the spacecraft also incorporates an active attitude control system which might consist of reaction wheels and attitude control thrusters. The complexity of the attitude control system is directly related to the spacecraft design. While certain basic aspects of the interactions between spacecraft components and the attitude control system (ACS) are straightforward and follow classical theory, there are other areas which are still evolving.

## D3.0 REVIEW OF EXISTING EMULATORS

Modeling of spacecraft attitude control systems is unique to the specific design. A literature search of recent modeling and emulation of spacecraft attitude control revealed that significant efforts are being made to develop accurate models of the various coupling effects associated with spacecraft appendages (antennas, solar panels, etc.). There are certain models of the basic functions of attitude control which are accepted and used by many ACS designers, but a generic model incorporating all the aspects needed to define any type of ACS was not found. Emulation of an ACS using hardware was also unavailable from the literature search. However, discussions with Air Force laboratories and industry disclosed work being conducted by Rockwell, Integrated Systems, Inc., and Boeing to develop such a capability.

Boeing is currently developing a sensor system simulation capability which incorporates simulation of the sensor, scene input phenomenology, and processing algorithms. While it would be advisable to maintain contact with their development, there does not appear to be an application for these simulators in the closed-loop test capability under development at AEDC.

Rockwell is developing a hardware emulator for the Kinetic Hardware in the Loop Simulation (KHILS) facility using a combination of parallel processors combined into a miniature multichip

module (MCM). A number of government and industry facilities are evaluating these processors developed by Rockwell. The current status of the KHILS emulator and its capabilities are unknown at this time. This approach for developing a processor to emulate the ACS should be evaluated further. In conversations with Rockwell personnel, it was stated that the lead time for fabricating an MCM for a specific closed-loop test capability is on the order of three years. Follow-up evaluation of this emulation approach will be conducted as work progresses.

Integrated Systems, Inc. has developed a versatile combination of software and programmable hardware which appears to have the potential for building a first-phase platform emulator. However, the expense of purchasing, developing, and maintaining this product is beyond the scope of our current effort. This approach to developing a platform emulator in the closed-loop test concept should not be abandoned. If resources become available, this system should be acquired for further evaluation.

This review of current emulation capability did not provide an existing software or hardware approach appropriate for our near-term POP demonstration. It did, however, uncover two hardware approaches which have the potential for building an emulator capability. Both approaches will require considerable resources in materials and manpower to develop and implement.

## D4.0 NEAR-TERM POP EMULATOR CONCEPT

Demonstration of the feasibility of the closed-loop test capability requires an affordable near-term solution. Our approach to satisfying this requirement is to model a system consisting of two coupled rigid bodies.

Currently, the line-of-sight pointing vector for the sensor is provided from a computer mouse which is manually manipulated by an observer. This is being used to assist in the development of the real-time scene rotation and translation algorithms needed by the DWSG projection electronics. The second step in the POP demonstration process is to build a satellite emulator which will model a rigid body platform on which is mounted a gimbaled sensor. In this system, the sensor gimbals will be programmed to step-stare as the satellite travels in its orbit. The sensor line-of-sight from the resultant motions of the two-body coupled system will be used to define the pointing vector for the input scene frames to the sensor.

## D5.0 SUMMARY

A concept for incorporating a real-time emulation of the satellite platform has been defined. A literature survey and capabilities search has indicated that there are no off-the-shelf capabilities for the types of emulators needed for the closed-loop test capability we envision. Two promising

approaches to developing a real-time emulator were found. One has a long lead time for the development of modular chips and the resulting processors; the other is too expensive for this program at present. A low-cost approach for providing a demonstration of the emulator concept has been defined and is being developed.

$c_i = \cos\theta_i$

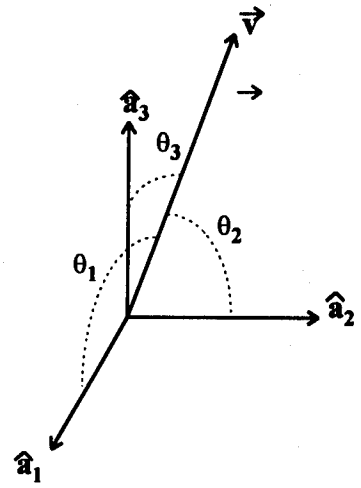


$\vec{v} = v(c_1\hat{a}_1 + c_2\hat{a}_2 + c_3\hat{a}_3)$

**Figure D-1. Direction cosines between v and a frame of reference.**

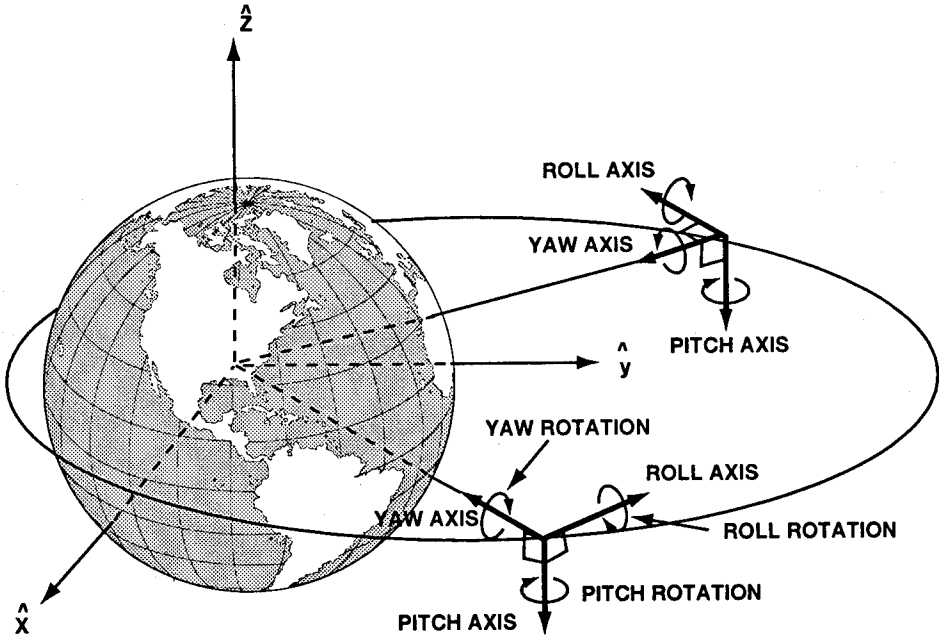


**Figure D-2. Reference frame coordinate system.**

# APPENDIX E
# DEVELOPMENT OF ALGORITHMS FOR SCENE MANIPULATION

S. L. Steely

## E1.0 INTRODUCTION

This appendix provides a synopsis of recent technology efforts at Arnold Engineering Development Center to provide real-time closed-loop image synthesis for the Focal Plane Array Test Capability (FPATC). Laser-based Direct-Write Scene Generation (DWSG) methods are used to simulate dynamic sensor operation and complex infrared scenes. New photonic image synthesis methods are being developed to employ image-to-object Whittaker-Shannon sampling, anisoplanatic optical convolution by quasi-isoplanatic spatial decomposition, and high-speed digital electronics for acousto-optic modulation. The development of the high-speed digital electronics is described in Appendix F. Recent research and technology efforts at AEDC provide new capabilities for laser-based DWSG (see Refs. E-1 – E-6).

High-speed photonic processing is required for closed-loop operation and simulation of dynamic and interactive sensor commands that reposition the sensor's field of view within the field of regard, and for high-fidelity simulation of optical blurring and temporal effects such as jitter. The real-time CLDWSG method requires that a number of operations be performed within the framing rate of the focal plane array of the sensor. These operations include selection and transfer of the scene background field of regard, calculation and inclusion of target intensities and positions, rotation and translation of the composite background and target scenes to simulate interactive sensor-pointing commands, simulation of sensor and satellite jitter, simulation of optical blurring resulting from aberrations and diffraction for broadband spectral radiation, integration of the photon flux over each FPA pixel element, FPA pixel responsivity calibration, and compensation for AO-cell optical modulation inefficiencies. Because of the large terabyte volume of data to be processed, the increased bandwidth requirements, and the increased simulation fidelity required for DT&E and OT&E of FPA sensors, the laser-based DWSG methodology is being extended to accommodate optical and computational decomposition methods to better exploit highly and massively parallel real-time image processing schemes.

## E2.0 RADIATION SOURCES

New DWSG photonic image synthesis methods are being incorporated to provide more realistic optical simulations with either real or synthetic scenes. These photonic image synthesis methods can more accurately generate and represent temporal power spectral densities and spatial Wiener spectrums for complex background and target scene simulations that are more

representative of scenes and convolved FPA images anticipated in and typical of real-world FPA sensor operation.

FPA sensor evaluation, modeling, and simulation ultimately depend on the mission and objectives of the electro-optical FPA sensor system and a sensor's modes of operation. Some emphasis is being devoted to understanding the mission, background and target phenomenologies, object-to-image mappings, scene distortions resulting from 3-D to 2-D radiance mappings from space to sensor FPA coordinates, temporal variations, etc. The "reality" or "truth" of any validation and verification effort has to be cast in context of the intended purpose and use of the sensor being evaluated.

Furthermore, no absolute truth table or matrix exists to determine or provide "absolute" scenes. In generation, detection, and simulation there are and will be natural photonic fluctuations and spatial/temporal variations that are necessary to provide the inherent fluctuations anticipated in real-world engagements. There are many stochastic and quasi-periodic fluctuations that cannot be simulated absolutely/exactly. Scene simulation and detection validation should be based on a statistical ensemble, instead of any concept of absolute scene "truth" data. Any potential object scene is then considered as one sample from an ensemble of possible scenes that represent the stochastic statistical population. Scene "truth" is then a relative measure of the ensemble mean, variance, and higher-order moments that ultimately describe the population's probability distribution. Accurate signal-to-noise simulations are therefore needed to judge the success or failure, not of any single event, but of an ensemble of detection events that can be described by the normal laws of stochastic processes and related detection criteria (probability of detection, probability of false alarms, etc.).

## E3.0 SENSOR VIEWING CONSIDERATIONS

To better understand potential methodologies being considered for closed-loop DWSG operation, a number of concepts will be briefly discussed to provide an overview of some basic principles being considered and evaluated. A sensor's geometry for above-the-horizon or below-the-horizon viewing is illustrated in Fig. E-1. The background and targets detected by a sensor will generally depend on the sensor's field of regard and the sensor's field of view, both of which can be time-dependent semi-deterministic processes or stochastic processes. Typical orbital positions will vary the field of regard that is viewed from space-based sensor systems, and corresponding background-to-FPA and target-to-FPA mappings have to be taken into consideration. In addition, differences resulting from using different wavebands for normal sensor operations in atmospheric absorption bands or ransmission windows of interest must also be accommodated. The background and target radiance levels reaching the sensor depend not only on the emission or scattering properties of the sources, but also on the transmission of the intervening medium such as the atmosphere and clouds.

A sensor's spatial location and relative orientation help to determine the field of regard, as illustrated in Fig. E-1. A 3-D geometry of space can be viewed as being either functionally or optically mapped onto a sensor's FPA, as illustrated in Fig. E-2. One can either think of the background and targets within the field of regard as being projected onto the FPA, or as the FPA being projected into the 3-D space as illustrated in Fig. E-3. A set of radiance field-of-regard mappings for selected orbital parameters can then be viewed as two-dimensional mappings onto an extended FPA and could, in principle, be precomputed or preselected for typical orbital parameters. The individual sensor FPA image frames could then be processed to include optical effects for time-dependent pointing vectors within the field of regard.

## E4.0 OPTICAL EFFECTS AND IMAGING

Sensor imaging of quasi-monochromatic, thermal, or blackbody sources generally depends on the theory of partial coherence. In many cases this generalization can be simplified to one of the two extreme cases of partial coherence, either totally coherent or totally incoherent, with the understanding that it is an approximation with known errors acceptable for the intended purpose of modeling and simulation. Neither of these two extremes (coherent or incoherent radiation) exists completely for real sources which are always partially coherent to some degree and also partially polarized. Thermal or blackbody sources are normally modeled using the simple incoherent superposition assumptions for adding or integrating the statistically independent object sources to obtain the integrated images with very good approximations to the "real world" for many cases. Each case is normally evaluated on an individual basis to ensure that the assumptions and simplifications are indeed representative of real-world engagement "reality."

Imaging and photodetection, as illustrated in Fig. E-4, follow the laws of optical diffraction. In addition optical components are not perfect. Therefore the images of "point" sources are not "point" sources because of the inherent wave-nature of photons and resulting diffraction and aberration effects. As a "point" source is moved within the field of view of a sensor, the corresponding image of the "point" source may noticeably vary, depending on the wavelength and the degree of aberrations present. For practical purposes, many optical systems can be considered spatially invariant and the image blur or point-spread function does not vary as measured, and, for a given wavelength range, the optical system can be considered diffraction limited. In other cases, there may be considerable distortions and variations in the point-spread function resulting from optical aberrations which must be considered. The optical components effectively map the object plane onto the image plane with potential aberrations, blurring, distortions, magnification, or minification, etc., that transform the object into the image. If one can compute this transformation function, then the image can be accurately determined and properly simulated. Simulations should consider the nature of the sensor mission, any integrated detector effects, and the corresponding algorithms. Verification and validation methods should be applied to ensure that the simulation is relevant for the intended purpose.

There are a number of concepts and methods for determining a sensor's point-spread function (PSF) or its OTF (see Appendices A and B). A sensor's image and the FPA's integrated photoflux can then be determined by basic integration methods or, for near spatially invariant FOV regions, by convolution methods or by way of the convolution theorem using OTF frequency-domain methods as illustrated in Fig. E-5. The method chosen depends on the desired fidelity as well as the computational performance desired. As with any computational/scientific model, these methods have inherent assumptions and simplifications. These have to be understood to provide a quantitative method to account for and potentially accommodate any resulting errors.

A geometrical point source is imaged into a diffraction pattern. Only as the geometrical image size increases relative to the PSF dimension do we see any structure or effects of the shape/size of the "point" source. Only after the geometrical image dimension increases to on the order of magnitude of the Airy radius do we even see the effects of its shape and size. Even square sources or arbitrary source shapes appear to be "point" sources when their maximum geometrical image dimension is small compared to the PSF dimension. The spatial and structural features are not observed until the geometrical image dimension is on the order of magnitude of the optical system's PSF dimension. In the frequency domain, one says the high-frequency content is stripped off and the image does not have sharp edges or discontinuous spatial features. If a small square's diffracted image has the same PSF as that produced by a small circular source, they can be indistinguishable. Under some circumstances we can then conceivably simulate images with sources that are distinctly different, yet yield the same effective image as detected by the FPA. Using the Whittaker-Shannon sampling theory, we can even use an array of sources that generate the same irradiance pattern if intensities are properly selected for OTF-filtered, bandwidth-limited optical images.

One distinct feature of the process of convolution is that when the point-spread function is "small," the image and object can be very similar. The image is also said to be of high fidelity when there are few or no aberrations present. In the limit of aberrationless, linear, shift-invariant, delta-function PSFs, the image will be an "exact" duplicate of the object scene (an idealism). As the point-spread function increases in relative dimension, the image will lose much of its clarity and fidelity; considerable differences between the object and the image can result. In the limit of very large PSFs, the image will blur into a uniform irradiance pattern with near-zero information content or modulation (maximum entropy), especially when the PSF's dimension is large compared with the largest geometrical image features present.

In the realm of Fourier optics, the object and PSF convolution can be viewed as a filtering process. With this perspective, the object is viewed in the frequency domain and the OTF filters or attenuates the high-frequency components (amplitude and phase) of the object scene, resulting in a low-frequency image. For incoherent imaging and when the geometrical image's spatial frequency is on the order of magnitude of the reciprocal of half the PSF dimension, then the contrast or modulation

reduces to zero and the image details or information is lost. Any spatial frequency beyond the cutoff frequency of the optical system will be attenuated in the image plane. The high-frequency details are essentially filtered out by the optical sensor's low-pass, spatial-frequency OTF.

## E5.0 ANISOPLANATIC OPTICAL SYSTEMS

For our applications, the scene and FPA are quantized into small grid-sampled regions (as illustrated in Fig. E-6) in order to perform the integrated image and detector photoflux computations. The degree or level of sampling needed for a scene and FPA combination depends on the desired DWSG simulation fidelity.

For optical scene simulations requiring real-time closed-loop operation, the satellite/sensor interactively updates the line-of-sight pointing vector relative to the sensor's position in space and to the background field of regard. To incorporate and support interactive CLDWSG operation and to accommodate simulation of nonuniform anisoplanatic optical systems, the scene is decomposed into quasi-isoplanatic regions for narrow spectral bands, as illustrated in Fig. E-7. For this method, the scene is decomposed into segments that allow application of direct convolutions or OTF methods via the convolution theorem for regions of quasi-isoplanatic patches. The spatial decomposition not only provides for improved optical fidelity in simulating anisoplanatic sensor optics, but also provides a method to decompose and compute the scene segments in parallel. When these methods are used, it is important to examine the effects of spatial decomposition and to mitigate edge effects, diffraction loss, etc., while at the same time providing anisoplanatic optical simulation.

With the scene decomposed into quasi-isoplanatic regions, one can use either direct methods or the convolution theorem for image computation and synthesis. For broadband radiation, effective PSFs can be used when sample points have the same relative spectral distribution. When there are regions in the scene that have considerable variation in spectral content (from region to region), then one could employ complete spectral decomposition and image synthesis for effective photon flux.

Spatial FOV decomposition, computation, and synthesis of the object/image scene provides a useful method that facilitates multiple PSFs to be used to determine and directly simulate an anisoplanatic optical system. Figures E-8 and E-9 illustrate that the spatial decomposition and computational methods may lead to anomalous computational artifacts resulting from simulated diffraction/PSFs, sampling, and other windowing effects. Various methods to improve the optical simulation and to mitigate computational artifacts have been investigated and illustrated in Fig. E-10. In these examples, extended domains help to improve the simulation fidelity and subsequently improve experimental testing results. Figure E-11 illustrates the improvement

obtained from using extended computational domains to simulate anisoplanatic optical aberrations with a reduction in computational artifacts and related errors.

For direct computation methods, the image is integrated over each FPA pixel element to determine the number of photoevents for each frame. However, the integrated detector photoflux can be viewed more generally as a convolution of the image irradiance with a detector, as illustrated in Fig. E-12. The detector convolution can then be computed directly, and integrated photoflux values can be obtained from the respective grid-point locations as desired, or arbitrary detector repositioning can be introduced to simulate perturbations in the detector's position, row offsets, alignment errors, etc.

For many applications and missions, a sensor will be detecting broadband radiation, and one needs to account for the spectral distribution of radiation as well as the spectral response of the sensor system. The PSF and OTF can vary considerably due to broad spectral distributions (see Fig. E-13). Also, there are other blurring effects such as jitter which vary the image considerably in real systems. When we introduce aberrations and polychromatic or broadband radiation, the total detectable irradiance on the FPA will deviate from the simple, deterministic one-case PSF/OTF normally used for simulation. However, in practice, a composite PSF from a polychromatic point source imaged with optical aberrations and vibrational blur can be approximated with a two-dimensional Gaussian-distributed PSF, as illustrated in Fig. E-14.

To help diagnose, investigate, and simulate the effects of potential real-time closed-loop DWSG operation that includes optical diffraction and aberration effects, a PC-based program has been developed. An example of the program's output using the OTF method for simulation is illustrated in Fig. E-15.

## E6.0 SUMMARY

To provide more optimized optical simulation fidelity and to reduce computational burdens, closed-loop DWSG image synthesis methods are being developed which employ image-to-object Whittaker-Shannon sampling, anisoplanatic optical convolution by quasi-isoplanatic spatial decomposition, and high-speed digital electronics for acousto-optic modulation. Optical and computational decomposition will not only provide high-fidelity optical simulation for anisoplanatic optical sensors and complex infrared scenes, but will also facilitate high-speed parallel processing schemes for real-time closed-loop DWSG and sensor operations. A computer testbed has been constructed and is being used to develop and evaluate the high-speed computational algorithms required for scene extraction and convolutions. This technology effort helps to provide new optical diagnostics for cost-effective and systematic DT&E and OT&E of large FPA sensors using parametric and statistical methods not amenable to costly field or flight testing methods.

## REFERENCES

E-1. Lowry, H. S., Tripp, D. M., and Elrod, P. D. "Current Status of Direct Write Scene Generation at AEDC." *SPIE Orlando Conference Proceedings*, April 1994.

E-2. Lowry, H. S., Tripp, D. M., and Elrod, P. D. "Equivalence of FPA Response to Continuous and Pulsed Laser Radiation." *SPIE Orlando Conference Proceedings*, April 1994.

E-3. Steely S. L. "Laser versus blackbody photostochastic fluctuations." *Annual OSA Conference Proceedings*, Vol. 16, October 1993.

E-4. Steely, S. L. "Aspects of laser versus blackbody photodetection: coherent versus thermal-source photonic fluctuations." *CLEO Conference Proceedings*, May 1994.

E-5. Steely, S. L., Lowry, H. S., Fugerer, R. H., and Elrod, P. D. "Real-Time Anisoplanatic Convolution Methods for Laser-Based Scene Generation: Closed-Loop Focal-Plane-Array Test and Evaluation Methods." *SPIE AeroSense Orlando '95 Conference on Targets and Backgrounds: Characterization and Representation*, Paper No. 2469-05, April 1995.

E-6. Steely, S. L., Lowry, H. S. and Tripp, D. M. "Aspects of Laser Versus Blackbody Photodetection: Laser-Based Photonics for Focal-Plane-Array Diagnostics." *SPIE AeroSense Orlando '95 Conference on Targets and Backgrounds: Characterization and Representation*, Paper No. 2469-35, April 1995.

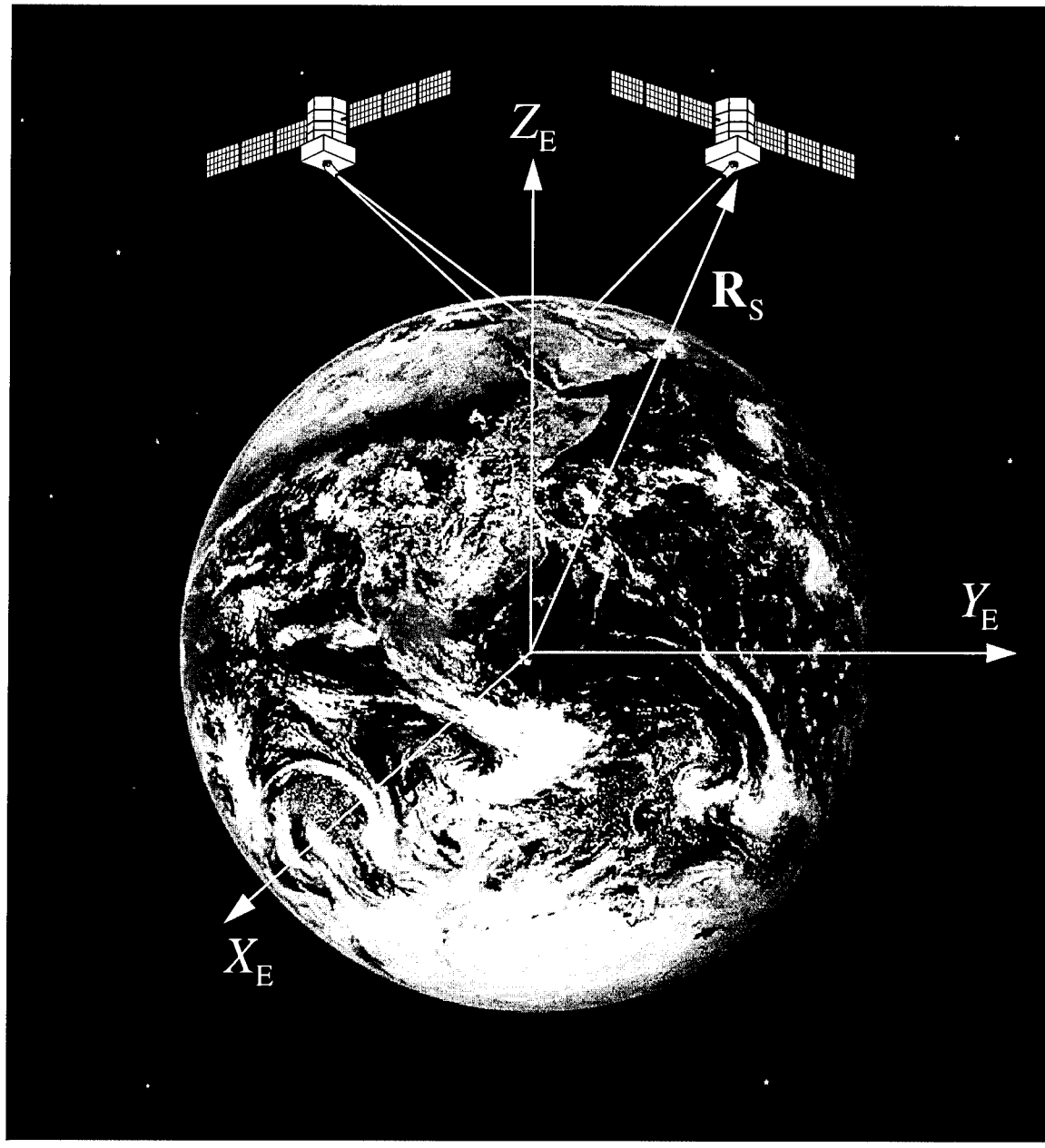


**Figure E-1. Multisensor perspective and simulation will depend on mission as well as on environmental and operational characteristics.**

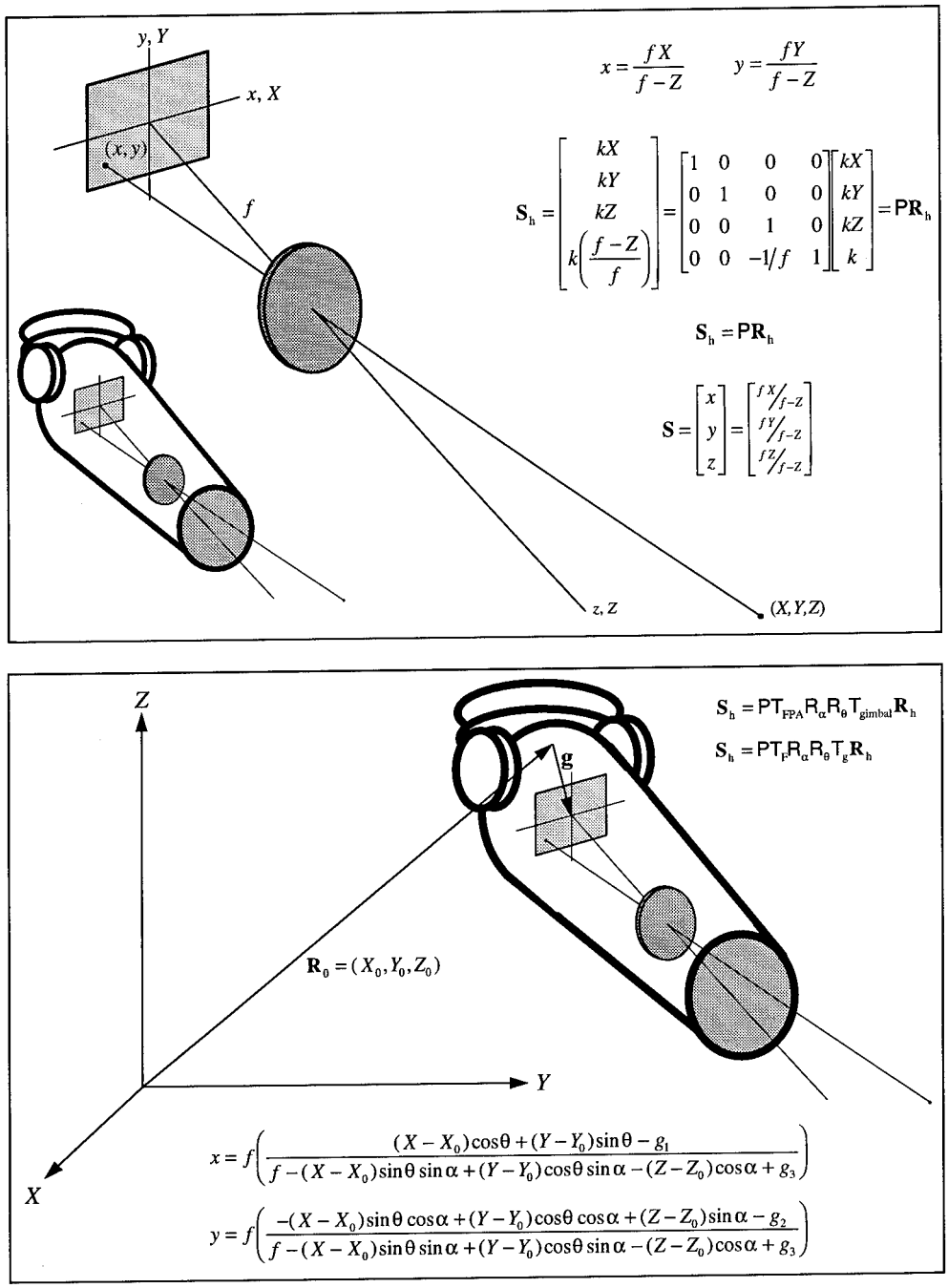


**Figure E-2. Illustration of a 3D-to-2D spatial mapping of space-based backgrounds and targets onto the FPA for DWSG optical simulation efforts.**

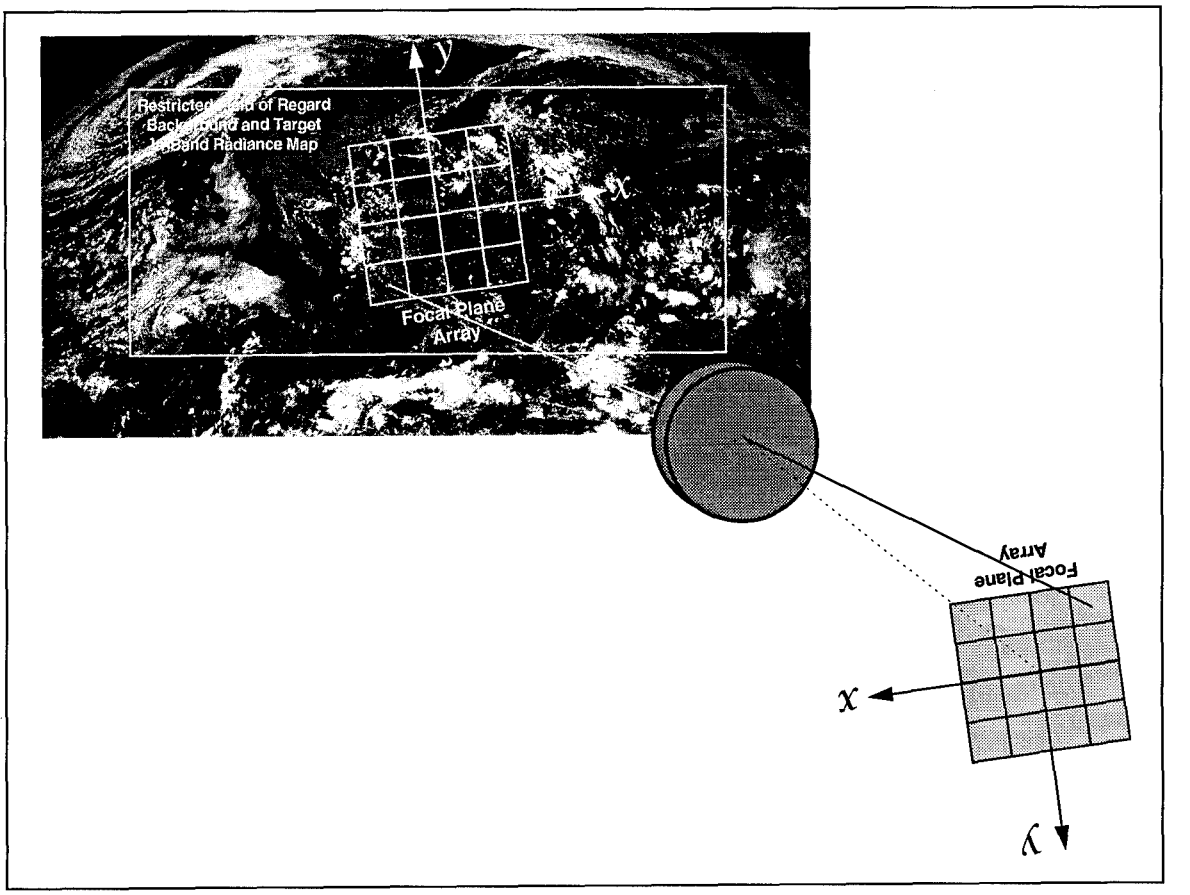


**Figure E-3. Concept illustration of the scene being mapped onto the FPA, which could also be usefully viewed as the FPA field of view being mapped onto the 2-D projection of the background and target scene.**

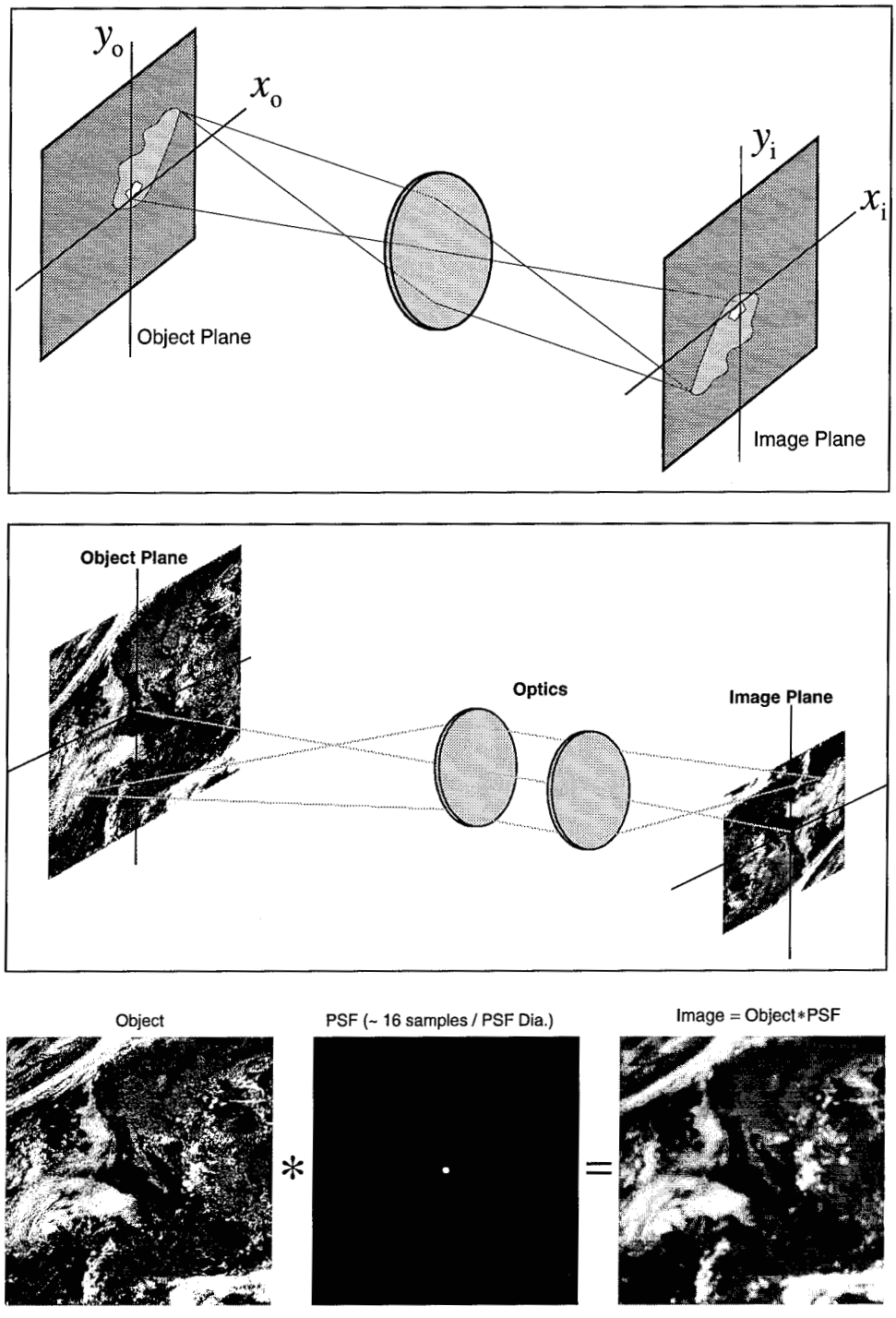


**Figure E-4. Illustration of the object plane being transformed to the image plane for FPA irradiation via the optical system for a simple background and target map.**

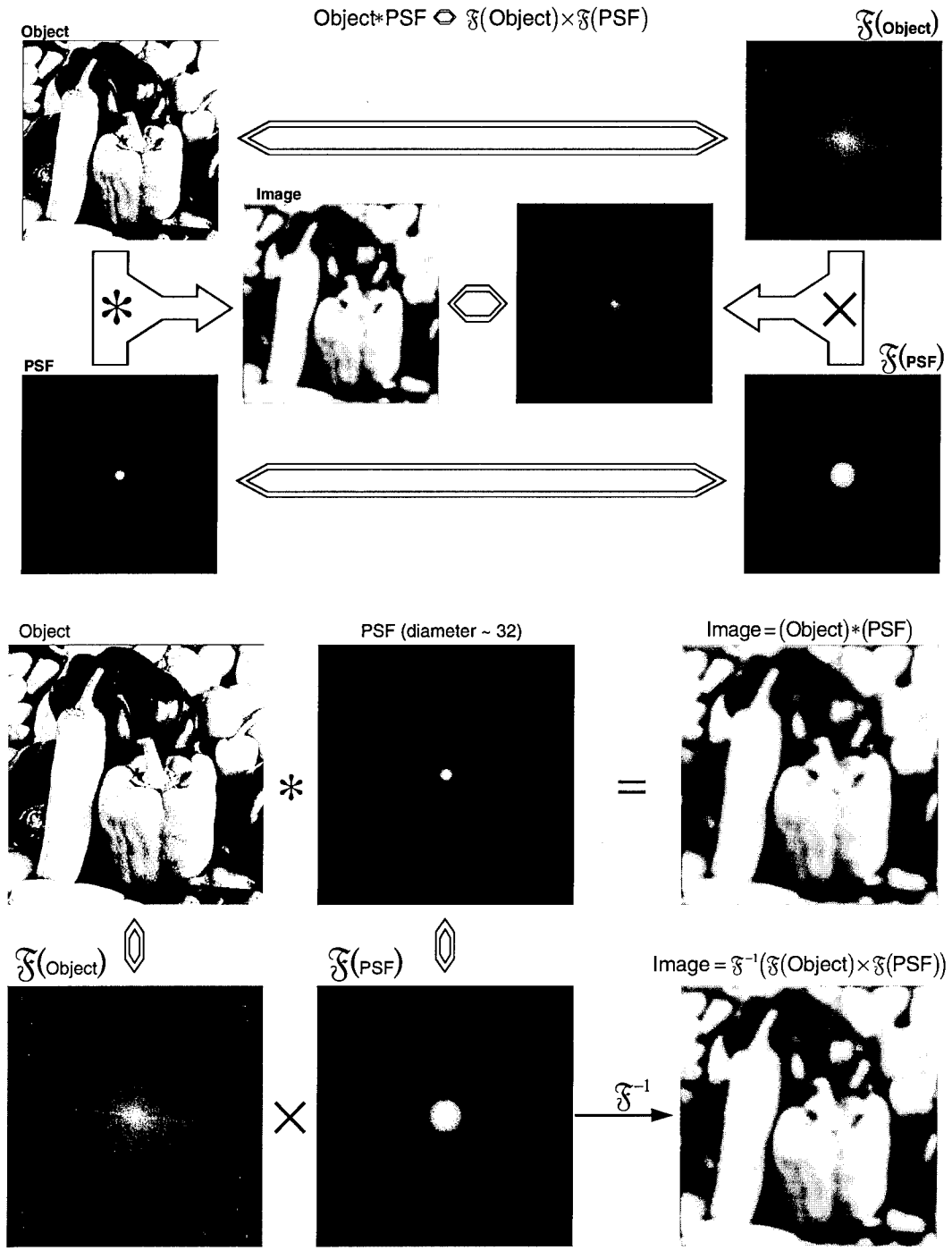


**Figure E-5. Optical convolution can be accomplished by either direct methods or by indirect FFT methods using the convolution theorem and the OTF of the sensor system (the method chosen depends on computational/photonic speed as well as fidelity issues/trades).**

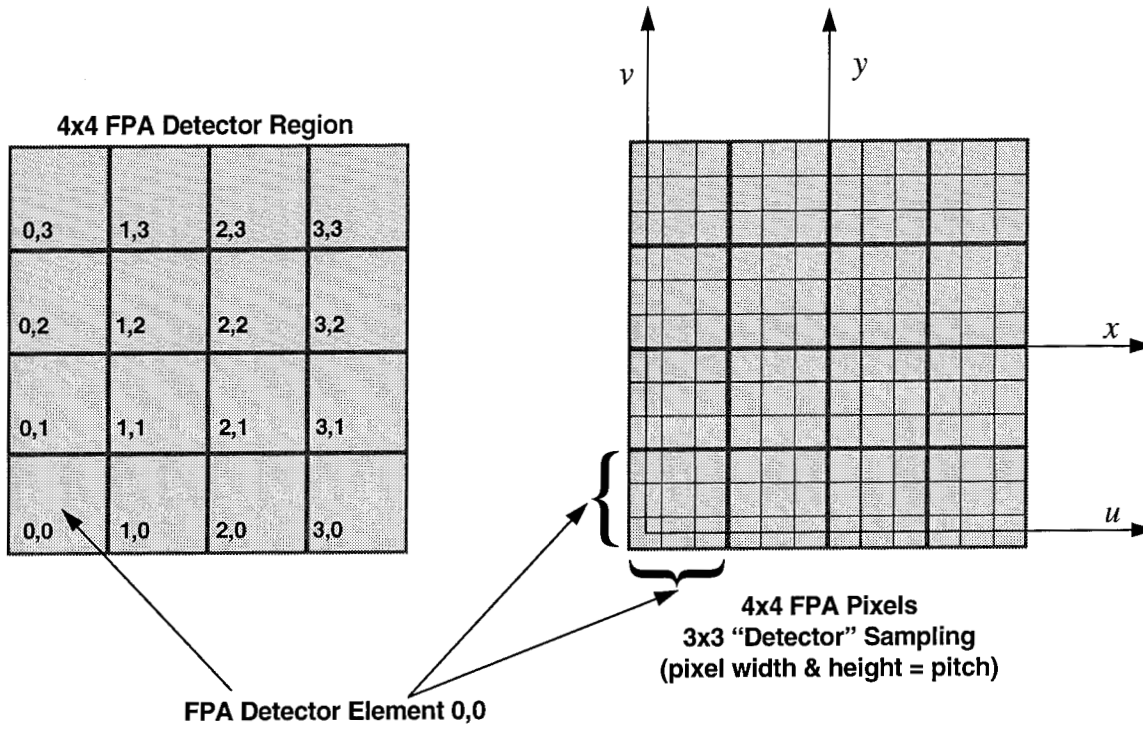


**Figure E-6. Background, target, and FPA sampling provide efficient and flexible computational schemes for scene extraction and image convolution by employing Whittaker-Shannon sampling ideas.**

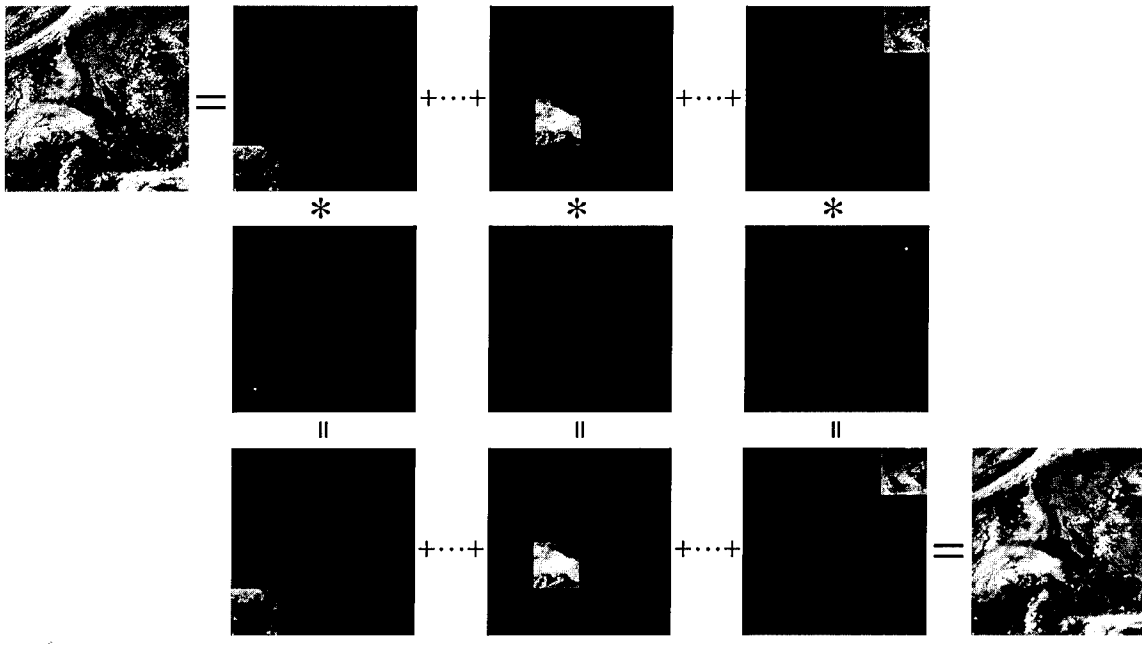

**Figure E-7. Illustration of a spatial decomposition method to support anisoplanatic optical simulation that could also support parallel and massively parallel processing schemes for the laser-based DWSG photonics.**

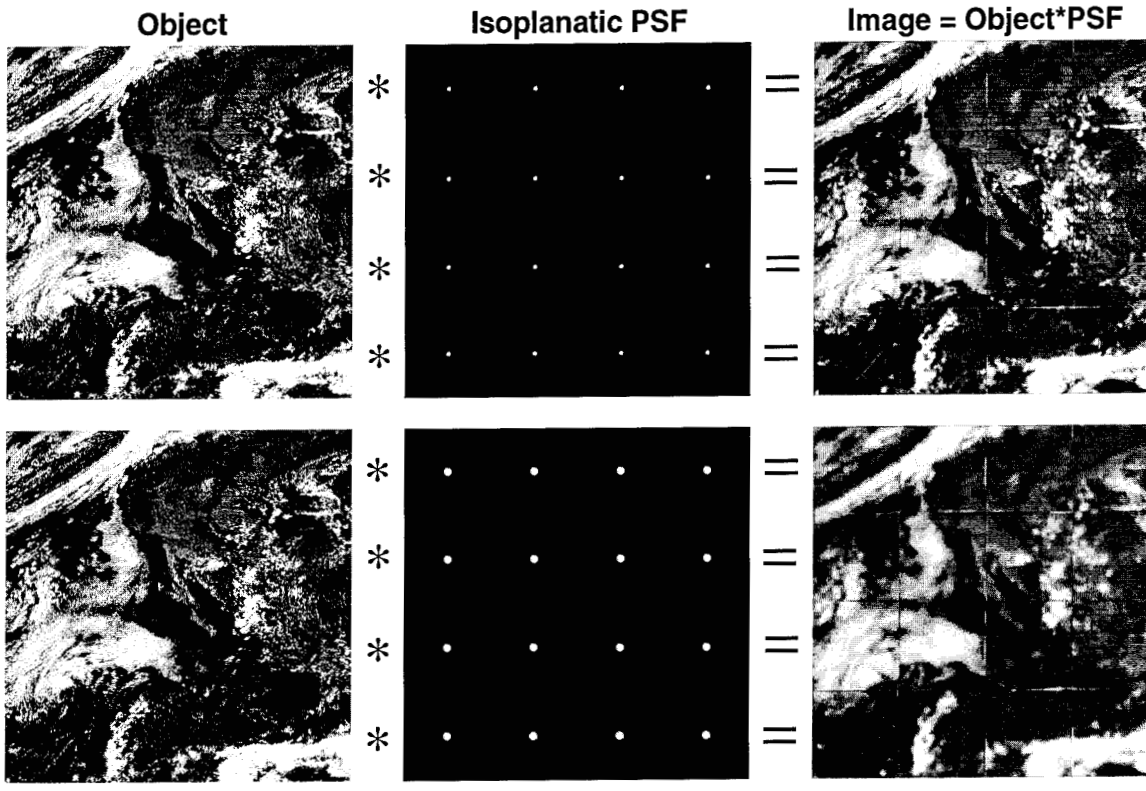


**Figure E-8. Illustration of a 4x4 optical decomposition to support parallel processing schemes and anisoplanatic optical simulation without any regard for diffraction effects/loss, spectral leakage, etc.**

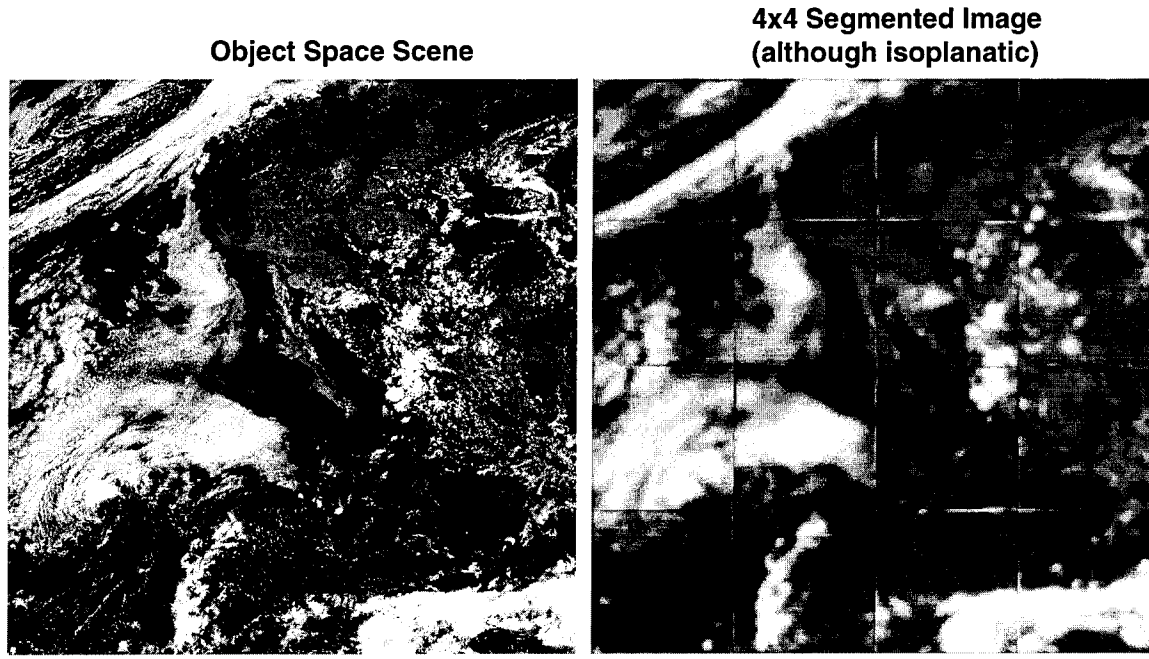


**Figure E-9. Illustration of potential simulation artifacts that can result from decomposition methods that fail to account for diffraction effects, spectral leakage, etc.**

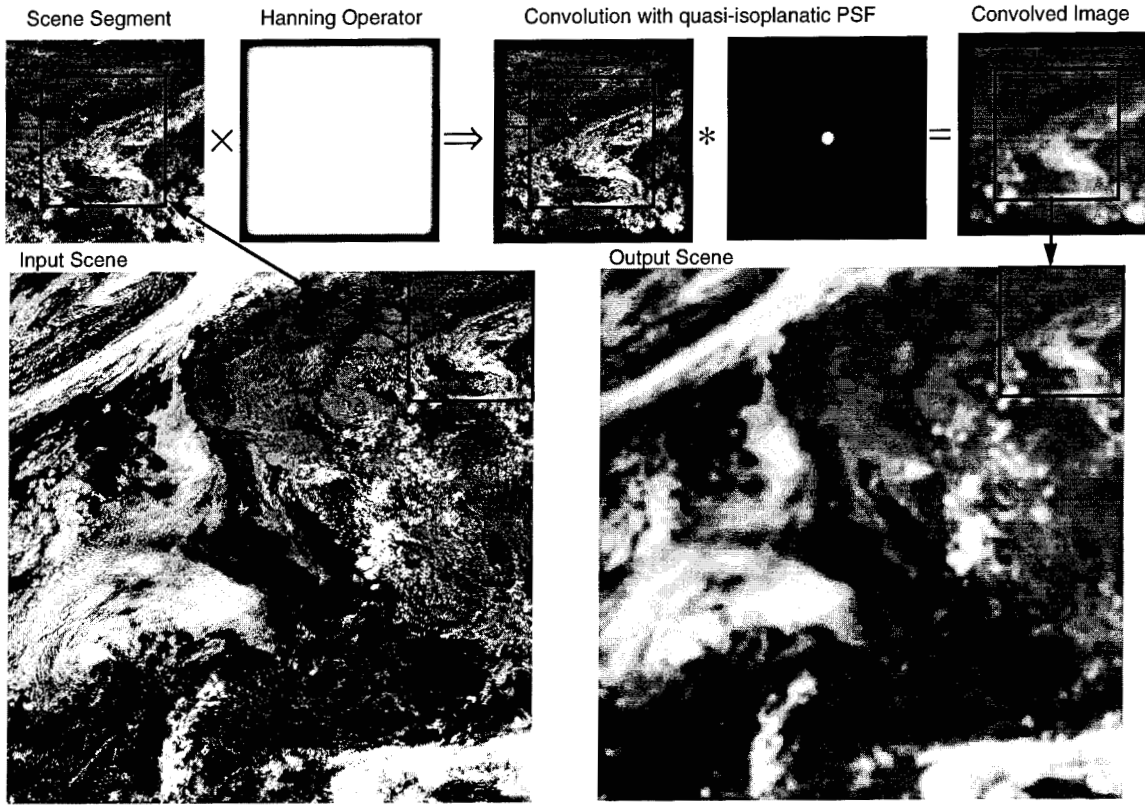


**Figure E-10. Methodology for using extended computational regions to not only support anisoplanatic decomposition for better fidelity and simulation, but to also support real-time closed-loop parallel processing schemes.**

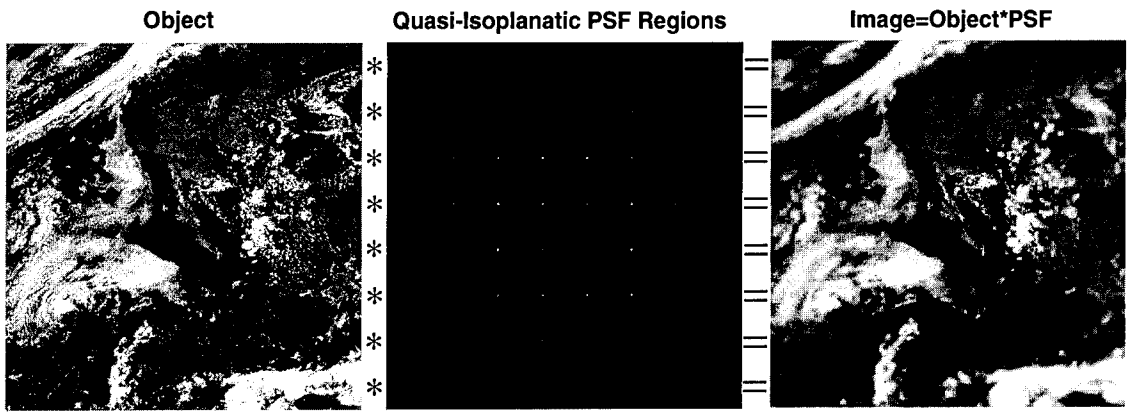


**Figure E-11. Illustration of a decomposition method to arrive at the composite field of view for an anisoplanatic optical system being simulated in the laser-based DWSG scene generation methodology.**

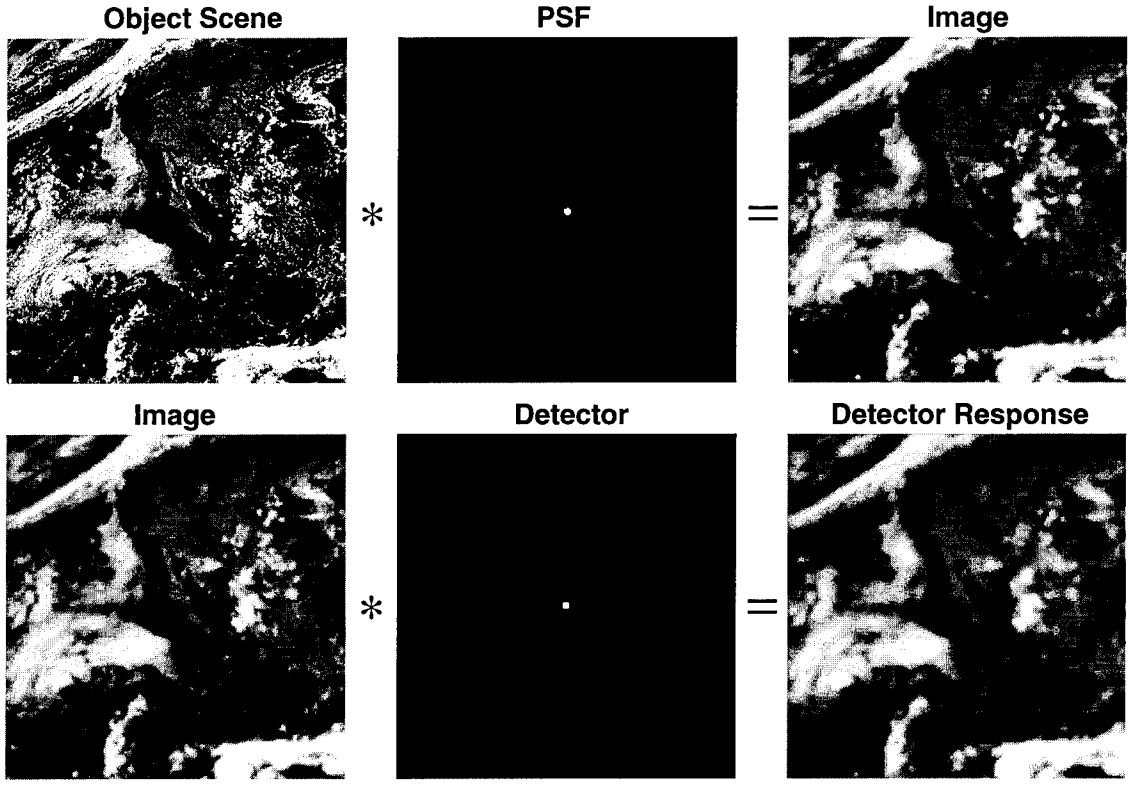


**Figure E-12. Illustration of methodology to derive the integrated photoflux from a double convolution process that can be accomplished from a more efficient system transfer function operation and application of the convolution theorem.**

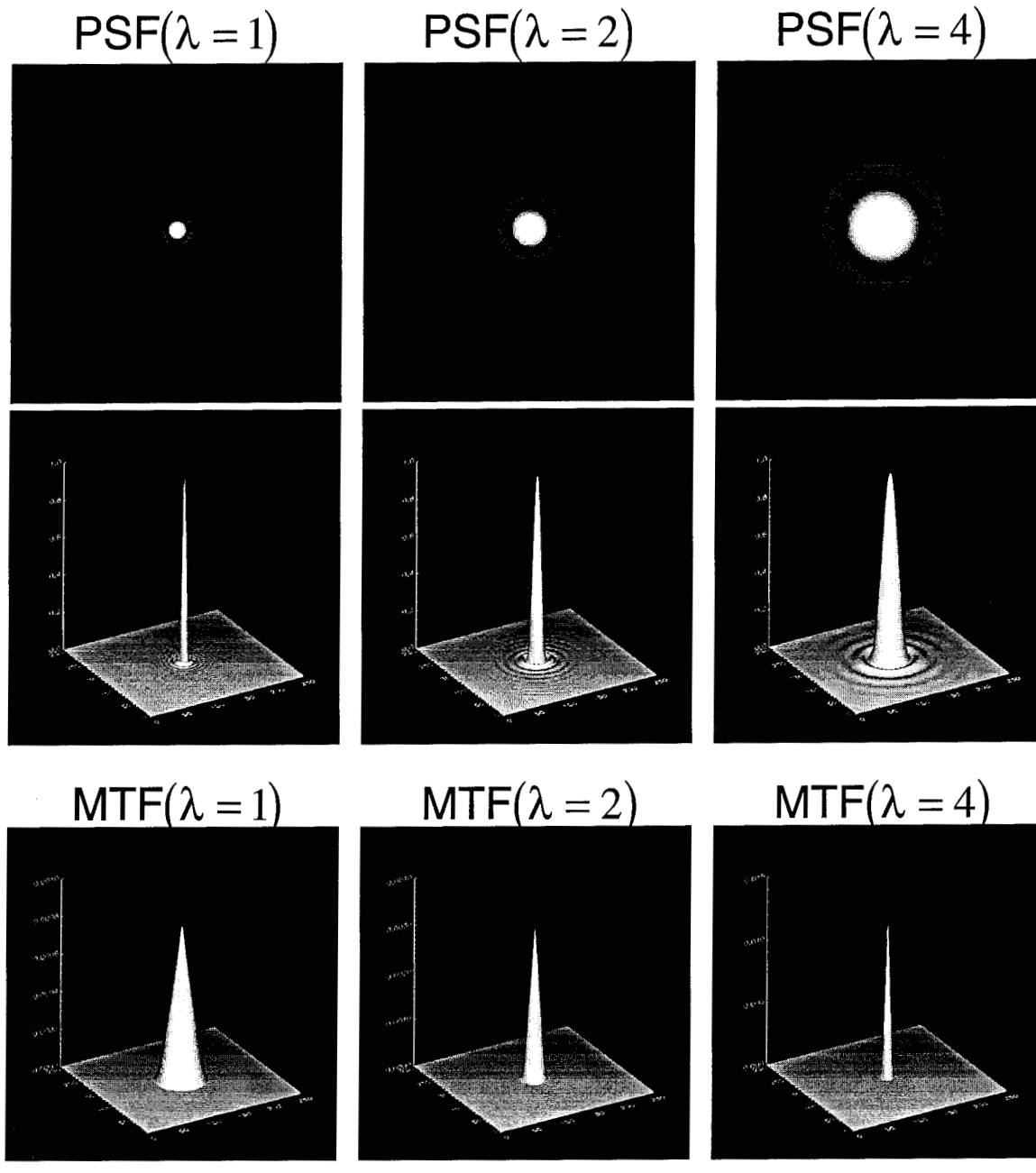


**Figure E-13. Illustration of the effects of wavelength-dependent variation of the PSF and optical cutoff frequency as seen in the magnitude of the OTF (modulation transfer function, MTF).**

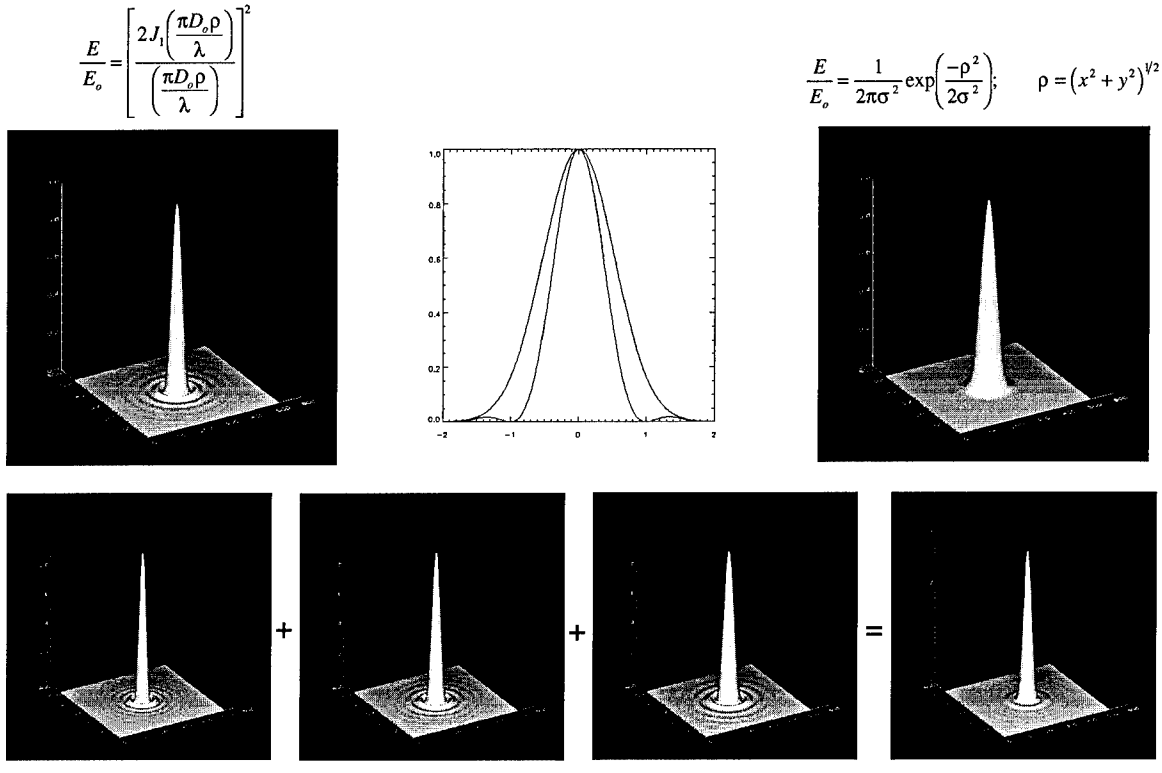


**Figure E-14. Illustration of the concept of an effective PSF resulting from a number of contributing sources such as broadband radiation, optical diffraction, deterministic and stochastic jitter and resulting blur, or other sources.**

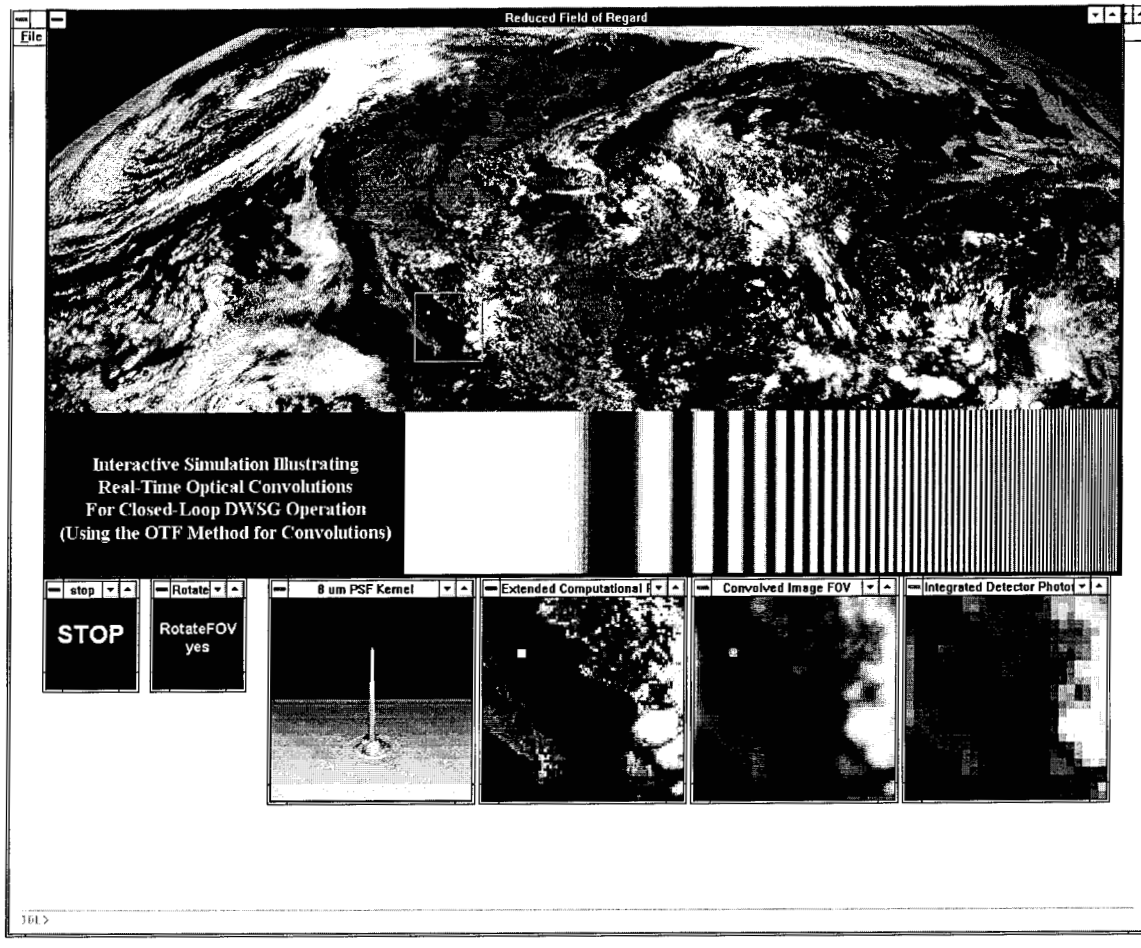


**Figure E-15. Example of the screen of the closed-loop simulator for algorithm development, diagnostic efforts, and demonstrations.**

# APPENDIX F
# SIGNAL PROCESSING REQUIREMENTS FOR CLOSED-LOOP TESTING

R.H. Fugerer

## F1.0 INTRODUCTION

This appendix describes the current methodology and status of the work to provide real-time and closed-loop scene manipulation methods using AEDC's FPATC signal processing systems. Figure F-1 shows the current FPATC open-loop capability using the Direct Write Scene Generator (DWSG) with emphasis on the electronics which drive the system. In this configuration, test scenarios are played into the sensor under test, and then captured at the sensor's output. Note that there is no feedback between the radio frequency (RF) electronics that control the projection of the scenario from the disk farm memory and the data acquisition electronics that capture and store the sensor output.

## F2.0 CLOSED-LOOP CONCEPT

Figure F-2 shows the changes to the open-loop hardware configured for the closed-loop FPATC concept. The test article is a sensor subsystem including FPA operational hardware and flight navigation hardware. Under closed-loop conditions, flight hardware tracking algorithms output new line-of-sight coordinates that are accepted by FPATC hardware and used to create the next sequential frame to be projected. Since the DWSG does not project through a sensor's optics, real-time digital simulation of sensor optical effects is a critical part of realistic simulations. Appendix E describes methods for digital simulation of anisoplanatic optics.

## F3.0 PROOF-OF-PRINCIPLE DEMONSTRATION

The initial closed-loop proof-of-principle (PoP1) demonstration focuses on using the FPATC to first, interactively manipulate or construct scenario frames by responding to changes in line of sight of the sensor, and second, to demonstrate computational capabilities for simulating optical effects in the constructed scene image. Before a PoP1 demonstration capability can be designed and integrated into the FPATC, it is necessary to understand some of the computational requirements for closed-loop in general, and the PoP1 demonstration in particular.

## F4.0 DETERMINATION OF THE COMPUTATIONAL REQUIREMENTS

Figure F-3 outlines the steps required to interactively compute a 2-D infrared rendered scenario frame based on a pointing vector input. These steps include rotation, translation, and extraction of the scene image; application of the OTF using a 2-D FFT and inverse FFT approach; detector integration for greater than 1:1 image sampling; radiometric, laser, and RF calibration; and projection buffer loading before outputting the frame. An equation, shown in Fig. F-3, was derived by predicting the number of compute cycles required for the whole process and summing the total. The equation is written as a function of test parameters such as oversampling ratio, number of FPA rows and columns, and point spread function size. To be conservative, no optimization was done on the calculation of compute cycles per step. A compute cycle is assumed to be the time required to perform an add, subtract, multiply, divide, or memory move. There are some optimizations that could be done to combine steps in the process and speed up the calculations. Figure F-4 shows the equation that would result if the FFT approach were substituted with direct convolution using a restricted kernel. Direct convolution is not always, however, the most optimal method to choose. Issues concerning kernel size relative to sampling ratio can cause fidelity problems in the simulation and create excessive computational loading. However, for applications that permit the fidelity levels associated with a smaller point spread function kernel, direct convolution is simpler and more efficient to implement. Figure F-5 tabulates direct convolution versus FFT methods and indicates a crossover point between FFT and direct convolution around a $9 \times 9$ kernel size.

After considering worst-case computational requirements for closed-loop, a three-fold implementation strategy was adopted. First, capabilities of existing FPATC hardware designs were evaluated for PoP1 demonstrations. Second, off-the-shelf hardware and software subsystems that could be integrated into the FPATC were investigated. Third, integration of off-the-shelf-subsystems and components with in-house developments that could meet closed-loop requirements was studied.

## F5.0 DESIGN OF COMPUTATIONAL HARDWARE

Figure F-6 shows an in-house designed DWSG RF control module. The module uses a TMS320C30 (C30) Digital Signal Processor (DSP) to control 16 RF channels (or FPA scan lines) during a mission simulation. In open-loop simulation, the system uses the DSP as a data pump to rapidly produce new frames during simulation. However, in closed-loop simulation, the DSP's computational capabilities could be tapped to execute the required closed-loop processing steps on scene data stored in each processor's memory. There are 32 C30's that work together in a Single Instruction Multi-Data (SIMD) architecture in the FPATC DWSG electronics. Since the SIMD architecture is very compatible with image processing and the decomposition methods required for optical anisoplanatic simulation, the PoP1 demonstration was implemented using existing FPATC

designs and hardware. Figure F-7 describes anticipated computational capabilities using all of the DWSG RF control electronics. Using the FPATC hardware and software for the PoP1 demonstration is cost effective since it delays, by at least a year, large material procurements for more advanced subsystems. This approach recognizes the obvious benefits of waiting for improved electronic capabilities and lower cost while demonstrating the principles of closed-loop operation.

## F6.0 SUMMARY

An analysis of the computational requirements for a closed-loop operation of the FPATC has been conducted. Current plans begin development of C30 codes for the PoP1 demonstration. Development of data formats for target and background data and scene visualization hardware concepts began in February 1995. Direct convolution will be implemented first to ensure that all of the system components are working properly. More advanced 2-D FFT approaches will be attempted as fidelity becomes more critical. Based on results from the PoP1 demonstration, a more detailed development plan will be completed for advanced hardware and software designs. As noted, AEDC has extensive experience in the development of advanced signal processing electronics for space sensor testing. As a result, AEDC is in a unique position to integrate off-the-shelf and in-house designs that meet the closed-loop requirement.

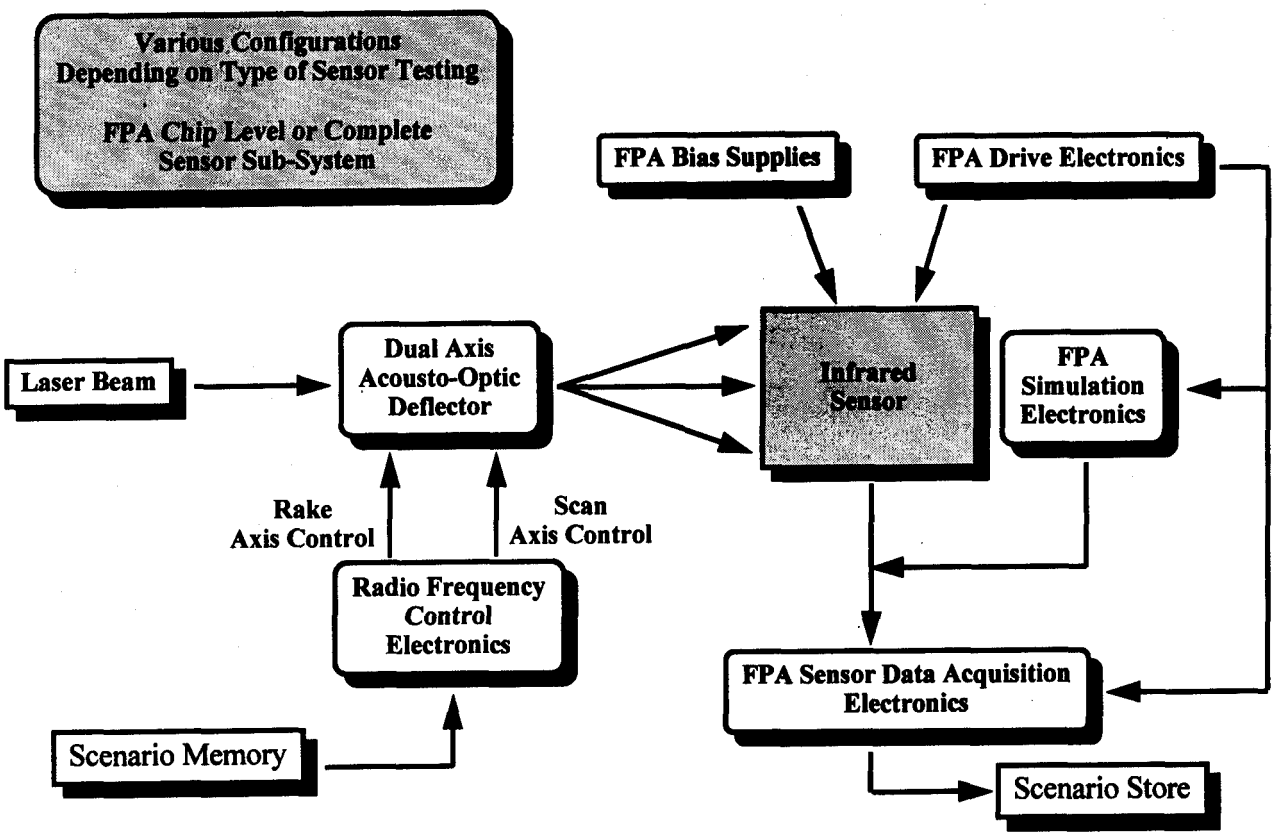


**Figure F-1. Open-loop FPATC concept.**

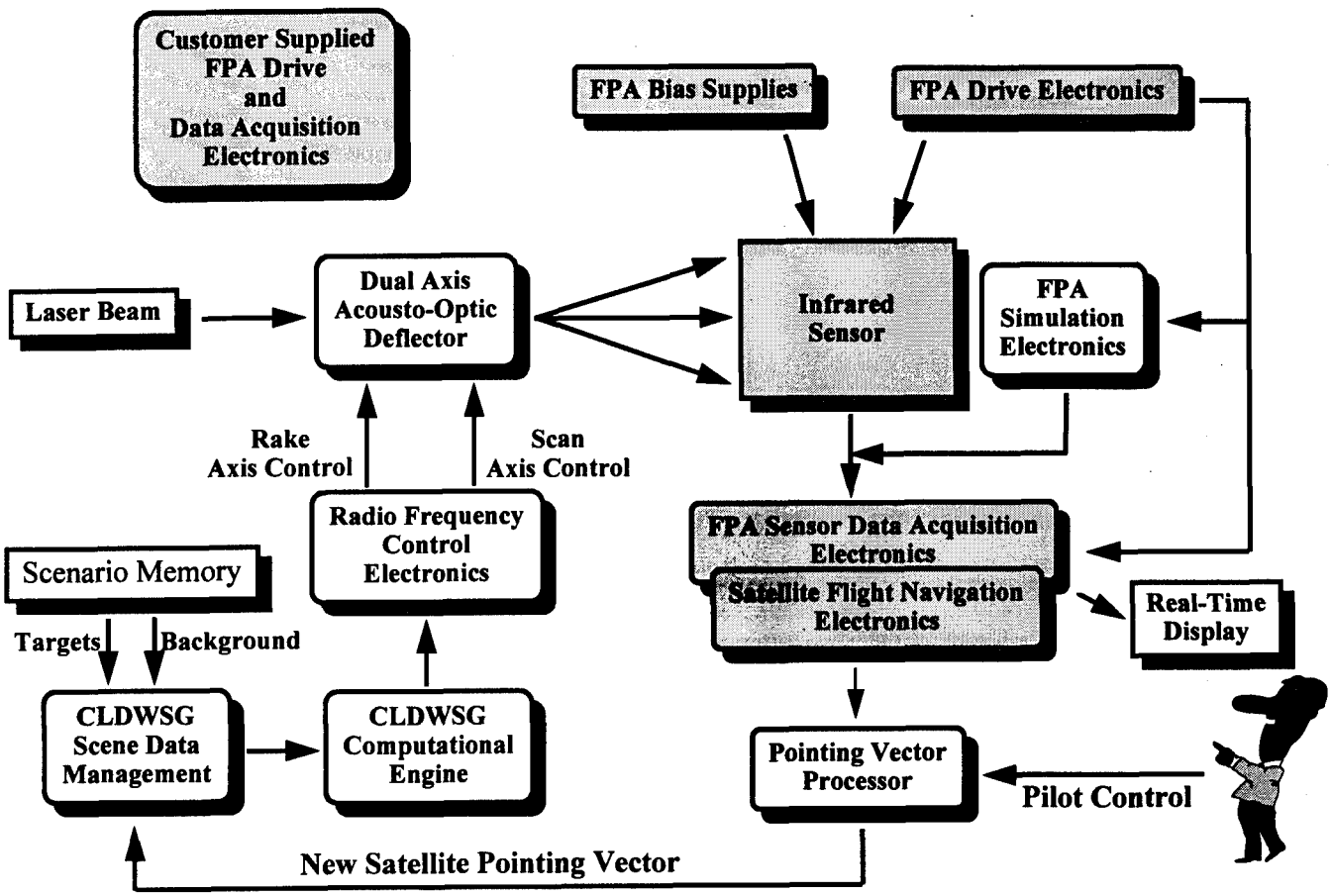


Figure F-2. Closed-loop FPATC concept.

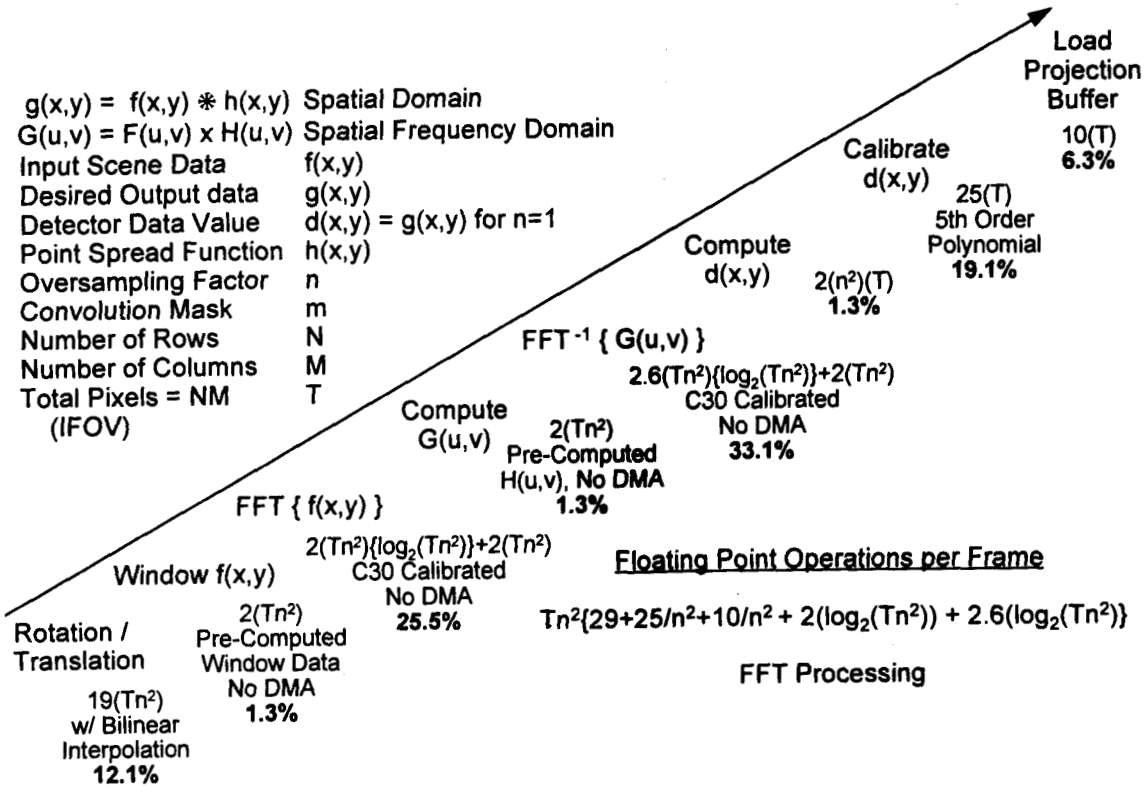


**Figure F-3. Computational steps required for FPATC closed-loop simulation.**

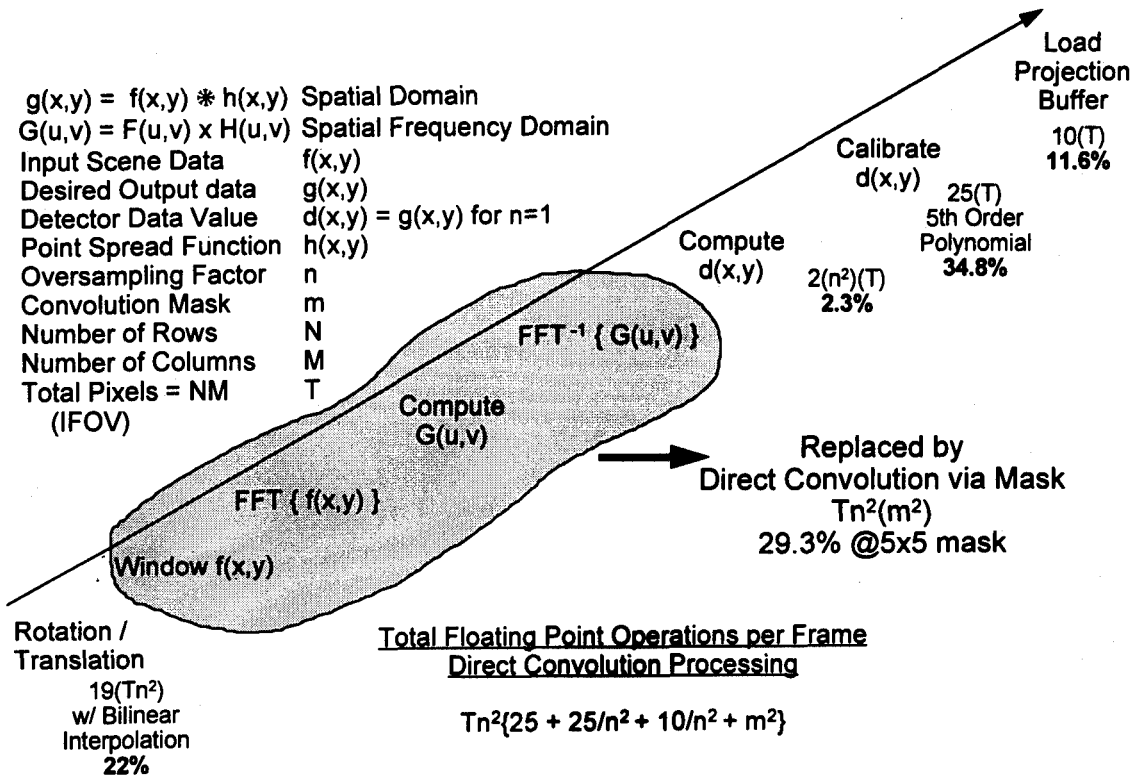


**Figure F-4. Closed-loop computational steps using direct convolution.**

Direct Convolution (mask=3x3)
MFLOP

| Row/Col | Oversampling (n) | | |
|---|---|---|---|
| NxM | 1 | 3 | 5 |
| 32x64 | 0.14 | 0.70 | 1.81 |
| 64x64 | 0.28 | 1.40 | 3.62 |
| 128x128 | 1.13 | 5.59 | 14.50 |
| 256x256 | 4.52 | 22.35 | 58.00 |
| 512x512 | 18.09 | 89.39 | 232.00 |

Direct Convolution (mask=9x9)
MFLOP

| Row/Col | Oversampling (n) | | |
|---|---|---|---|
| NxM | 1 | 3 | 5 |
| 32x64 | 0.29 | 2.03 | 5.50 |
| 64x64 | 0.58 | 4.05 | 11.00 |
| 128x128 | 2.31 | 16.20 | 43.99 |
| 256x256 | 9.24 | 64.82 | 175.96 |
| 512x512 | 36.96 | 259.26 | 703.86 |

- Trade-offs exsist between FFT / direct methods
- Need to consider effective PSF affect on final data
- DSP optimization for convolution may speed calculations and data management

FFT Algorithm
MFLOP

| Row/Col | Oversampling (n) | | |
|---|---|---|---|
| NxM | 1 | 3 | 5 |
| 32x64 | 0.23 | 1.73 | 5.04 |
| 64x64 | 0.47 | 3.64 | 10.54 |
| 128x128 | 2.04 | 15.91 | 45.94 |
| 256x256 | 8.76 | 69.05 | 198.84 |
| 512x512 | 37.43 | 297.91 | 855.65 |

**Figure F-5. Comparison of direct convolution and FFT computational methods.**

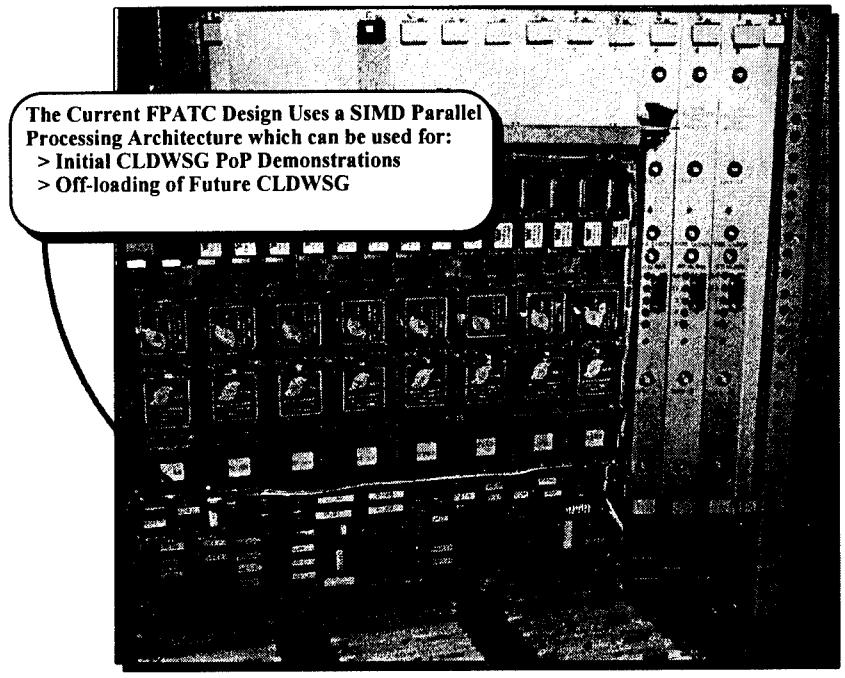


Figure F-6. DWSG RF Control Electronics Module.

**Computational Throughput (Frames/Sec)**
**DRES C30 Baseline**

| Row/Col | Oversampling (n) | | | |
|---|---|---|---|---|
| NxM | 1 | 3 | 5 | |
| 32x64 | 2825.50 | 369.11 | 127.08 | 11.2 Mb/s |
| 64x64 | 1356.34 | 175.95 | 60.70 | 10.83 Mb/s |
| 128x128 | 314.01 | 40.24 | 13.93 | 10.05 Mb/s |
| 256x256 | 73.10 | 9.27 | 3.22 | 9.37 Mb/s |
| 512x512 | 17.10 | 2.15 | 0.75 | 8.78 Mb/s |

Assume 32 C30's
640 MFLOPS
Rating
1.28 GFLOPS

C40 CPU Capability
25% increase
over C30

52-1280Mb/s
20,000
Frames/Sec
20x64 array

Need to
Reconfigure
Disk Farms
for Higher
Throughput

Required Bandwidth
Based On Computational Throughput

Figure F-7. Theoretical FPATC RF control electronics capabilities.

# APPENDIX G
# SENSOR PARAMETERS WHICH INFLUENCE T&E REQUIREMENTS

R. Menzel

## G1.0 INTRODUCTION

The specifications for surveillance sensors needed to guard against a missile attack on the United States or its areas of interest have been in review since the end of the Cold War. Sensor systems conceptualized and designed during that era to detect and track a potential Soviet first-strike attack on the United States are no longer considered to be cost effective because the threat of a massive attack is no longer apparent. Nevertheless, the Gulf War demonstrated the need for a threat or missile defense warning system. The difference between pre- and post-Cold War system needs is not in detection and tracking requirements, but rather in the number of missiles that may have to be detected and tracked, with a shift in emphasis from space-looking sensors to Earth-looking sensors. With the reduced scale of the threat dimension, new system requirements are currently being studied.

Because of the state of flux of system requirements, surveillance sensor system designs were not specified when this report was being written. This has the cascading effect that in trying to derive the impact that sensor systems impose on associated test and evaluation systems such as the DWSG, there are no specific examples to be followed. Instead, the driving requirements for the scene simulator must be addressed by generalities based on a best guess as to what the sensor system specifications will eventually be.

The scene generation requirements are further complicated because one step in calculating the scene composition is to convolve the scene with the sensor's OTF. The impact of this mathematical step is that the scenes presented to a focal plane are specifically tailored according to the characteristics of the particular sensor into which the focal plane will be installed. When the sensor's OTF is not available, the default calculation is made by assuming an OTF (perhaps idealized as for perfect optics). This assumption is not likely to be seen as an acceptable representative test of the focal plane because, as stated by Bob Jackson of Martin Marietta during a presentation of the Brilliant Eyes Final Program Review in February 1992, "[detection and tracking] algorithm design is driven as much by sensor characteristics as by the target/cluster conditions; . . . simulated data are useful but changes [to the algorithms] are required when the real sensor is finally in the target environment; . . . nearly half of the algorithm design concerns sensor effects." Clearly, there are no generic scenes that are applicable to testing a focal plane and its processor because each test case requires scenes specifically tailored by the intended sensor's OTF and the anticipated threat environment.

Aside from the OTF problem, the test scenes are dependent on a permutation of three groups of information: the type of sensor being considered, the particulars of the background scene conditions, and the choice of targets. The sensor design may be for surveillance or for an interceptor, the operational mode may be staring or scanning, the frame rates and/or scene revisit times may vary, and the sensor's orbital location and orientation must be specified. Various background scenes that may be required are day/night, sunlit, cloud covered, over land, over water, atmospheric absorption, seasonal dependence, Earth-limb, or deep space. Different targets might be the rocket type (i.e., spectral dependence), ascending plume, mid-course warm body, reentry heating, decoys, cruise missiles, etc. A collection of test scenes for the various combinations of these variables would result in an encyclopedic matrix of cases. Even so, it may not anticipate some particular test requirement.

Nevertheless, some boundaries must be placed on the size of the scene that may be required so the storage memory and data management problem can be sized. This decision necessitated a selection of sensor parameters, a candidate background scene, and a target scene. A review of the GPALS literature suggested that the more stressing cases involve using a staring sensor in a low-Earth orbit, an Earth background scene, and an ascending SCUD-like missile as the target information

## G2.0 SCENE CONTENT CONSIDERATIONS

Concepts for low Earth-orbit surveillance systems have been developed by the government and private contractors. Although there are significant differences in the specific designs, there are some commonalties resulting from the common mission requirements and the state of the art in IR sensor technology. The basic mission as defined is to detect a missile launch, track the missile in the early part of the launch with sufficient accuracy to hand over its launch coordinates to an attack plane, and to predict its potential impact point. As the tracking continues, the tracking accuracy should increase to the point where aimpoint vectors can be supplied to an anti-missile system. These mission requirements result in some generic properties of the surveillance system. First, launch detection implies a wide-field-of-view monitoring capability. However, a wide-field-of-view system would not have the accuracy to meet the tracking requirement. This would suggest a narrow-field-of-view sensor. The tracking accuracy requirement also suggests a low-altitude system versus a geosynchronous sensor. Low-altitude satellite systems must consider the Van Allen belts as a possible hazard. From these considerations, a generic surveillance system would consist of a satellite in about a 1,600-km orbit with both a wide-angle and a narrow-field-of-view system. In a similar fashion it can be surmised that a downward-looking surveillance system searching for a rocket launch would maximize the sensitivity by looking in the IR band of maximum emission from the plume. This is in the shorter wavelengths. Since detectability is a function of signal to noise, it is appropriate to consider maximizing the plume signal and minimizing the clutter from the Earth background. This can be accomplished by using the Earth's atmosphere as an Earth absorption

filter. Examination of the atmospheric transmission properties shows that there are two strong absorption bands in the shorter wavelengths, one between 2.5 and 2.8 μm, and the other between 4.2 and 4.5 μm. Bandpasses within these absorption bands are, therefore, of prime interest. This starts to define the requirements for the sensor's focal planes.

The most stressing sensors for ground testing will be the tracking sensors. These have a small field of view and high stability and high precision requirements.

Table G-1 shows additional assumptions and their justification made about the sensor design; these parameters are a best guess at the sensor characteristics that might satisfy a GPALS-like low-Earth-orbiting surveillance sensor. In order for a sensor to determine the location of a target with 15- to 20-μrad accuracy, it must either have a very small pixel IFOV, or it must employ some means of extracting the target position from lower-resolution data. The sizes of the available focal planes and the need for some reasonable field of view (so that the target doesn't get lost out of the field of view of a soda straw) preclude designing a system with 15- to 20-μrad pixels. In addition, there are limits placed by the physical properties of infrared telescopes. Diffraction effects define the focused spot size for reasonably sized mid-IR telescopes around 45 μrad. If the target spot size is as large or slightly larger than the detector pixel, then the target detection and tracking algorithms use centroiding techniques to determine the target position to values as small as one third of the pixel dimensions. Thus, a telescope with a 45-μrad IFOV pixel can be expected to provide 15-μrad placement of the target in its field of view. If the sensor has this capability, then the ground test chamber must provide the same accuracy in the target position in the scenes.

There are two methods of providing this type of accuracy in a test chamber. The first is to use an analog positioner to move the target. This positioner must have a minimum step resolution of at least 15 μrad. In an all-digital system where the target must be placed in a digitized background, the target placement resolution can be attained by requiring that the background database be built on a 15-μrad pixel matrix. The target can thus be co-added to the background.

This implies that the background is oversampled by 3 to 1 relative to the information deposited on each pixel of the focal plane, and the target is placed within one element of the $3 \times 3$ background matrix (for those pixels that contain target information) without having to further interpolate its position within the scene information grid while still meeting the position resolution requirement. The Earth surface footprint for each scene element at the chosen slant viewing angle is $54 \times 94$ meters. The best resolution of the SSGM for cloud backgrounds is about 175 meters. To obtain the desired scene element resolution will require that the SSGM maps be artificially subdivided into smaller grids so interpolation to the scene element unit sizes may be accomplished.

# G3.0 SCENE CHARACTERISTIC CONSIDERATION

The exact scene requirements of a particular focal plane test are mission- and sensor-dependent. Each test will require detailed scene preparation calculations and post-test analysis. The following text discusses a few of the scene characteristics that will be a concern for all scene compositions.

## G3.1 LINE-OF-SIGHT POINTING ACCURACY

The uncertainty of the target line of sight (LOS) is a combination of a bias uncertainty and a relative location uncertainty. These are combined using the root-sum-squared (RSS) method if the bias and relative uncertainties are independent (i.e., random). Bias corresponds to an absolute pointing accuracy dependent on how accurately the target track can be located relative to the Earth's geodesic coordinates, which are considered to be an absolute reference. Bias error is introduced by an uncertainty in determining the missile launch point. Generally, it is desired to know the launch coordinate within a circle of error of approximately 1 km. This uncertainty, divided by the viewing distance, gives the bias in terms of the scene resolution on the focal plane. The bias error affects the scene generation process by how accurately the target track origin is spatially coregistered on the background. As noted in Table G-2, the target positioning resolution suggests that the scene simulation must locate targets to better than 50 meters relative to the geodesic coordinates.

The relative track location uncertainty is the cumulative uncertainty introduced in the frame-to-frame repositioning of the target. This uncertainty is complicated because it is dependent on the history of the cumulated uncertainties (i.e., time dependence). Generally, the uncertainty decreases as more of the track history becomes available; the objective is to reduce the track uncertainties so that an impact point prediction uncertainty can be calculated within the operational specifications. The relative uncertainty affects the scene generation process by how accurately the track files can be represented by the spatially quantized scene element grid, by the round-off errors of the scene-element/sensor OTF convolution calculation, and by the sub-pixel spatial resolution of the focal plane algorithm.

## G3.2 TARGET RESOLUTION: PLUME SIZES

The rocket plume sizes depend on the rocket type, the fuel used, atmospheric conditions, and altitude. It is anticipated that most target track projections will be composed using classified information; unless otherwise supplied, the target plume's spatial and spectral characteristics can be obtained from the BMDO Plume Data Center at AEDC, albeit it may need to be filtered for variances in atmospheric conditions, viewing distances, and viewing perspective.

Typically, at low altitudes the high-intensity portion or core of the plumes is similar in size to the length of the rocket hardbody. Even at the shortest viewing distance (nadir), these plumes are not resolved to better than one focal plane pixel (54 μm), especially when seen in cross section rather than in profile. If the rocket burn lasts until high altitudes, the plume may grow in extent such that more than one pixel is illuminated

## G3.3 TARGET RADIANCE

The ratio of target intensity to background intensity depends on the size of the background "footprint" seen by each pixel; if the background area is large enough, the integrated background illumination can obscure the target illumination. Consequently, an important design parameter for a sensor system is to choose the per pixel "footprint" small enough so that the anticipated target information will be detected. Typically, a detection probability of greater than 0.95 is the design goal. Another design goal is that the focal plane operate at a signal/noise ratio of about 5. The consequence for the scene generator is that it answers the question of whether or not the background scene illumination would overwhelm the target illumination. To satisfy a S/N = 5 and a 0.95 detection probability (after the target passes through cloud obscuration) will require that the target illumination be significantly larger than the background within the detection bandwidth for any target illuminated pixel.

The power spectral density (PSD) of the background reduces approximately 4 orders of magnitude from a spatial frequency of one cycle/100 km to one cycle/km. The high spatial frequency portion of the PSD represents the high contrast portion of the background scene.

## G3.4 SCENE JITTER

Spacecraft jitter can be simulated by scene jitter. The effect of jitter on the scene content depends on the jitter frequency, amplitude, and on the focal plane frame rate, i.e., the integration period for each "snapshot." Jitter with frequencies higher than the integration period has the effect of blurring the scene. This can be simulated by degrading the OTF used to calculate the per pixel scene content.

Low-frequency jitter is manifested by an oscillation of the scene content relative to the focal plane pixel positions. The scene is not blurred, but it wanders about on the focal plane. This does not affect the metrics of the scene content, as long as each "snapshot" has within it a reference location from which relative measurements are made, or if the spacecraft IMU has an adequately accurate orientation/motion detection resolution.

Scene jitter may be an important perturbation when the focal planes of interceptors are tested. Interceptors undergo large lateral accelerations during their mission. These forces may cause the interceptor body (a) to enter a ringing mode, (b) to flex about its center line, and/or (c) to rotate the body orientation. Any of these perturbations can cause severe line-of-sight jitter, centroid jitter, and image size variations.

In contrast, surveillance sensors operate in a very benign environment. Typical operational requirements call for a jitter of less than about 10 μrad at 10 Hz. This is small enough that image blurring is much smaller than one pixel resolution and image dancing can be seen only if sub-pixel centroid resolution of approximately one-tenth of the pixel size can be discerned.

## G4.0 SUMMARY

Some generically derived requirements for the scene generation needed for the test and evaluation of surveillance sensors are presented. Because the sensor requirements are currently being reassessed to reflect the changes in the post-Cold War threat projections, the test scene compositions are based on a best guess of the functional requirements that a missile launch detection and tracking sensor must satisfy. The principal derived scene requirement is to simulate a plume target superimposed on an Earth background such that location and track vectors are known within 15 to 20 μrad of an Earth grid reference. The scene resolution is satisfied when the scene is oversampled by a factor of three in each dimension relative to the sensor's instantaneous field of view per pixel. In general, this resolution is greater than that supplied by the SSGM. This in turn necessitates that the SSGM maps be artificially subdivided into a smaller grid so that interpolation to the required scene area elemental units may be accomplished.

The parametric requirements of the scene applied for test and evaluation of a sensor are uniquely dependent on the particular sensor, its mission, and the contents of the target and scene information. Each test will require detailed scene preparation calculations and post-test analysis for the preparation of the uncertainty analysis. Some of the key ingredients of the uncertainty analysis are the line-of-sight accuracy, the target resolution, the irradiance characteristics, and intentional and unintentional scene jitter.

**Table G-1. Parameters Influencing the Sensor Design**

| Parameter | Assumption | Reason |
|---|---|---|
| Ratio: (PSF)/Pixel Size | 1.5 to 1.0 | Allows sub-pixel resolution algorithm |
| Focal Plane: Array Size | 64 × 64<br>128 × 128<br>256 × 256 | State of the art for InSb, MCT, and doped Si arrays |
| Sensor Optics: Field-of-view | 0.4 to 1.0 deg | Typical narrow-field-of-view IR telescope design |
| Focal Plane Frame Rate | 30 to 100 Hz | Typical clocking rate for staring sensors |
| Orbital Height | 1,600 to 1,700 km | Just below the Van Allen belts |
| Slant Viewing Distance | 3,000 to 4,500 km | Arbitrary mid-range values assuming that the satellites will operate as pairs in complementary orbits to obtain stereo viewing |
| Target Position Resolution | 15 – 20 μrad | Determine tracking accuracy for handover |
| Target Velocity Against Background | 0.5 to 2 km/sec | Average missile velocity |
| Background Scene | | Sun irradiance with clouds over a terrain background |
| Scene Duration | 60 sec<br>300 sec | Typical rocket burn time for Scud<br>Burn times for a 3-stage rocket |

**Table G-2. Derived Scene Parameters**

| Parameter | Derived | Method |
|---|---|---|
| IFOV per pixel | 45 to 55 μrad | Estimate of diffraction-limited spot, and possible telescope design (0.4 deg)/128 |
| Observed Target Motion | 0.67 mrad/sec | (2 km/sec)/ (3,000 km) motion at distance |
| Target Motion per Frame | 22 μrad | (0.67 mrad/sec)/ (30 Hz) target position resolution per frame |
| Scene Element Resolution | 15 to 18 μrad | Target position requirement for digital backgrounds |
| Scene Elements per Pixel | 3 × 3 | (55 μrad)/(18 μrad) = 3 |
| | | |
| IFOV Footprint per Pixel | 165 × 288 m | (55 μrad) * (3,000 km) at a 55-deg slant angle |
| Footprint per Scene Element | 54 × 94 m | (18 μrad) * (3,000 km) at a 55-deg slant angle |

## NOMENCLATURE

| | |
|---|---|
| AEDC | Arnold Engineering Development Center |
| ASTC | Advanced Sensor Test Capability |
| $BMC^3$ | Battle Management Command Control Communications |
| BMDO | Ballistic Missile Defense Organization |
| $C^2E$ | Command and Control Element |
| COEA | Cost and Operating Effectiveness Analysis |
| CSO | Closely spaced object |
| CTEIP | Central Test and Evaluation Investment Program |
| DIS | Distributed Interactive Simulation |
| DNA | Defense Nuclear Agency |
| DoD | Department of Defense |
| DSP | Digital signal processor |
| DT&E | Development Test & Evaluation |
| DWSG | Direct Write Scene Generator |
| EMD | Engineering Manufacturing Development |
| ERD | Element Requirements Document |
| FFT | Fast Fourier Transform |
| FOV | Field of view |
| FPA | Focal plane array |
| FPATC | Focal Plane Array Test Chamber |
| FPCC | Focal Plane Characterization Chamber |
| FSD | Full-scale development |
| HIC | Human-in-control |
| IMU | Inertial Measurement Unit |
| IOC | Initial Operating Capability |
| IR | Infrared |
| ISTC | Integrated System Test Capability |
| LAN | Local Area Network |
| LOS | Line-of-sight |
| LWIR | Long wavelength infrared |
| M&S | Modeling and simulation |
| MNS | Mission Need Statement |
| MOE | Measures of Effectiveness |
| MOP | Measures of Performance |
| MWIR | Middle wavelength infrared |
| NIST | National Institute of Standards and Technology |
| ODP | Object-dependent processor |

| | |
|---|---|
| ORD | Operational Requirements Document |
| OSD | Office of Secretary of Defense |
| OT&E | Operational Test and Evaluation |
| OTF | Optical transfer function |
| PDU | Protocol data units |
| PoP | Proof-of-principle |
| RF | Radio frequency |
| RV | Reentry vehicle |
| SIMD | Single instruction multi-data |
| SONET | Synchronous Optical Network |
| SSGM | Strategic Scene Generation Model |
| STAR | System Threat Assessment Report |
| SWIR | Short wavelength infrared |
| TDP | Time-dependent processor |
| TEMP | Test and Evaluation Master Plan |
| TMD | Theater Missile Defense |
| WAN | Wide Area Network |